

Intersectional Targeting Reveals Heterogeneous Nature of Glp1r- and Lepr- expressing POMC Neurons

INAUGURAL-DISSERTATION



zur Erlangung des Doktorgrades
der Mathematisch-Naturwissenschaftlichen Fakultät
der Universität zu Köln

vorgelegt von
Nasim Biglari
geboren in Zanzan, Iran

Köln, 2020

Berichtersteller

Prof. Dr. Jens C. Brüning
Prof. Dr. Peter Kloppenburg

Tag der mündlichen Prüfung: 22.01.2021

Jahr der Veröffentlichung: 2022

Table of Contents

1	INTRODUCTION	1
1.1	Global obesity epidemic	1
1.1.1	Obesity, its prevalence and causes.....	1
1.1.2	Associated comorbidities of obesity	2
1.1.2.1	The metabolic syndrome and type 2 Diabetes Mellitus (T2DM)	2
1.2	Energy homeostasis	3
1.2.1	Anatomy and functions of the hypothalamus and its nuclei	4
1.2.2	Hypothalamic control of energy homeostasis	6
1.2.3	The arcuate melanocortin system.....	7
1.3	POMC-expressing neurons of the ARC (POMC^{ARC}).....	8
1.3.1	The <i>Pomc</i> gene, its sites of expression and functional relevance	9
1.3.2	The posttranslational cleavage products of POMC and the melanocortin receptors	10
1.3.3	Neural inputs into POMC neurons and their projection sites	13
1.4	Stimuli of POMC neurons	13
1.4.1	Leptin and its action on POMC neurons	14
1.4.2	Glp1 and its action on POMC neurons	15
1.5	Heterogeneity of POMC neurons	18
1.6	Genetic-based tools for studying heterogeneity	20
1.6.1	Tools used in this study for investigating the heterogeneity of POMC neurons.....	21
1.7	Objectives	22
2	MATERIALS AND METHODS.....	23
2.1	Animal and experimental ethics.....	23
2.2	Animal housing and care.....	23
2.3	Commercially available or previously published driver lines used in this study	23
2.4	In-house developed transgenic mouse lines	24
2.5	Generation of experimental animals	24
2.6	Glucose tolerance tests (GTT)	24
2.7	NMR for body weight composition.....	24
2.8	Indirect calorimetry	25

2.9	Study design of DREADD animals	25
2.9.1	CNO administration.....	25
2.9.2	Corticosterone ELISA.....	26
2.10	Perfusion and tissue fixation	26
2.11	Immunohistochemistry	26
2.12	Imaging and quantification of immunohistochemistry	27
2.13	RNA <i>in situ</i> hybridization	27
2.14	Imaging and quantification of RNA <i>in situ</i> hybridization	28
2.15	Tissue clearing, image acquisition and analysis	29
2.15.1	uDISCO whole-brain clearing and image acquisition.....	29
2.15.2	Whole brain immunostaining.....	30
2.15.3	Co-registration using VINCI.....	30
2.15.4	Extraction of neuronal coordinates using Arivis and 3D scatter plots.....	31
2.15.5	Isosurface density plots.....	32
2.15.6	Data analysis of 3D projections.....	32
2.16	Study design of bacTRAP (EGFPL10a) mice	32
2.16.1	Purification of mRNA from triple positive EGFPL10a Mice and RNA sequencing.....	33
2.16.2	Gene Ontology Analysis.....	33
2.16.3	Overlap analysis.....	33
2.17	Electrophysiological experiments	34
2.17.1	Animals and brain slice preparation.....	34
2.17.2	Electrophysiology.....	35
2.17.3	Intrinsic electrophysiological properties.....	36
2.17.4	Peptide signaling.....	37
2.18	Quantification and Statistical Analysis	37
2.19	Statistical analyses	37
2.19.1	Statistical analysis of 3D data.....	38
2.19.2	RNA-Sequencing Analysis Workflow.....	38
3	RESULTS	40
3.1	Generation of POMC-Dre driver line	40
3.2	Combinatorial recombinase-dependent labeling of heterogeneous POMC neuron populations	44
3.3	Distinct anatomical distribution of POMC^{Lep^r+} and POMC^{Glp1^r+} neurons in the ARC 47	

3.4	Similar projection patterns of POMC^{Lep^r+} and POMC^{Glp1^r+} neurons.....	51
3.5	DREADD-dependent activation of POMC^{Lep^r+} and POMC^{Glp1^r+} neurons differentially regulates food intake.....	54
3.6	Distinct translational signatures of POMC^{Lep^r+} and POMC^{Glp1^r+} neurons.....	62
3.7	Verification of endogenously expressed, differentially regulated genes in POMC^{Lep^r+} and POMC^{Glp1^r+} neurons	67
3.8	POMC^{Lep^r+} and POMC^{Glp1^r+} neurons have distinct intrinsic electrophysiological properties.....	69
3.8.1	Specific regulation of POMC ^{Lep^r+} and POMC ^{Glp1^r+} neurons by energy state sensing signals	71
4	DISCUSSION	74
4.1	The POMC-Dre driver mouse is a versatile tool for studying POMC neurons	74
4.2	The Cre/Dre combinatorial recombinase system for studying heterogeneity.....	75
4.3	Anatomical localization of POMC^{Lep^r+} and POMC^{Glp1^r+} neurons	76
4.4	Similar projection patterns of POMC^{Lep^r+} and POMC^{Glp1^r+} neurons	78
4.5	Physiological effects of POMC^{Lep^r+} and POMC^{Glp1^r+} neuron activation.....	79
4.6	Molecular and electrophysiological differences between POMC^{Lep^r+} and POMC^{Glp1^r+} neurons	82
4.7	Conclusion.....	85
5	BIBLIOGRAPHY	86
6	SUMMARY	99
7	ZUSAMMENFASSUNG	100
8	ERKLÄRUNG.....	101
9	ACKNOWLEDGEMENTS	102

Figure index

Figure 1.1 Diagram of the hypothalamus and its major nuclei.....	5
Figure 1.2 Bioactive POMC products and their interactions with the melanocortin receptors.....	11
Figure 1.3 The expression system used for intersectional Cre/Dre dependent targeting of heterogenic populations.....	20
Figure 3.1 The POMC ^{Dre} driver line successfully targets POMC neurons.....	41
Figure 3.2 The POMC ^{Dre} transgene does not cause any metabolic phenotypes compared to wildtype controls.	43
Figure 3.3 Co-expression of <i>Pomc</i> with either <i>Glp1r</i> or <i>LepR</i> in the ARC.....	44
Figure 3.4 Breeding scheme used for generating experimental mice that shows the triple transgenic mice as well as their littermate controls.....	45
Figure 3.5 ZsGreen labeling of POMC ^{LepR+} and POMC ^{Glp1r+} neurons using the Dre/Cre-dependent ROSA26 SlrSrZsGreen reporter line.....	46
Figure 3.6 POMC ^{LepR} and POMC ^{Glp1r} have different spatial distribution patterns in the ARC.....	48
Figure 3.7 Similar coronal distribution pattern of transgenic-labeled and endogenously-expressed POMC ^{LepR+} and POMC ^{Glp1r+} neurons.	50
Figure 3.8 ZsGreen expression in ARC is only detected in mice expressing both Cre and Dre recombinases.....	51
Figure 3.9 Three-dimensional analysis of the projections of POMC ^{LepR+} and POMC ^{Glp1r+} neurons shows similar patterns.	53
Figure 3.10 Cre/Dre-dependent hM3Dq transgenic lines allow for specific neuronal activation solely in triple transgenic mice.	55
Figure 3.11 Chemogenetic activation of POMC ^{LepR+} and POMC ^{Glp1r+} neurons differentially suppresses food intake in male mice without eliciting a response in genotype controls.....	57
Figure 3.12 Chemogenetic activation of POMC ^{LepR+} and POMC ^{Glp1r+} neurons does not affect food intake in female mice.....	58

Figure 3.13 Chemogenetic activation of POMC^{Lep^r+} and POMC^{Glp1^r+} neurons leads to reduced RER.....	59
Figure 3.14 <i>Vgat</i> or <i>Vglut2</i> expression in POMC^{Lep^r+} and POMC^{Glp1^r+} neurons.....	60
Figure 3.15 No effects observed on circulating corticosterone levels upon chemogenetic activation of POMC^{Lep^r+} and POMC^{Glp1^r+} neurons.....	61
Figure 3.16 Transcriptomic profiling of POMC^{Lep^r+} or POMC^{Glp1^r+} neurons via targeted EGFP10a expression.	63
Figure 3.17 GO-term analysis on of the differently expressed genes between the POMC^{Lep^r+} and POMC^{Glp1^r+}.....	65
Figure 3.18 Overlap analysis of the publicly available single-cell RNA-sequencing data from mouse hypothalamic with our dataset.....	66
Figure 3.19 Differential expression of endogenous mRNA for identified candidates in POMC^{Lep^r+} and POMC^{Glp1^r+} neurons.....	68
Figure 3.20 POMC^{Lep^r} and POMC^{Glp1^r} neurons exhibit different intrinsic properties.	69
Figure 3.21 Electrophysiological recordings of the effect of leptin and Glp1 on transgenic labeled POMC^{Lep^r} and POMC^{Glp1^r} neurons, respectively.....	71
Figure 3.22 Representative traces showing the effect of Glp1 and leptin on transgenic labeled POMC^{Lep^r} and POMC^{Glp1^r} neurons, respectively.....	72

Abbreviations

Acb	nucleus accumbens
ACTH	adrenocorticotropic hormone
AGRP	agouti related peptide
AH	anterior hypothalamus
ARC	arcuate nucleus of the hypothalamus
BAC	bacterial artificial chromosome
BBB	blood-brain-barrier
BMI	body mass index
BNST	bed nucleus of the stria terminalis
cAMP	cyclic adenosine monophosphate
Cartpt	cocaine and amphetamine regulated transcript protein
CLIP	corticotrophin-like intermediate peptide
CNO	clozapine-n-oxide
CNS	central nervous system
CVD	cardiovascular disease
DAG	diacyl glycerol
DB	diagonal band of Broca
DIO	diet-induced obesity
DMH	dorsomedial nucleus of the hypothalamus
DpMe	deep mesencephalic nucleus
DPP4	dipeptidyl peptidase
DREADD	Designer receptors exclusively activated by designer drugs
EGFP	enhanced green fluorescent protein
FPKM	fragments per kilobase million
GABA	gamma-Aminobutyric acid
Gad	glutamate decarboxylase
Gal	galanin
Gcg	glucagon

Gck	glucokinase
GH	growth hormone
Glp1	glucagon-like peptide-1
Glp1r	glucagon-like peptide-1 receptor
GLUT	glucose transporter
GO	gene ontology
G-protein	guanine nucleotide binding protein
hM3D	human M3 muscarinic DREADD
IP	immunopurified
IP3	and inositol 1,4,5-trisphosphate
IRES	internal ribosome entry site
JAK	Janus kinase
Lepr	leptin receptor
LH	lateral hypothalamus
LPH	lipotrophins
LS	lateral septum
MC	melanocortin
mCPP	meta-chlorophenylpiperazine
MCR	melanocortin receptor
ME	median eminence
MPO	medial preoptic nucleus
MSH	melanocyte-stimulating hormone
NLS	nuclear localization signal
Nmur2	neuromedin-2 receptor
NMU	neuromedin-U
Npy	neuropeptide Y
NTS	nucleus tractus solitarius
Opr	opioid receptor
PAG	periaqueductal grey
PC	prohormone convertase

PCE	POMC converting enzyme
Pdyn	prodynorphin
Penk	preproenkephalin
pG	deep gray layer of the superior colliculus
PIP2	phosphatidylinositol 4,5-bisphosphate
PKA	protein kinase
Pomc	pro-opiomelanocortin
PVH	paraventricular nucleus of the hypothalamus
RIN	RNA Integrity values
Rpl10a	ribosomal protein L10a
T2D	type 2 diabetes mellitus
TSH	thyroid stimulating hormone
Vglut	vesicular glutamate transporter
VMH	Ventromedial nucleus of the hypothalamus
WHO	World Health Organization
WSS	Westphal-Stop-Sequences

1 Introduction

1.1 Global obesity epidemic

1.1.1 Obesity, its prevalence and causes

Obesity is described as an excessive accumulation of body fat that poses as a health risk. The body mass index (BMI) has been widely used as a crude determinant of obesity and is calculated by dividing the weight of an individual (in kilograms) by the square of their height (in meters). If the calculated BMI is equal or greater than 30 kg/m², the individual is generally considered obese, whereas a BMI of 25 kg/m² or greater is an indication that the person is overweight (Organization, 2018). Use of the BMI as a determinant of obesity has been scrutinized due to its inability to discern between fat and lean mass and to consider the localization of adiposity (Snijder et al., 2006). An accumulation of visceral versus subcutaneous fat is a greater proponent in development of associated comorbidities (Bergman et al., 2006). Therefore, factors such as waist-to-hip ratio, waist circumference or body fat percentage have also been taken into consideration for a better categorization of stages of overweight and obesity (Snijder et al., 2006).

The prevalence of obesity varies depending on factors such as age, socioeconomic group, education, and region within each population. However, according to the World Health Organization (WHO), obesity has tripled since 1975, across the globe (Organization, 2018). In 2016, 1.9 million adults were overweight (39% of the total), of which, 650 million adults (13% of total) were classified as obese (Organization, 2018). At the same time, an estimated number of more than 41 million children aged less than five years were overweight (Organization, 2018). Notably, overweight and obesity in childhood often persist throughout an individual's lifetime. In addition to the increasing incidence of childhood obesity, the global prevalence of maternal and gestational obesity is rapidly rising in low and high-income populations (Hanson et al., 2016). Maternal obesity during pregnancy increases the risk of the offspring to become obese, creating a "vicious cycle". Not only does this lead to higher risk of the offspring to develop type 2 diabetes mellitus (T2DM) and cardiovascular comorbidities such as stroke, coronary heart disease or asthma but also it is found that maternal obesity

influences the cognitive performance of the child and increases the risk of neurodevelopmental diseases (Brion et al., 2011; Hanson et al., 2016).

Obesity, at its basis, results from an imbalance in energy intake relative to energy expenditure that comes down to increased caloric intake and a reduction in energy expenditure. This can be attributed to the modern lifestyle of humans that has brought around an increase in accessibility in calorie-dense food (high fat, high sugar) and increased sedentary states. Despite this, the etiology of obesity is known to be complex, influenced by behavioral, socioeconomic, environmental, and genetic factors. With respect to the latter, monogenic mutations causative of drastic obese phenotypes are indeed a rarity in the human population. Although the epidemic magnitudes of obesity cannot be attributed to them, studying mutations of single genes has led to the identification of several key components of energy homeostasis regulation, including the *melanocortin 4 receptor (Mc4r)*, *proopiomelanocortin (Pomc)*, or *leptin (Ob)* genes (Farooqi, 2008; Krude et al., 1998; Montague et al., 1997; Santini et al., 2009). From a genetic standpoint, common obesity is likely to have many genetic determinants, mapped by genome-wide association studies (GWAS) that through their interaction with obesogenic environmental factors lay the grounds for the escalating prevalence of this disorder (Hetherington and Cecil, 2010).

1.1.2 Associated comorbidities of obesity

The obese state leads to dysfunction in energy homeostasis as well as a myriad of metabolic processes within the body. Obesity is thus associated with or exacerbates a multitude of chronic disorders such as osteoarthritis, liver and kidney disease, sleep apnea, type 2 diabetes mellitus, cardiovascular disease (CVD) and depression (Apovian, 2016).

1.1.2.1 The metabolic syndrome and type 2 Diabetes Mellitus (T2DM)

Metabolic syndrome (MetS), or syndrome X, is a metabolic disorder, characterized by a clustering of at least three clinical representations of the following five risk factors: glucose intolerance (type 2 diabetes, impaired glucose tolerance, or impaired fasting glycaemia), insulin resistance, central obesity, dyslipidemia, and hypertension (Grundy, 2008). The prevalence of this disorder ranges between 20-30% within the adult population (Grundy, 2008). T2DM is the state of chronic hyperglycemia that results from insulin resistance in the

key target regions of this hormone such as liver, white adipose tissue, muscle, and the central nervous system (CNS) (Biddinger and Kahn, 2006). According to the international diabetes federation (IDF) approximately 463 million adults were living with diabetes in 2019, 90% of which is accounted by T2DM (Edition). Since obesity is associated with chronic insulin resistance and hyperglycemia, it serves as an established risk factor for both MetS and T2DM, each of which give rise to a multitude of disorders including CVD (Vasudevan et al., 2006). When introducing MetS at the American Diabetes Association national meeting, Gerald Reaven mainly attributed it to insulin resistance and suggested that all other symptoms arise from this (Roberts et al., 2013).

Based on a buildup of evidence, the Endocrine Society has suggested that obesity might be due to dysfunction of the system controlling energy homeostasis than simply a passive weight accumulation (Schwartz et al., 2017). Despite the fact that dysfunctions in this system lead to obesity, the increase in prevalence is likely attributable to the inability of the regulatory system to cope with the high-caloric, sedentary lifestyle (O'Rahilly et al., 2003). It has been considered that obesity results from a lack of discipline, the inability to reduce calorie intake and to increase physical activity leading to a social stigmatization of affected individuals, which based on extensive studies suggest a complex interplay of factors impacting the regulation of homeostasis (Friedman, 2004). If this is indeed the case, we need to gain better understanding of the regulation of energy homeostasis and its components. Since the system can modulate both energy intake and expenditure, it would employ compensatory mechanisms in instances of calorie restriction and exercise, for maintenance of a certain homeostatic state. Thus, investigation into the homeostatic control and the molecular machinery behind the compensatory mechanism is crucial for development of effective therapeutics.

1.2 Energy homeostasis

Energy consumption and homeostasis requires an efficient regulatory system that has the ability to sense and monitor nutrients, adapt to internal and external fluctuations and adjust energy intake and metabolism accordingly (Berthoud et al., 2017). The French physiologist, Claude Bernard, was the first to devise the concept of a constant internal environment (*milieu intérieur*) and that the bodily systems function to maintain it despite

varying external conditions (Cooper, 2008). Walter Cannon extended this concept and formulated the word “homeostasis” (Cannon, 1932). His theories addressed *how* this internal constant is maintained and thus suggested that the brain regulates systems within the body in order to maintain set values for internal variables (Cooper, 2008). In vertebrates, the central nervous system (CNS) has developed mechanisms through which it detects external and internal nutritional states, integrates this information to control eating behavior and energy expenditure, and thereby regulates body weight (reviewed in (Berthoud et al., 2017)). The hypothalamus has emerged as the main integration site for factors originating from both central and peripheral systems for the regulation of energy homeostasis (Timper and Bruning, 2017). The involvement of the hypothalamus in metabolic regulation is elaborated on in the following sections.

1.2.1 Anatomy and functions of the hypothalamus and its nuclei

The hypothalamus derives its name on the basis of its position, being situated below the thalamus. It is located in the ventral diencephalon and is part of the limbic system. The hypothalamus is constructed of 11 main nuclei in addition to several smaller ones that are symmetrically arranged around the third ventricle and form bidirectional neuronal connections with various nuclei in the brain (Simerley, 1995). An outline of the anatomy of major hypothalamic nuclei addressed here are displayed in Figure 1.1. The position and anatomy of the hypothalamus allows it to act as a bridge between the nervous and endocrine system as well as the periphery by adjacency to the third ventricle and being linked to the pituitary (Pop et al., 2018). In general the hypothalamus regulates autonomous and endocrinological processes (Pop et al., 2018). The hypothalamic nuclei are each involved in various functions such as arousal, sleep, circadian rhythms, hunger and satiety, thermoregulation and thirst (Waterson and Horvath, 2015).

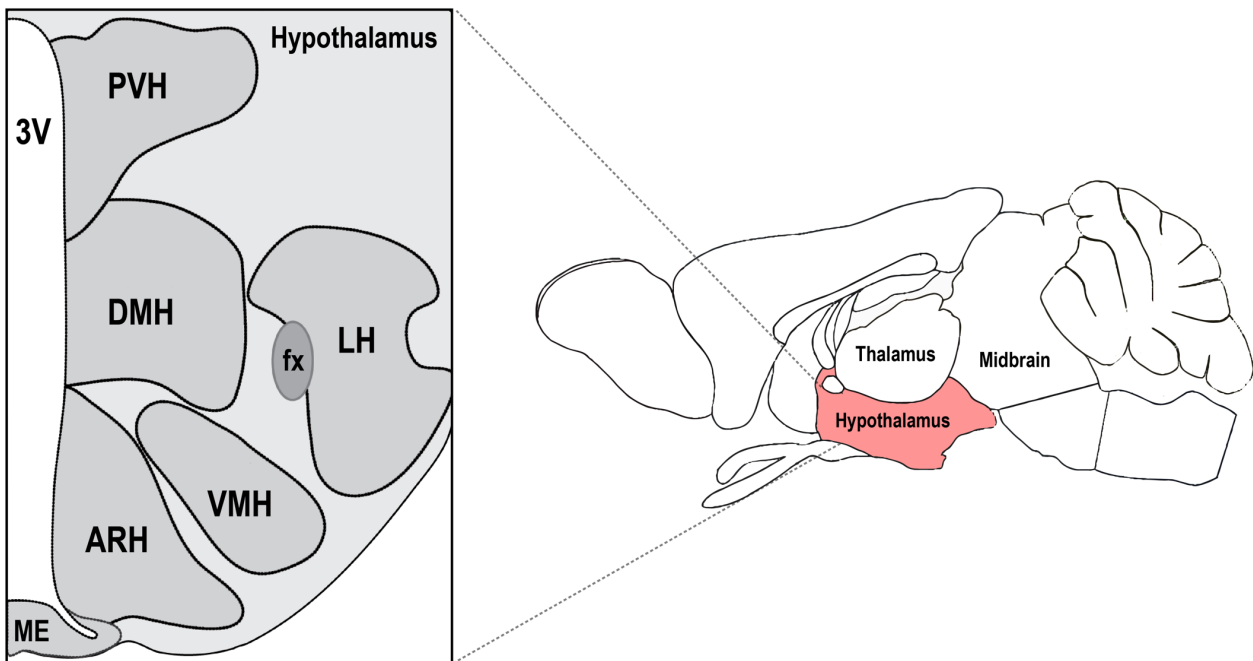


Figure 1.1 Diagram of the hypothalamus and its major nuclei.

The hypothalamus is situated below the thalamus next to the midbrain. Hypothalamic nuclei are located symmetrically around the third ventricle, adjacent to the median eminence. ME, median eminence; ARC, arcuate nucleus of the hypothalamus; VMH, ventromedial nucleus of the hypothalamus; DMH, dorsomedial nucleus of the hypothalamus; PVH, paraventricular nucleus of the hypothalamus; LH, lateral hypothalamic area; fx, fornix; 3V, third ventricle.

The aggregation of neurons in direct vicinity to the third ventricle and the median eminence form the arcuate nucleus of the hypothalamus (ARC). Extensive studies on the neurons of this area divulge its critical role in metabolic process control, further elaborated on in Section 1.2.3. Another main nucleus of the hypothalamus is the PVH, which is located rostrally in the periventricular area and regulates the hormones expressed in the pituitary in addition to integrating inputs to formulate autonomic outputs in response to fluctuating conditions (Ferguson et al., 2008). The VMH is located above the ARC and regulates energy intake and glucose homeostasis (Beverly et al., 1995; Levin et al., 2008). Dorsal to the VMH is the dorsomedial hypothalamus (DMH) that receives input from many other hypothalamic nuclei thus it likely acts as a relay for ARC to the PVH through which it modulates appetite and emotional behavior (Chao et al., 2011; Thompson and Swanson, 1998). In comparison to other

hypothalamic nuclei, the lateral hypothalamus spans extensively across the rostrocaudal axis. The LH is implicated in physiological functions including feeding behavior, reward systems, sleep/wakefulness cycle, stress regulation and inhibition of inflammatory pain (Stuber and Wise, 2016). Throughout the years and subsequent to the pioneering experiments in the 19th century, a great deal of research has focused on unraveling the mechanisms and circuitry through which each of these hypothalamic nuclei function to maintain homeostatic conditions within the body. The new developments in neuroscience will aid a great deal in comprehension of the fine details that are involved in these processes.

1.2.2 Hypothalamic control of energy homeostasis

Initial evidence revealing the involvement of the brain and the hypothalamus in regulating metabolism came from Claude Bernard who observed that lesions to the fourth ventricle led to glucose level alterations in dogs (Bernard, 1855). Gradually, subsequent studies on various regions of the hypothalamus suggested a more refined function of these areas in metabolic control (Brobeck, 1946b; Hess, 1949). Classic studies conducted in the mid-20th century showed that ventromedial hypothalamus (VMH) lesioning increased food intake whereas electrical stimulation of the ventrolateral hypothalamus (vLH) led to reduced feeding, gaining the respective labels of “feeding center” and “satiety center” (Anand and Brobeck, 1951). Evidence also existed in the involvement of the hypothalamus in energy homeostasis based on the rapid weight gain observed in patients with pituitary adenomas, Erdheim formulated the hypothesis that damage to the hypothalamus caused by the adenoma led to the observed obesity (Fröhlich, 1901, Erdheim, 1904). First experimental insights into the neuronal regulation of food intake by different nuclei were obtained from lesion studies in rats about 30 years later. The destruction of the hypothalamic ventromedial (VMH), paraventricular (PVH) and dorsomedial (DMH) nuclei led to the induction of hyperphagia and obesity (Brobeck, 1946a; Hetherington and Ranson, 1942). In contrast, lesions of the lateral hypothalamus (LH) resulted in hypophagia (Anand and Brobeck, 1951). This suggested more specified roles for the nuclei.

Interestingly, a GWAS illustrated that a great deal of genes linked to BMI are expressed in the central nervous system and the hypothalamus (Locke et al., 2015). More recent studies have revealed that the hypothalamus works in conjunction with the corticolimbic system and

the brainstem to control and exert functions for food intake regulation. The brainstem integrates information from vagal and non-vagal visceral afferents and nutrients and can regulate ingestion, digestion and absorption (Schwartz, 2000). The corticolimbic system includes large cortical areas, basal ganglia, hippocampus, and amygdala and provides emotional, executive and cognitive input (Kelley et al., 2005). Both these systems provide dense inputs into the hypothalamus, which functions as the hub within this network and integrates both internal and external inputs on the metabolic state (Berthoud et al., 2017). While the massive research effort launched since then has both refined and expanded this original portrayal, at its core it remains the same and even more research is required out to advance our understanding.

1.2.3 The arcuate melanocortin system

The arcuate nucleus of the hypothalamus (ARC), resides at the mediobasal hypothalamus, proximal to the third ventricle and the median eminence (ME). The ME is one of the seven circumventricular organs in the brain that are described by their dense vascularization of fenestrated capillaries and a “leaky” blood-brain barrier (BBB) (Ciofi et al., 2009; Rodriguez et al., 2010). This unique localization enables neurons of the ARC to sense nutrients and hormonal stimuli from the periphery, incorporating them with neuronal inputs and responding accordingly to control energy homeostasis (Timper and Bruning, 2017).

The melanocortin system within the ARC is comprised of a collection of neurons with functionally antagonistic roles that have thus far been very well studied. They are the orexigenic agouti-related neuropeptide (AgRP)- and neuropeptide Y (NPY)-expressing cells (AgRP neurons) and the anorexigenic proopiomelanocortin (POMC) and cocaine-amphetamine regulated transcript protein (CARTPT)-expressing neurons (POMC neurons) (Cone, 2005; Garfield et al., 2009). In addition to the neurons in the ARC, the melanocortin system also includes their downstream targets in the PVN that express melanocortin-3 (MC3R) and melanocortin-4 receptors (MC4R) plus a small population of POMC neurons in the NTS. AgRP neurons are stimulated by calorie deficit thus driving food intake, energy conservation and promote weight gain (Aponte et al., 2011; Cone, 2005; Krashes et al., 2011; Liu et al., 2012; Yang et al., 2011). On the other hand, POMC neurons respond to satiated states to cease feeding, increase in energy expenditure and weight gain (Atasoy et al., 2012;

Dodd et al., 2015; Zhan et al., 2013). The MC3 and MC4 receptors belong to a family of five melanocortin receptors (MC1-5R) and are the only two expressed in the brain. MC4Rs are mainly expressed in the PVH and are involved in the regulation of energy metabolism (Cone, 2005; Yang et al., 2011). In satiated states, α -MSH released from POMC neurons binds to this receptor and activates the downstream neuron through an increase in intracellular cAMP levels (Lee et al., 2001). In contrast, during states of hunger, AgRP released onto the MC4R functions as an antagonist (Ollmann et al., 1997). NPY, also released from terminals of AgRP neurons, has a similar function to AgRP, i.e., it drives feeding and reduces energy expenditure (Stanley and Leibowitz, 1984). NPY binds to NPYRs, a group of Gi-coupled-protein receptors that inhibit the downstream neurons via decrease in cAMP levels (Gerald et al., 1996). Another mechanism through which AgRP neurons mediate their orexigenic effects is through synaptic release of the neurotransmitter gamma-aminobutyric acid (GABA) onto POMC neurons, thereby inhibiting them (Cowley et al., 2001; Horvath et al., 1997).

The pivotal role of the melanocortin system in the control of energy homeostasis is corroborated by reports demonstrating that deletions or mutations in molecular constituents of this system such as POMC, MC3R, MC4R or Agouti in agouti viable yellow mutant mice (Avy) lead to hyperphagia, obesity, hyperinsulinemia and hyperglycemia, both in rodents and humans (Chen et al., 2000; Huszar et al., 1997; Lu et al., 1994; Smart et al., 2007; Yaswen et al., 1999). Intracerebroventricular (ICV) injection of α -MSH decreases food intake and AgRP or NPY increase it (Clark et al., 1984; Millington et al., 2001) In a study in 2010, it was reported that *Pomc* is expressed in the majority of hypothalamic neurons during embryonic development in transient. Interestingly, they identified that roughly 25% of AgRP neurons derive from a *Pomc*-expressing lineage (Padilla et al., 2010).

1.3 POMC-expressing neurons of the ARC (POMC^{ARC})

The importance of POMC neurons and their connections with regards to various metabolic processes is implicated in both human and rodent studies. Primary experiments on genetic manipulation and ablation of POMC via targeted expression of diphtheria toxin receptor (DTR) demonstrated that POMC^{ARC} neuron ablation led to overeating and decreased energy expenditure (Luquet et al., 2005; Zhan et al., 2013). With regards to their antagonistic counterparts, genetic ablation of AgRP and/or NPY in developmental stages in mice causes

mild changes in body weight and food intake, though ablating them in adult mice causes extreme weight loss and eventually leads to death indicating the necessity of AgRP neuron action in feeding behavior in adult mice (Gropp et al., 2005; Luquet et al., 2005). Development of optogenetic and chemogenetic techniques allowed for targeted and remote manipulation of circuits involved in feeding behavior neurons (Krashes, 2017; Rogan and Roth, 2011). Upon chronic optogenetic stimulation, the POMC^{ARC} neurons reduce food intake and body weight in mice, however, these effects were lost on an *A^y* background, pointing to the fact that the satiating actions of POMC^{ARC} neurons are MC4R-dependent (Aponte et al., 2011; Zhan et al., 2013). Similarly, chemogenetic activation of these neurons via hM3Dq resulted in 50% reduced food intake and 6% body weight loss while acute activation of POMC^{NTS} neurons reduced food intake (Zhan et al., 2013). Other studies also show that acute and prolonged activation of POMC neurons results in decreased food intake without exerting any effects on glucose metabolism and insulin sensitivity (Steculorum et al., 2016). Moreover, hM4Di-mediated chronic inhibition of POMC^{ARC} neurons caused hyperphagia after 24 hours. Intriguingly, stimulation by endocannabinoid via CB1R-expressing POMC neurons that released β -endorphin onto neurons in the PVN has induced feeding via POMC neuron activity (Koch et al., 2015).

1.3.1 The *Pomc* gene, its sites of expression and functional relevance

It has been speculated that *Pomc* was created as a result of an insertion of the melanocortin DNA segments into a prepro-endorphin gene more than 500 million years ago (Navarro et al., 2016). This gene contains 3 exons, two of which undergo translation (De Souza et al., 2005). There are key tissues where the POMC gene expression leads to release of functionally bioactive peptides derived from the POMC precursor that include the pituitary, the arcuate nucleus of the hypothalamus, the nucleus tractus solitarius, and the skin. *Pomc* expression has been detected in various tissues including testis, ovary, spleen, lung, liver, thymus, thyroid, heart, kidney, lymphocytes, duodenum, colon, and adrenal gland though protein expression has not been reported (Harno et al., 2018).

In an early human study, a microsatellite polymorphism mapped to chromosome 2 in a region containing the *Pomc* gene was linked to obesity in Mexican Americans (Comuzzie et al., 1997). Subsequently, it was shown that mutations in exons 3 and 2 either caused aberrances

in ACTH, α - and β -MSH or abolished *Pomc* translation manifesting as early onset obesity, adrenal insufficiency and red hair pigmentation (Krude et al., 1998). In addition, mutations altering the cleavage site between β -MSH and β -endorphin correlated with childhood obesity cases (Challis et al., 2002). Mice with a whole-body *Pomc* knockout displayed early onset obesity, altered pigmentation and adrenal insufficiency, much similar to the symptoms observed in humans (Yaswen et al., 1999). *Pomc* deficiency in mice increases food intake and reduces energy expenditure (Challis et al., 2004). Mutations in enzymes involved in POMC processing, i.e., PC1 are obesity-associated while PC2-null mice exhibit hypoglycemia, glucagon deficiency and no major alteration in weight or growth (Furuta et al., 1997; Jackson et al., 1997; Zhu et al., 2002). The phenotype of PC2-null mice is likely due to the fact that it is involved in cleavage of other precursors. Different MC4R agonists have been developed to treat obesity caused by POMC and it could be shown that treatment with the MC4R agonist Setmelanotide leads to body weight loss in mice, rats, dogs and monkeys as well as in humans (Chen et al., 2015; Collet et al., 2017; Kievit et al., 2013). Thus, correct POMC processing is required for energy homeostasis regulation.

In the hypothalamus, *Pomc* transcription is regulated by various factors that include the energy state of the animal. It was shown that acute food deprivation lowers POMC levels in rodents but overfeeding increases it (Bergendahl et al., 1992; Brady et al., 1990; Hagan et al., 1999). Mice that lack the leptin hormone or its receptor, show lower levels of *Pomc* mRNA in the hypothalamus compared to their controls indicating a role of leptin in *Pomc* transcription regulation (Mizuno et al., 1998). Similarly, other hormones and nutrients like insulin, glucose and glucocorticoids have been shown to affect hypothalamic *Pomc* expression (Kim et al., 1999; Mizuno et al., 1998; Wardlaw et al., 1998).

1.3.2 The posttranslational cleavage products of POMC and the melanocortin receptors

The POMC gene encodes a precursor for various polypeptide bioactive peptides and hormones involved in energy balance modulation. Tissue-specific posttranslational processing of the precursor gives rise to the functionally active peptides such as adrenocorticotropin (ACTH), α -, β - and γ -MSHs, and β -endorphin. This precursor undergoes cleavage at defined dibasic amino acid sequences containing lysine and/or arginine by pro-

hormone convertases (PCs), the types of which and their resulting peptides are dependent on the tissue they are expressed in (Pritchard et al., 2002). Figure 1.2 presents the POMC cleavage products and their interaction with the melanocortin receptors (Modified from (Butler et al., 2017)).

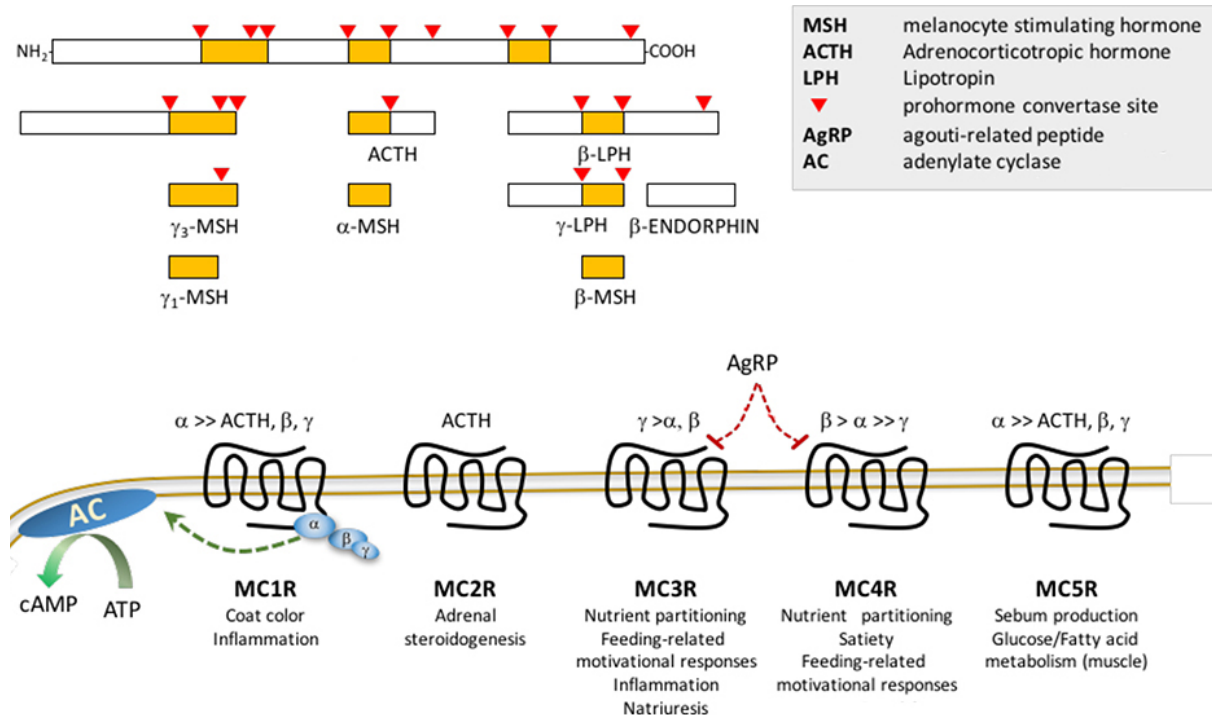


Figure 1.2 Bioactive POMC products and their interactions with the melanocortin receptors.

In corticotrophs of the anterior pituitary, the 285-amino acid polypeptide precursor is cleaved by PC1/3 to yield ACTH as an end product (Cawley et al., 2016). ACTH is a hormone that stimulates release of cortisol from adrenal glands. In addition to ACTH, β -lipotropin (β -LPH), and a 16-kDa N-terminal fragment result from the POMC precursor in the aforementioned cells. In the intermediate lobe of the pituitary, POMC neurons of the ARC and the skin, ACTH is further cleaved by PC2 to produce ACTH (amino acids 1–17) and corticotropin-like intermediate peptide (CLIP). ACTH (1–17) serves as a substrate to enzymes carboxypeptidase E (CPE) and peptidyl α -amidating monooxygenase (PAM) to produce des-acetyl α -MSH (DA- α -MSH) which is acetylated to α -MSH by *N*-acetyltransferase (N-AT). On the other hand, PC2 cleaves β -LPH to β -endorphin (β -EP) and γ -LPH, finally yielding β -MSH (Harno et al., 2018). The biological function of intermediate peptides like β -LPH, γ -LPH is not

yet fully described (Millington, 2007). Interestingly, acetylation of α -MSH is also cell type specific and is an important regulator of POMC function (Millington, 2007). In general, the diverse cell-type specific cleavage and posttranslational modifications of POMC illustrates the importance of this gene in a variety of physiological processes including energy homeostasis, food intake, reproduction, stress regulation, immune response, cardiovascular and melanocyte function (Dunbar and Lu, 2000; Millington and Buckingham, 1992; Millington, 2006; Sawchenko et al., 1996; Van der Ploeg et al., 2002).

The melanocortins, namely, α -, β -, γ -MSH, and ACTH can bind to the melanocortin receptors via the amino acid motif His-Phe-Arg-Trp, required for MCR binding. Five MCRs (MC1-5R) are known. The MCRs are a part of the G-protein coupled heptahelix receptor family, which upon activation lead to an increase in intracellular cyclic adenosine monophosphate (cAMP) (Getting, 2006). Some studies indicate an involvement of additional signaling pathways such as phosphoinositol for the MC3R (Konda et al., 1994) and the JAK/STAT pathway for the MC5R (Buggy, 1998). Moreover, MCRs contain a consensus binding sequence for protein kinase C (Wikberg et al., 2000). Sequence similarities between all five receptors range from 40-60%, pointing towards a partial overlap in binding characteristics. MC1R is expressed in melanocytes as well as other peripheral tissues. In the brain it is limited to a few neurons in the periaqueductal grey matter (Xia et al., 1995). It mainly binds to α -MSH and ACTH with less affinity. The interaction of MC1R with both ligands is known to regulate pigmentation, skin type and hair color (Wikberg et al., 2000). MC2R is found mainly in the adrenal cortex and through its specific binding to ACTH, it regulates mineralocorticoid and glucocorticoid production (Schiöth et al., 1996). As previously alluded to, MC3R and MC4R are abundant in the brain. MC3R is mostly restricted to the hypothalamus and the limbic system, though MC4R is found in various brain regions (Roselli-Rehfuß et al., 1993). MC4R has a higher affinity to β -MSH than α -MSH whereas MC3R readily binds to γ -MSH in comparison to other possible ligands (Getting, 2006). The main function of both receptors is within the regulation of energy homeostasis (Getting, 2006). β -endorphin that also results from POMC prohormone processing, binds to μ -opioid receptors, also expressed on POMC neurons thereby leading to inhibition of their activity (Millington, 2007).

1.3.3 Neural inputs into POMC neurons and their projection sites

In an endeavor to gain an overview of the neuronal network of POMC and AgRP neurons, a study carried out in 2015 specifically looked into the projection sites and neuronal inputs of these neurons (Wang et al., 2015). AgRP and POMC neurons in the ARC send projections to nuclei within the hypothalamus as well as to other brain regions. Their converging intrahypothalamic pattern includes the PVH, LH, VMH, posterior hypothalamus, DMH, and medial preoptic nucleus/area (Bagnol et al., 1999). Outside of the hypothalamus, POMC^{ARC} neurons innervate regions such as the bed nucleus of the stria terminalis (BNST), the lateral septum (LS), the diagonal band of Broca (DB) and the accumbens nucleus (Acb), the periaqueductal grey (PAG), the deep gray layer of the superior colliculus (pG) and the deep mesencephalic nucleus (DpMe) and the dorsal motor nucleus of the vagus (DMX), whereas AgRP neurons connect to the BNST, and the lateral parabrachial nucleus (LPB), central nucleus of the amygdala (CEA), and PAG (Betley et al., 2013; Wang et al., 2015). Despite the overlaps in projection areas between POMC and AgRP neurons, POMC neurons innervate extrahypothalamic regions such as the DMX that are not innervated by AgRP neurons indicating the multifaceted function of POMC neurons in control of metabolism.

Interestingly, POMC^{ARC} neurons received direct input from more than 40000 neurons while AgRP neurons were innervated by approximately 17000 neurons across the brain. Both neuronal groups are innervated by PVH, DMH, VMH, LH, LS and BNST. The hippocampus, medial mammillary nucleus, and VTA seem to connect specifically to POMC^{ARC} neurons. POMC^{NTS} neurons are innervated by other brainstem neurons as well as PVH and the amygdala (Wang et al., 2015).

1.4 Stimuli of POMC neurons

Neurons of the ARC have the ability to sense and integrate hormonal and nutrient stimuli from the periphery in line with their role in regulating metabolic processes. POMC neurons are also not exempt from this and can thus sense stimuli such as insulin, leptin, serotonin, glucose, glucagon-like peptide 1 (Glp1), glucocorticoids, endocannabinoids, nicotine, fatty acids and amino acids (Belgardt et al., 2009; Dodd et al., 2015; Parton et al., 2007; Pinto et al., 2004; Toda et al., 2017).

1.4.1 Leptin and its action on POMC neurons

Leptin is an adipokine, released by white adipose tissue (WAT). The leptin (otherwise known as *Ob*) gene produces a 143-amino-acid peptide and its plasma concentration levels are directly proportional to the mass of adipose tissue (Barrios-Correa et al., 2018). Leptin is considered to be one of the major players in the regulation of feeding and energy metabolism (Barrios-Correa et al., 2018). Mice lacking leptin (*ob/ob*) cannot synthesize the hormone due to the introduction of a mutation in the *Ob* gene and this leads to profound obesity symptoms, restored by leptin treatment. In addition, lack of leptin is accompanied by infertility, short stature, diabetes and a variety of other endocrine, autonomic and behavioral abnormalities (Flak and Myers, 2016). On the other hand, *db/db* mice have high levels of circulating leptin but a truncated form of the LepRb (ObR) and also display an obese phenotype (Chehab, 2014). Studies in humans illustrating the relationship between obesity and mutations in either the leptin gene or its receptor, show that leptin is essential for body weight regulation (Flak and Myers, 2016).

Leptin exerts its intracellular effects by binding to leptin receptors (LEPRs). Six LEPRs have been identified in mammals (LEPRa-LEPRf), types LEPRa-LEPRd are found in humans (Bacart et al., 2010) LEPRs are expressed in tissues such as the kidney, liver, heart, gastrointestinal tract, ovaries, testes, spleen, pancreas and brain (Fei et al., 1997). Of the six isoforms, LEPRb is the only long receptor isoform. It contains a long cytoplasmic domain, which retains full signaling capability. This domain is known to activate the Janus kinase 2/signal transducer and activator of transcription-3 signaling pathway (JAK2/STAT3) (Barrios-Correa et al., 2018). Nonetheless, other pathways have been described to be involved in LEPR signaling. These include ERK, STAT5, PI3K, AMPK and mTOR pathways (reviewed in detail in (Barrios-Correa et al., 2018)).

Experimental evidence for the importance of the long isoforms of LepRs stems from the finding that the classical leptin receptor mutant (*db/db*) mouse, which lacks only the long form of the leptin receptor, presents a phenotype not different than *ob/ob* mice (Chen et al., 1996). Along those lines, restoration of LepRb alone in mice lacking all leptin receptor isoforms suffices to normalize physiology (de Luca et al. 2005).

Within the CNS, the expression of LepRb is much higher than in other organs, specifically in the hypothalamic nuclei ARC, VMH and DMH (Barrios-Correa, Estrada, and

Contreras 2018). Strikingly, ablation of the *LepRb* specifically in the hypothalamus of mice leads to a phenotype similar to *db/db* mice including increased weight gain and adiposity, hyperphagia, cold intolerance and insulin resistance (Ring and Zeltser, 2010), highlighting the importance of *Lepr* expression by ARC neurons in the signaling of leptin to maintain whole body energy homeostasis.

POMC neurons in the ARC express the *Lepr* gene (Hakansson and Meister, 1998). Cowley et al. demonstrated with electrophysiological studies that POMC neurons are activated by leptin (Cowley et al., 2001). Moreover, mice with a specific deletion of *Lepr* in POMC neurons show a mild obese phenotype, are hyperleptinemic and have altered expression of hypothalamic neuropeptides (Balthasar et al., 2004). Another study using an inducible POMC-Cre line could dissociate the effect of leptin on food intake and glucose homeostasis in POMC neurons: knockout of *Lepr* in POMC neurons of adult mice led to hyperglycemia, hyperleptinemia and worsened liver insulin sensitivity, but unaltered energy balance (Caron et al., 2018).

In another model, *Lepr* was re-expressed in POMC neurons of *db/db* mice, which partially normalized energy expenditure and modestly reduced body weight as well as normalized blood glucose and ameliorated hepatic insulin resistance, hyperglucagonemia and dyslipidemia (Berglund et al., 2013). Moreover, it was shown that POMC neurons of diet-induced obese (DIO) mice were resistant to LEPR-STAT3 signaling (Gamber et al., 2012). Overexpression of *Lepr* in POMC cells was reported to cause increased sensitivity to diet-induced obesity most likely due to the induction of leptin resistance in POMC cells (Gamber et al., 2012).

In conclusion, leptin is one of the best studied stimuli of POMC neurons and leptin sensing by POMC neurons is important to maintain glucose homeostasis and likely also body weight homeostasis.

1.4.2 Glp1 and its action on POMC neurons

Glp1, a posttranslational product of proglucagon, is specific to L-cells in the small and large intestines in addition to neurons of the NTS. The pre-proglucagon precursor also gives rise to Glp2, glicentin and oxyntomodulin and glucagon via tissue-dependent cleavage by PC1/PC3 (Bell et al., 1983; Kieffer and Francis Habener, 1999). The *Gcg* gene is mainly

expressed in the endocrine pancreas, gut and brain. In pancreatic α -cells, PC2 cleaves proglucagon mainly into glucagon (Rouille et al., 1995), whereas cleavage in the intestine and brain by PC1 and PC3 results in Glp1, Glp2, glicentin and oxyntomodulin (Zhu et al., 2002). Thus, PC1 and PC3 double knock-out mice are Glp1 and Glp2 deficient (Zhu et al., 2002). Glp1 is released in response to meals and plays an important role in the regulation of glucose homeostasis. The incretin effect of Glp1 means that it is a compound that promotes insulin secretion dependent on glucose intake. It is released within minutes after ingestion (Muscogiuri et al., 2017). Glp1 is subjected to rapid degradation via the enzyme dipeptidyl-peptidase-4 (DPP-IV). Approximately 25% of its active form is secreted into the portal vein to be further degradation in the liver so that ~10–15% of endogenously secreted intact Glp1 would end up in systemic circulation (Hansen et al., 1999).

Glp1 acts via the Glp1r that is a G-coupled receptor composed of 463 amino acids in humans (Graaf et al., 2016). It is expressed in various tissues such as the pancreas, lung, brain, pituitary, stomach, heart, kidney, and hepatoportal region though its expression on insulin-target tissues such as the liver, skeletal muscle, and adipose tissue is debatable (Graaf et al., 2016). Homozygous knockout of Glp1r in mice leads to glucose intolerance and an impairment of glucose-stimulated insulin release, and this phenotype is rescued by re-expression of Glp1r in the pancreas (Chen et al., 2011). The effect of Glp1 in the pancreas is possibly the best studied (Lee and Lee, 2017). The beta-cells of the pancreas express the Glp1r that is coupled to adenylate cyclase and produces cAMP when activated. This leads to an increase in intracellular Ca^{2+} via PKA, finally translating to an increase in insulin release. Glp1 also acts on pancreatic alpha-cells and reduces glucagon release (Cho et al., 2014). Intravenous (IV) Glp1 infusion dose-dependently slows down gastric emptying in humans and suppresses postprandial increases in triglycerides and free fatty acids. Within the cardiovascular system, it exerts positive effects on repair after ischemia and also reduces blood pressure. Actions on other tissues include colonic transit time, satiety action, hepatic glucose production, cardiac function, energy expenditure, thermogenesis, food intake and body weight regulation (Lee and Lee, 2017).

The quick degradation of this hormone has raised the question whether peripheral Glp1 would be able to reach the CNS and affect the Glp1r-expressing neurons there (Hansen et al., 1999). Therefore, it is likely that peripheral effects of Glp1 are mediated through Glp1rs in

enteric or vagal sensory neurons, supported by the observation that Glp1rs are present in the nodose ganglion and the vagal nerve terminals innervating the portal vein in rats (Holst, 2007; Richards et al., 2014). The following idea formulated that Glp1r in the hepatoportal region activate neurons of the nodose ganglion resulting in the activation of brain circuits involved in metabolic regulation. In line with this, it was demonstrated that peripheral Glp1 injections stimulate vagal afferent fibers and denervation of the vagus nerve below the diaphragm prevents the anorexic effect induced by peripherally administered Glp1 in rats (Abbott et al., 2005; Nishizawa et al., 1996). In addition, intraportal infusion of the Glp1r agonist exendin 4 resulted in glucose intolerance (Vahl et al., 2007). On the other hand, studies with radioactively labeled Glp1 suggest that it can penetrate the BBB and can possibly also act on neurons of the hypothalamus (Kastin et al., 2002; Orskov et al., 1996). Moreover, neurons of the NTS produce Glp1 and project to DMH, PVH and ARC thus strengthening the need for further research on Glp1 effects in the CNS (Baggio and Drucker, 2014).

Glp1 decreases food intake, however, the exact mechanisms are not fully understood. The Glp1r is expressed in the hypothalamic nuclei, thalamus, hippocampus, lateral septum, and subfornical organ in the brain and ICV-administrated Glp1 decreases food intake (Burmeister et al., 2017). Many hypothalamic nuclei express the Glp1r corroborated by experiments showing neuronal activation after central administration of Glp1 (Barrera et al., 2011). Interestingly, it was revealed that fluorescently labeled liraglutide injected into the periphery could be detected in the PVH and the ARC 6 hours after the injection though the weight loss observed in these animals could be traced back to the arcuate neurons and not those of the PVH (Secher et al., 2014). First experiments showed that ICV administration of Glp1 caused a reduction in food intake and body weight in rats, whereas administration of exendin 9-39, a Glp1 receptor (Glp1r) agonist, led to an increased food intake in rats (Meeran et al., 1999). In line with these findings, the knockdown of the Glp1 encoding gene proglucagon in the NTS promoted hyperphagia and weight gain in rats (Barrera et al., 2011). By deletion of Glp1r in the visceral nerves or the brain and testing the effects of liraglutide, Sisley et al. show that neuronal Glp1rs mediate body weight and anorectic effects of Glp1, but are not required for glucose-lowering effects (Sisley et al., 2014).

A study further pointed out the complexity of Glp1 action on the CNS when they examined the effect of Glp1 on the PVH and ARC by site-specific injections and found that PVH

injections reduced in food intake but did not affect glucose homeostasis. On the other hand, Glp1 injections into the ARC had no effect on food intake, but reduced hepatic glucose production during hyperinsulinemic-euglycemic clamp experiments in rats (Sandoval et al., 2008). Another group looked into Glp1-mediated central regulation of energy expenditure and found that Glp1r in the VMH to be important in this context (Beiroa et al., 2014). Despite this, the centrally targeted role of Glp1 on other aforementioned physiological processes (e.g., gastric motility or colon transit time) is less well studied and requires further research (Muscogiuri et al., 2017). In general, the effect of central Glp1 on food intake and appetite regulation is established, although more research is needed to delineate which brain areas are involved in these processes.

Various studies have been carried out to elucidate the role of Glp1 and Glp1r on POMC neurons. It has been shown that 70% of all POMC neurons in the ARC express the Glp1r and that exendin-4 (EX-4) treatment leads to POMC neuron activation (Dalvi et al., 2012; Sandoval et al., 2008). In a human study, the Glp1r expression was decreased in T2DM patients in the infundibular nucleus (IFN, the equivalent of ARC in humans) and PVN. Moreover, sporadic co-expression of Glp1r with NPY/AgRP and POMC was observed in the IFN indicating a potential mediatory effect of Glp1 through these neurons in humans (Ten Kulve et al., 2016). Electrophysiological studies confirmed a direct activation of POMC neurons by Glp1 (Secher et al., 2014). Moreover, injection of exendin-4 into the ARC reduced hepatic glucose production (Sandoval et al., 2008). Further research is needed to fully understand the role of POMC neurons in the context of central Glp1-mediated alterations in energy metabolism.

1.5 Heterogeneity of POMC neurons

Defined by the expression of POMC, these neurons have been considered to be a homogeneous population. Gradually evidence emerged based on their functional and molecular properties hinting that these neurons segregated into different subpopulations. To begin with, the fact that POMC neurons react to different stimuli is noteworthy. The percentage of POMC neurons expressing *Lepr* is around 80% and Glp1r is approximately 68% (Lima et al., 2016; Sandoval et al., 2008). The fact that manipulation of these different subsets of POMC neurons has partly distinct effects is supporting the hypothesis that different subsets of POMC neurons might differ in their regulation of physiological processes. One of the initial

hypotheses of the heterogeneity of POMC neurons formulated on the basis of the diversity of the projection areas described for them. POMC/CART neurons in rats located in the mainly innervate autonomic areas such as the dorsal vagal complex and the intermediolateral cell column (IML) (Swanson and Kuypers, 1980), (Elias et al., 1998; Zheng et al., 2005) while more caudal POMC neurons projected to the PVN and LH (Baker and Herkenham, 1995; Elias et al., 1999). Electrophysiological experiments from the Elmquist laboratory initially opened the field of POMC neuron heterogeneity research. In a series of studies, it was demonstrated that POMC neurons responding to different key stimuli are distinct from each other. Recording electrophysiological behavior of POMC neurons in response to the serotonin receptor agonist meta-chlorophenylpiperazine (mCPP) and leptin showed that cells responding to one of the stimuli did not respond to the other, and vice versa (Sohn et al., 2011). In addition, they described that leptin-activated POMC neurons are located more laterally in the ARC than the serotonin-responsive cells (Sohn et al., 2011). Similarly, they described two distinct POMC populations in response to leptin and insulin, which were also anatomically segregated (Williams et al., 2010). Interestingly, Sandoval et al. already reported that two POMC subpopulation, *Glp1r*-positive and *Glp1r*-negative cells, cluster in different areas of the ARC. One population, found mostly in the medio-lateral part of the ARC, co-expressed *Glp1r*, while the other population was reported to be localized close to the lateral edge of the ARC and largely did not co-express *Glp1r* mRNA (Sandoval et al., 2008). Differential clustering and specific anatomical localization of subpopulations of neurons would be in line with the hypothesis that different subpopulations regulate different physiological processes.

Heterogeneity on the basis of neurotransmitter release also exists for POMC neurons. It was shown that POMC neurons express either glutamate or GABA, or both (Jarvie and Hentges, 2012). Interesting in this context is that the expression of these markers is dynamic. While vesicular glutamate transporter 2 (*Vglut2*) expression is highest at P1 and then decreases, glutamate decarboxylase 67 (*Gad67*) expression is lowest at P1 and increases over time (Dennison et al., 2016).

The recent single cell datasets highlighted the molecular heterogeneity of POMC neurons. (Campbell et al., 2017; Lam et al., 2017). The sequencing and subsequent unbiased hierarchical clustering of cells of the ARC and the ME resulted in 50 clusters, three of which expressed *Pomc* (Campbell et al., 2017). The other dataset focused on sequencing FACS-sorted

EGFP-tagged POMC neurons through which four different clusters were identified (Lam et al., 2017). Thus, functional analysis and single cell sequencing have revealed heterogeneity in POMC neurons while the functional relevance remains elusive.

1.6 Genetic-based tools for studying heterogeneity

At the moment, the best available method for monitoring and manipulating specific cell types with the aim of gaining a better understanding of their function is through genetic targeting (Huang and Zeng, 2013). The Cre-loxP system in mice has been widely utilized to target cell types of interest by driving Cre recombinase expression under the control of known promoters (Gong et al., 2007). When it comes to heterogeneous cell populations an additional level of specificity is required. Several intersectional gene-targeting approaches have been developed by combining Cre with other recombinases (Belteki et al., 2003; Buchholz et al., 1998). The Dre-rox system, derived from bacteriophage D6 is homologous to the Cre-loxP system and can work in conjunction with it. (Anastassiadis et al., 2009).

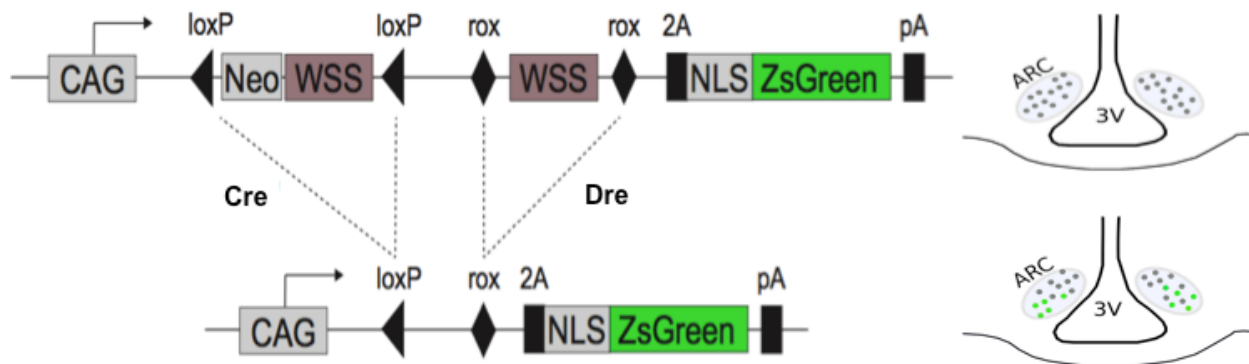


Figure 1.3 The expression system used for intersectional Cre/Dre dependent targeting of heterogenic populations.

The transgene expression is prevented by two STOP cassettes: a Dre-specific rox-flanked and a Cre-dependent loxP-flanked cassette. CAG: CMV-chicken beta actin promoter; loxP site: Cre-recognition site; rox site: Dre-recognition site; NEO: neomycin resistance gene; 2A: self-cleaving T2A peptide sequence. WPRE sequence: woodchuck hepatitis virus post-transcriptional regulatory element, WSS: Westphal Stop Sequence and PA: poly A tail.

Within this scope, transgenic mouse lines were generated to express a gene of interest in a Dre- and Cre-dependent manner. In these models, the transgene is usually preceded by two transcriptional STOP cassette; i.e., loxP-flanked (LSL) and an additional rox-flanked (rSr). An example of such a double recombinase system and also the one developed for and utilized in the present study is displayed in Figure 3.2. In this exemplary image, the fluorescent marker protein ZsGreen coupled to a nuclear localization signal (NLS) (Lohr et al., 2018). This expression system is targeted to the ubiquitously expressed ROSA26 locus (R26) in mice (Zambrowicz et al., 1997). The addition of a cytomegalovirus enhancer and chicken beta-actin (CAG)-promoter allow for enhanced expression of the gene of interest. To extend the purpose of cellular and molecular interrogation or manipulation an array of tools can be incorporated as the transgene.

1.6.1 Tools used in this study for investigating the heterogeneity of POMC neurons

In order to visualize the neurons and their corresponding axonal fibers, we made use of the ZsGreen and tdTomato fluorophores, respectively. The coding sequence from both is integrated into the previously described intersectional expression system (Fig. 1.3). Within this system, the ZsGreen fluorophore is coupled to an NLS, enabling us to fully visualize the soma while the expression of the tdTomato in the projections serves as a great tool for fiber density analysis (Lohr et al., 2018; Madisen et al., 2015).

Designer receptors exclusively activated by designer drugs, famously referred to as DREADDs, are G-protein coupled receptors, genetically modified so they only get activated by compounds that are in other instances inert (Rogan and Roth, 2011). An example is hM3Dq, a modified form of the human M3 muscarinic (hM3) receptor, which binds specifically to the physiologically inert clozapine metabolite clozapine-n-oxide (CNO) (Armbruster et al., 2007). Binding of the ligand hM3Dq leads to direct depolarization of expressing cells and has been demonstrated to be an indispensable tool for targeted neuronal application with low invasiveness (Urban and Roth, 2015).

The ribosomal protein L10a (Rpl10a) is a subunit of the ribosome and through fusion with enhanced GFP (EGFP), it has been transformed into a tool for isolating polysomes and polysome-bound mRNA (Heiman et al., 2008). Cell type specific expression of EGFP-L10a and subsequent immunoprecipitation and sequencing of bound RNA has been successfully

performed in various studies and is commonly known as the translating ribosome affinity purification (TRAP) technique (Heiman et al. 2008; Doyle et al. 2008).

1.7 Objectives

The global increase in obesity and its associated co-morbidities has called for attention in developing strategies for prevention and control of this disorder. Gaining understanding of the underlying aberrant mechanisms in obesity is crucial in the endeavor to design and produce suitable therapeutics for metabolic disorders. Unraveling the intricacies of the central system that regulates energy expenditure and homeostasis has become pivotal in designing appropriate therapeutics in battling obesity and its associated comorbidities. This endeavor includes gaining understanding about the molecular mechanisms and interwoven neural circuitry through which the system exerts its functions. POMC neurons, an important part of the central melanocortin system, have been shown to respond distinctly to various hormones, indicating their heterogeneous nature. Understanding this and the possible divergent melanocortin pathways through which they control homeostasis will be crucial for development of therapeutics against obesity.

Leptin and Glp1 are important regulators of POMC neuronal activity; however, their mechanisms of action in control of energy homeostasis through POMC neurons are not yet fully understood. The objective of this study is to investigate the heterogeneity of POMC neurons expressing *Lepr* and *Glp1r*- and to gain further understanding in the characteristics of these neurons. To this end, we utilized double recombinase-based expression systems to target these neuronal subtypes. The aim was to decipher the anatomical localization and intra- as well as extra-hypothalamic projection patterns of *Lepr* and *Glp1r*-expressing POMC neurons through specific fluorophore expression. Subpopulation-specific activation of these neurons using the DREADD system would allow us to gain better understanding of their physiological function in the regulation of metabolism. Finally, the molecular characteristics and electrophysiological properties of these neurons will also be examined.

2 Materials and Methods

2.1 Animal and experimental ethics

Animal housing and experiments were carried out in accordance with protocols approved by local governmental authorities responsible for animal ethics in the city of Cologne (Bezirksregierung Köln). Breeding and experimental ethics approval were issued by the Department for Environment and Consumer Protection - Veterinary Section, Cologne, North Rhine-Westphalia, Germany ((§11) 576.1.35.2.G 07/18, 84-02.04.2017.A058).

2.2 Animal housing and care

Animals used in the present study were housed in individually ventilated cages (IVCs) with a 12-hour light/dark cycle and the ambient temperature was regulated at 22°C–24°C. The mice had ad libitum access to food and water. The mice received normal chow diet (NCD; Teklad Global Rodent 2018, Harlan) containing 53.5% carbohydrate, 18.5% protein and 5.5% fat (12% of calories from fat) or high-fat diet (HFD; C1057, Altromin) consisted of 32.7% carbohydrate, 20% protein and 35.5% fat (55.2% of calories from fat).

2.3 Commercially available or previously published driver lines used in this study

The LeprCre mouse line was kindly provided to us by G Meyers (Leshan et al., 2006). In LeprCre mice the expression of the Cre recombinase is coupled to the Lepr expression via an internal ribosome entry site (IRES). The Glp1rCre mouse line was provided by Stefan Trapp and developed with BAC transgenesis (Richards et al., 2014). In this line, the Cre recombinase is expressed under the control of the promoter and regulating sequences of the Glp1r gene. The knock-in line ROSA26ISrSrZsGreen (ROSA26-CAGS-lox-STOP-lox-rox-STOP-rox-ZsGreen) was generated in-house (Lohr et al., 2018). Line ROSA26rSrlSlttdTomato (ROSA26-CAGS-rox-STOP-rox-lox-STOP-lox-ZsGreen) was purchased through the Jackson Laboratory (Madisen et al., 2015).

2.4 In-house developed transgenic mouse lines

The knock-in lines ROSA26ISlrSrhM3Dq (ROSA26-CAGS-lox-STOP-lox-rox-STOP-rox-hM3Dq-2A-ZsGreen-WPRE) and ROSA26ISlrSrEGFPL10a (ROSA26-CAGS-lox-STOP-lox-rox-STOP-rox-EGFP L10a-WPRE) were generated in-house (Please refer to thesis of Dr. Jonas Schumacher for further details).

2.5 Generation of experimental animals

POMC^{Dre} ROSA26rSrZsGreen: the breeding scheme was mating heterozygous POMC^{Dre} mice to homozygous ROSA26^{rx/rx} mice of the ZsGreen construct.

Mouse lines POMC^{Dre} Lepr^{Cre} ROSA26ISlrSrZsGreen, POMC^{Dre} Glp1r^{Cre} ROSA26ISlrSrZsGreen, POMC^{Dre} Lepr^{Cre} ROSA26rSrlSltDTomato, POMC^{Dre} Glp1r^{Cre} ROSA26rSrlSltDTomato, POMC^{Dre} Lepr^{Cre} ROSA26ISlrSrhM3Dq, POMC^{Dre} Glp1r^{Cre} ROSA26ISlrSrhM3Dq, POMC^{Dre} Lepr^{Cre} ROSA26ISlrSrEGFPL10a, POMC^{Dre} Glp1r^{Cre} ROSA26ISlrSrEGFPL10a were generated via mating heterozygous double transgenic mice to homozygous ROSA26^{fl;rx/fl;rx} mice of the corresponding functional transgene construct. Resulting triple transgenic Cre^{+/-} Dre^{+/-} ROSA26^{fl;rx/wt} mice were used as experimental animals and compared to genotype controls as stated in the figure legends. Littermates of both sexes were used for experiments as indicated in text and figures. The C57BL/6N mouse line was purchased from Charles River, France.

2.6 Glucose tolerance tests (GTT)

Glucose tolerance tests were performed at 13 weeks of age with 16-hour fasted mice. Body weights of mice and their basal blood glucose were determined before the start of the experiment. Mice were injected with 20% glucose and blood glucose was measured using a glucometer and glucose strips (Contour Next, Bayer HealthCare, Germany) prior to and 15, 30, 60 and 120 min post injection.

2.7 NMR for body weight composition

Lean and fat mass were determined via nuclear magnetic resonance (NMR Analyzer minispec mq 7.5; Bruker Optik, Ettlingen, Germany) in live mice. Alternatively, body

composition was analyzed by computed tomography (CT) in isoflurane-anesthetized mice (Dräger and Piramal Healthcare). For data acquisition on an IVIS Spectrum CT scanner (Caliper LifeScience, USA) we used IVIS Living Image Software V4.3.1. Quantification of lean and fat mass contents were determined with a modification of the previously described Vinci software package 4.61.0. developed at our institution (available at: <https://vinci.sf.mpg.de/>).

2.8 Indirect calorimetry

Metabolic phenotyping and food intake were measured by an automated PhenoMaster open-circuit indirect, calorimetry system (TSE Systems). Mice were allowed to acclimatize to the experimental setup for 4 days before the start of each experiment. Food and water was available *ad libitum*.

2.9 Study design of DREADD animals

POMC^{Dre} Lepr^{Cre} ROSA26|SlrSrhM3Dq and POMC^{Dre} Glp1r^{Cre} ROSA26|SlrSrhM3Dq mice and corresponding genotype controls were characterized at 13-15 weeks of age with *ad libitum* access to NCD. Saline (0.9%) or CNO injections (3 mg/kg body weight) were administered intraperitoneally. For measurements of food intake (as described under “Indirect calorimetry”), mice were injected with saline at 18:00 and 23:00, followed by one-day recovery and subsequent CNO injections at 18:00 and 23:00 on the next day. For measurements of energy expenditure, RER and locomotion (as described under “Indirect calorimetry”), mice were injected with saline at 17:00, 22:00 and 07:00 followed by CNO at 17:00, 22:00 and 07:00 on the next day. Prior to perfusions at 22-26 weeks of age, mice were fasted for 2 h and injected with saline or CNO 1 h before perfusion. Serum for the corticosterone ELISA was obtained from mice fasted for 2 hours and injected with CNO one hour before blood collection. Littermates of both sexes were used for experiments as indicated in text and figures.

2.9.1 CNO administration

CNO (abcam, #ab141704) powder was dissolved in DMSO (100mg/mL) and diluted 1:333 in 0,9% NaCl (saline).

2.9.2 Corticosterone ELISA

Concentrations were determined using a commercial Corticosterone ELISA kit from CrystalChem as described in the user's manual (Cat. ID: 80556).

2.10 Perfusion and tissue fixation

With the exception of DREADD animals, all mice were perfused in a random-fed state. Mice were deeply anesthetized and perfused transcardially with 1X PBS followed by ice-cold 4% paraformaldehyde (PFA; in 1X PBS; pH 7.4). The brain was removed from the skull and post-fixed in 4% PFA at 4°C for approximately 24 h, and then moved to 20% sucrose solution (in 1X PBS) at 4°C. The brains were cut at 20µm on a sliding microtome (Leica Microsystems, model SM2010R) equipped with a stage for dry ice. For immunohistochemistry, sections were collected in bins containing anti-freeze solution (30% ethylene glycol and 20% glycerol in PBS), and subsequently stored at -20 °C until further processing. For RNA *in situ* hybridization, sections were mounted on SuperFrost Plus Gold slides (Cat No. FT4981Glp1LUS; ThermoFisher) and subsequently stored at -80 °C until further processing.

2.11 Immunohistochemistry

For immunofluorescent stainings against ZsGreen all incubation steps were performed at room temperature unless otherwise stated. Floating sections were washed once for 10 min in PBS, incubated for 10 min in 0.3% glycine, washed again for 5 min in PBS and incubated for 10 min in 0.03% SDS/PBS. Subsequently, sections were blocked for 1 h in 3% donkey serum in PBS containing 0.25% TritonX. Thereafter sections were incubated overnight at 4°C in primary antibody diluted in Signal Stain (Cell Signaling). Primary antibodies rabbit anti-ZsGreen (Takara Bio Clontech no. 632474, 1:100) was used. The following morning, sections were washed three times for 10 min in PBS containing 0.1% TritonX and incubated for 1 h in secondary antibody in PBS containing 0.25% TritonX. Secondary antibody, donkey anti-rabbit-Alexa488 (ThermoFisher no. A21206, 1:500) were used for 1 hr at room temperature. Sections were washed three times for 10 min in PBS containing 0.1% TritonX, fixed for 5 min in PFA, washed twice for 5 min in PBS and blocked for 30 min in 3% donkey serum in PBS containing 0.25% Triton-X. After three washing steps for 10 min in PBS containing 0.1%

TritonX, sections were mounted in Vectashield DAPI-containing mounting medium (Vector Laboratories, #VEC-H-1200) and stored at 4°C in the dark until imaging.

2.12 Imaging and quantification of immunohistochemistry

Images were captured using a confocal Leica TCS SP-8-X microscope, equipped with a 40x/1.30 oil objective. Z-stacks were taken with optical sections of 0.9 µm. Laser intensities were kept constant throughout all related conditions. Images were imported into FIJI (NIH) where maximum intensities were projected. For representative images adjustments in brightness and contrast for each channel were kept constant throughout all related conditions.

2.13 RNA *in situ* hybridization

The fluorescent *in situ* hybridization technique (RNAscope®) was used to detect mRNA of *Pomc*, *Agrp*, *Lepr-tv1*, *Glp1r*, *ZsGreen*, *Fos*, *Cartpt*, *Vglut2*, *Vgat*, *Npy1r*, *Oprm1* and *Nmur2*. All reagents were purchased from Advanced Cell Diagnostics (ACD, Hayward, CA) if not otherwise stated. The *Pomc* probe (Cat No. 314081) contained 10 oligo pairs targeting region 19–995 (Acc. No. NM_008895.3) of the *Pomc* transcript, the *Agrp* probe (Cat No. 400711-C2) contained 16 oligo pairs targeting region 11–764 (Acc. No. NM_001271806.1) of the *Agrp* transcript, the *Lepr-tv1* probe (Cat No. 471171) contained 19 oligo pairs targeting region 3220-4109 (Acc. No. NM_146146.2) of the *Lepr* transcript variant 1, the *Glp1r* probe (Cat No. 418851) contained 20 oligo pairs targeting region 108-1203 (Acc. No. NM_021332.2) of the *Glp1r* transcript, the *ZsGreen* probe (Cat No. 461251) contained 15 oligo pairs targeting region 980-1655 (Acc. No. JQ071441.1) of the *ZsGreen* transcript, the *Fos* probe (Cat No. 316921) contained 20 oligo pairs targeting region 407–1427 (Acc. No. NM_010234.2) of the *Fos* transcript, the *Cartpt* probe (Cat No. 432001) contained 17 oligo pairs targeting region 11–860 (Acc. No. NM_013732.7) of the *Cartpt* transcript, the *Vglut2* probe (Cat No. 319171) contained 20 oligo pairs targeting region 1986 - 2998 (Acc. No. NM_080853.3) of the *Vglut2* transcript, the *Vgat* probe (Cat No. 319191) contained 20 oligo pairs targeting region 894 - 2037 (Acc. No. NM_009508.2) of the *Vgat* transcript, the *NPY1R* probe (Cat No. 427021) contained 20 oligo pairs targeting region 227-1169 (Acc. No. NM_010934.4) of the *Npy1r* transcript, the *Oprm1* probe (Cat No. 315841) contained 20 oligo pairs targeting region 1135-

2162 (Acc. No. NM_001039652.1) of the *Oprm1* transcript and the *Nmur2* probe (Cat No. 314111) contained 20 oligo pairs targeting region 69-1085 (Acc. No. NM_153079.4) of the *Nmur2* transcript. 4-plex negative (Cat No. 321831) and positive control probes (Cat No. 321811), were processed in parallel with the target probes. All incubation steps were performed at 40°C using the ACD HybEz hybridization system (Cat No. 321462) if not stated otherwise. One day prior to the assay, sections were mounted on SuperFrost Plus Gold slides (Cat No. FT4981Glp1LUS; ThermoFisher), dried at RT, briefly rinsed in autoclaved Millipore water, air-dried and incubated at 60°C for 4-6 hours. Subsequently, slides were submerged in Target Retrieval (Cat No. 322000) at a temperature of 99.5°C for 10 min, rinsed once in autoclaved Millipore water and dehydrated in 100% ethanol for 3 minutes. Slides were allowed to air dry for 5 min, a hydrophobic barrier was created around the sections using an ImmEdge hydrophobic barrier pen (Cat No. 310018) and slides were stored at room temperature until assaying. The following day, slides were incubated with Protease Plus (Cat No. 322330) for 25 min. The subsequent steps, i.e., hybridization of the probes, amplification and detection steps, were performed according to the manufacturer's protocol for RNAscope® Fluorescent Multiplex Detection Reagent kit v2 (Cat No. 323110) and, if more than 3 probes were to be detected, RNAscope® 4-Plex Ancillary Kit for Multiplex Fluorescent Kit v2 (Cat No. 323120). The probes were detected using tyramide diluted Opal690 (1:2000), Opal650 (1:1500), Opal620 (1:1000), Opal570 (1:1000), Opal520 (1:750) or Cy3 (1:750). Sections were counterstained with DAPI and coverslipped with ProLong Gold Antifade Mountant (Cat No. P36931; ThermoFisher) and stored in the dark at 4°C until imaged.

2.14 Imaging and quantification of RNA *in situ* hybridization

Images were captured using a confocal Leica TCS SP-8-X microscope, equipped with a 40x/1.30 oil objective. Z-stacks were taken with optical sections of 0.9 µm. Laser intensities were kept constant throughout all related conditions. Images were imported into FIJI (NIH) where maximum intensities were projected. For representative images adjustments in brightness and contrast for each channel were kept constant throughout all related conditions, whereas for quantifications all channels were kept unmodified and approximately 5-10 sections were quantified per mouse and, if so stated, area. For intensity quantification of endogenous *Lepr*, *Glp1r* and *Pomc* expression in C57BL/6N mice, all channels were imported

and fused into the Halo software (Indica Labs). The software relies on the DAPI stain for cellular identification and calculates the cell intensity for each cell and probe (a number integrating both the fluorescent intensity and the covered probe area within the designated cell). The threshold for probe recognition was determined by visual judgement, considering approximately 5 or more signals per cell as positive. For generation of the distribution pattern of POMC neuron subpopulations throughout a coronal cross-section, comparable anatomic locations within the ARC were analysed correspondingly by the Halo software and 3 mice per replicate have been merged. For quantification of *Cartpt*, *Npy1r*, *Oprm1* and *Nmur2* in C57BL/6N mice, integrated density was assessed via FIJI (NIH) in previously defined single cell ROIs showing *Pomc* signal and 5 or more signals of the *Lepr* or *Glp1r* probe. Cell counting of ROSA26rSrZsGreen and ROSA26lSlrSrM3DGq mice was performed manually, defining single cell ROIs showing *Pomc* and *ZsGreen* signal, and considering 5 or more probe signals per ROI of *Agrp*, *Lepr*, *Glp1r*, *Fos*, *Vglut2* or *Vgat* as positive.

2.15 Tissue clearing, image acquisition and analysis

2.15.1 uDISCO whole-brain clearing and image acquisition

The protocol was adapted from the uDISCO clearing method (Pan et al., 2016). POMC^{Dre} ROSA26rSrZsGreen^{+/-}, POMC^{Dre} *Lepr*^{Cre} ROSA26lSlrSrZsGreen^{+/-} and POMC^{Dre} *Glp1r*^{Cre} ROSA26lSlrSrZsGreen^{+/-} male and female mice were perfused with 1X PBS (pH 7.4) for 10 minutes followed by 4% PFA/PBS for 10 minutes. The brains were post-fixed for 24 hours in 4% PFA/PBS (pH 7.4) at 4°C. The brains were dehydrated in a gradient manner via incubations in tert-Butanol diluted in distilled water: 30, 50, 70, 80, 90, 96 (vol%) for 10-16 hours at 37°C. The brains were subsequently incubated in dichloromethane (DCM) for 60-90 minutes at RT to remove lipids. Next, BABB-D4 was used as the reagent-matching solution for 6 hours at RT to complete the clearing process. (BABB: benzyl alcohol + benzyl benzoate 1:2 ratio respectively, BABB-D4: a mixture of BABB and diphenyl ether (DPE) at a ratio 4:1 (vol/vol)). The cleared brains were imaged with a LaVision Bio Tec Ultramicroscope II. Whole brain and magnified scans of the ARC were obtained using 1.6X and 8X total magnification, respectively. For the projection density analysis, cleared brains from POMC^{Dre} *Lepr*^{Cre}

ROSA26^{IslrSrt}tdTomato^{+/-} and POMC^{Dre} Glp1r^{Cre} ROSA26^{IslrSrt}tdTomato^{+/-} were imaged using 1.6X magnification with the same laser intensity across all samples.

2.15.2 Whole brain immunostaining

Pre-treatment prior to staining was as follows: the fixed brains were washed two times in PBS for 1 hr, incubated in 50% methanol (in PBS) for 1 hr, 80% methanol for 1 hr and two times in 100% methanol for 1 hr. The samples were bleached with 5% H₂O₂ in 20% DMSO/methanol (1 vol 30% H₂O₂/1 vol DMSO/4 vol methanol) at 4°C overnight. Subsequently, samples were transferred to methanol for 1 hr twice, then in 20% DMSO/methanol for 1 hr twice, then in 80% methanol for 1 hr, 50% methanol for 1 hr, PBS for 1 hr twice, and finally in PBS/0.2% Triton X-100 for 1 hr twice before further staining procedures. Pre-treated samples were incubated in PBS/0.2% Triton X-100/20% DMSO/0.3 M glycine at 37°C overnight, then blocked in PBS/0.2% Triton X-100/10% DMSO/6% Donkey Serum at 37°C overnight. This was followed by a wash in PBS/0.2% Tween-20 with 10 µg/ml heparin (PTwH) for 1 hr twice, then incubated in rat anti-mCherry (for tdTomato, 1:500 Thermo Fisher Scientific, #M11217) in PTwH/5% DMSO/3% Donkey Serum at 37°C for 8 days. After a one-day long wash in PTwH, the samples were incubated in anti-rabbit Alexa594 antibody (ThermoFisher no. A21207, 1:300) in PTwH/3% Donkey Serum at 37°C for 4 days. Samples were finally washed in PTwH before clearing and imaging.

2.15.3 Co-registration using VINCI

An automated workflow for co-registering each 4X-magnified scan of each brain was registered to its full-brain image. Each full-brain image was subsequently registered to the Allen Brain 25 µm reference mouse brain atlas, using rigid-body correlation-coefficient (CC) and 12-parameter affine mutual information schemas, resp. in VINCI (Cizek et al., 2004). Originally VINCI was developed for co-registration of clinical data but can also be utilized in animal studies (Lippert et al., 2019). The parameters were adapted for the multi-scale approach and pre-processing (quantile filtering) for microscopy data (VINCI version 4.96.0). However, the size of the microscopy scans meant that further optimization was required, we needed to co-register 32 GB size image files (8×10^9 voxels), while typical use cases in PET, MRI and CT for animal and human data are in the order of 2×10^7 voxels. The

processing of these large data sets was sped up through multi-threading and the co-registration time on a dedicated system (56 cores) could be reduced from over 24 hours to 0.7 hours. The transformation matrix of the 4X-image to the atlas was derived as the combination of the two transformations. Quality of registration was determined based on a visual inspection of the registration result (a match of the interhemispheric fissures and the anatomical surface at the base of the hypothalamus).

The scans with the best co-registration in each group were identified and the 4X-images from each mouse were aligned to the 4X-scan of the reference mouse within each group. This was done using another specially adapted 12-parameter affine mutual information schema combined with the known transformation of the reference mouse full brain image to the atlas. The CC values for the reference brain for the POMC, Lepr and Glp1r were 0.85, 0.75 and 0.90, respectively. The quality of registration for the Glp1r group was not optimal so the Glp1r scans with were co-registered the 4X-4X script but to the reference mouse of the POMC group.

2.15.4 Extraction of neuronal coordinates using Arivis and 3D scatter plots

The output NIFTI file of the co-registered 4X brain scans were uploaded into the Arivis software. Individual neurons were identified using the Blob Finder feature in the software and their XYZ coordinates were extracted. A python script was used to visualize the 3D scatter plots for each neuronal group where the quality of registration was checked once again. For the coronal view of the 3D distribution, the 3D scatter plot of 3 mice (per group) were plotted and a coronal snapshot was created from rostral locations within the ARC comparable to that of the 2D coronal distribution. The coordinates of the 2D coronal distributions were also extracted using the Arivis software from the Halo output files (as described under Imaging and quantification of RNA ISH) that had been previously aligned manually. The final distribution graph was plotted using the Prism software.

2.15.5 Isosurface density plots

In order to create the isosurface density plots, a python script was used (V 2.7.12). The Probability density function (PDF) of 3D distribution of neurons was estimated for the whole POMC population as well as the *Lepr* and *Glp1r* subpopulations. This was done using the non-parametric Kernel Density Estimation (KDE) method. The density of neurons within the ARC is thus calculated based on the 3D neuronal coordinates to demonstrate the spatial concentration which was then color coded to visualize the regions within the ARC with higher neuronal count for each subpopulation.

2.15.6 Data analysis of 3D projections

Brain scans were co-registered to an annotated atlas (<https://scalablebrainatlas.incf.org/mouse/ABA12#downloads>) using VINCI. Thresholding was achieved using the Threshold function on VINCI by applying a value across all scans. Using the Automated calculation function of VINCI, a mask was created from the regions of interest in 3D and the intensity profile of each region was determined using the VOI define function on VINCI. Representative images in the areas of interest were rendered using the Arivis software (V.3.3.0).

2.16 Study design of bacTRAP (EGFPL10a) mice

For $\text{POMC}^{\text{Dre}} \text{Lepr}^{\text{Cre}} \text{ROSA26ISlrSrEGFPL10a}$ and $\text{POMC}^{\text{Dre}} \text{Glp1r}^{\text{Cre}} \text{ROSA26ISlrSrEGFPL10a}$ animals, six triple transgenic bacTRAP mice (three females, three males) and twelve triple transgenic bacTRAP mice (six females, six males) were pooled for each replicate respectively, accounting for 3-4 replicates per POMC subpopulation. Mice were sacrificed at 12 weeks of age in a random-fed state by decapitation. Whole hypothalami were obtained using a mouse brain slicer matrix and snap frozen in liquid nitrogen until translating ribosome affinity purification (TRAP).

2.16.1 Purification of mRNA from triple positive EGFP10a Mice and RNA sequencing

The TRAP technique was performed using a modified version of a previous study on hypothalami of mice described under “Study design of bacTRAP (EGFP10a) mice”(Heiman et al., 2008). For sequencing (performed by the Cologne Center for Genomics), pre-amplification was carried out using the Ovation RNASeq System V2 was performed. Total RNA was used for first strand cDNA synthesis, using both poly(T) and random primers, followed by second strand synthesis and isothermal strand-displacement amplification. For library preparation, the Illumina Nextera XT DNA sample preparation protocol was used, with 1 ng cDNA input. After validation (Agilent 2200 TapeStation) and quantification (Invitrogen Qubit System) transcriptome libraries were pooled. The pool was quantified using the Peqlab KAPA Library Quantification Kit and the Applied Biosystems 7900HT Sequence Detection and sequenced on an Illumina HiSeq4000 sequencing instrument with a 2x75bp paired-end read length protocol.

2.16.2 Gene Ontology Analysis

The regulated Gene Ontology (GO)(Ashburner et al., 2000) terms were derived using the clusterProfiler R package(Yu et al., 2012) and visualized by mapping the percentage of regulated genes to the total GO term gene count against significant gene count and adjusted p-value per term. We visualized the GO-term as a heat map, where each row represents a DE gene belonging to the term and each column represents a sample. To ensure visual differentiation between the rows not being skewed by highly expressed genes, the values of each sample were converted to z-scores with respect to the individual genes (Dr. Paul Klemm).

2.16.3 Overlap analysis

We employed publicly available single-cell RNA-sequencing data from mouse hypothalami to detect overlaps with markers identified in our Glp1r and Lepr datasets. The first data source used was single-cell RNA-sequencing of 20,921 cells from the arcuate-median eminence complex of mice (Campbell et al., 2017). We filtered cells expressing POMC (4,248/20,921 cells) and clustered them using the R Seurat package(Butler et al., 2018) . The clustering result was visualized using the UMAP plot of Seurat. The second data source used

was from the single-cell RNA-sequencing dataset of 163 POMC-expressing neurons in mice yielding four clusters (Lam et al., 2017).

2.17 Electrophysiological experiments

2.17.1 Animals and brain slice preparation

Experiments were performed on brain slices from 12-15 week-old genetically marked (with ZsGreen) *Glp1r*⁻ and *Lepr*-expressing POMC neurons employing *POMC^{Dre} Lepr^{Cre} ROSA26^{ISlrSrZsGreen}^{+/-}* or *POMC^{Dre} Glp1r^{Cre} ROSA26^{ISlrSrZsGreen}^{+/-}* male and female mice. Animals were kept under standard laboratory conditions, with tap water and chow available ad libitum, on a 12h light/dark cycle. The animals were lightly anesthetized with isoflurane (B506; AbbVie Deutschland GmbH and Co KG, Ludwigshafen, Germany) and decapitated. Coronal slices (270 – 300 μm) containing the arcuate nucleus of the hypothalamus were cut with a vibration microtome (HM-650 V; Thermo Scientific, Walldorf, Germany) under cold (4°C), carbogenated (95% O₂ and 5% CO₂), glycerol-based modified artificial cerebrospinal fluid (GaCSF; (Ye et al., 2006). GaCSF contained (in mM): 244 Glycerol, 2.5 KCl, 2 MgCl₂, 2 CaCl₂, 1.2 NaH₂PO₄, 10 HEPES, 21 NaHCO₃, and 5 Glucose adjusted to pH 7.2 with NaOH. If not mentioned otherwise, the brain slices were continuously superfused with carbogenated aCSF at a flow rate of $\sim 2.5 \text{ ml}\cdot\text{min}^{-1}$. aCSF contained (in mM): 125 NaCl, 2.5 KCl, 2 MgCl₂, 2 CaCl₂, 1.2 NaH₂PO₄, 21 NaHCO₃, 10 HEPES, and 5 Glucose adjusted to pH 7.2 with NaOH. To prevent GABAergic and glutamatergic synaptic input the aCSF contained 10⁻⁴ M PTX (picrotoxin, P1675; Sigma-Aldrich), 5 x 10⁻⁶ M CGP (CGP-54626 hydrochloride, BN0597, Biotrend), 5 x 10⁻⁵ M DL-AP5 (DL-2-amino-5-phosphonopentanoic acid, BN0086, Biotrend), and 10⁻⁵ M CNQX (6-cyano-7-nitroquinoxaline-2,3-dione, C127; Sigma-Aldrich). To suppress action potential-dependent synaptic release, we have blocked voltage-dependent Na⁺ channels by tetrodotoxin (10⁻⁶ M, TTX, T-550, Alomone, Jerusalem, Israel) in some experiments.

2.17.2 Electrophysiology

Current-clamp and voltage-clamp recordings of ZsGreen-expressing POMC neurons were performed at $\sim 32^{\circ}\text{C}$ in the perforated patch clamp configuration. Neurons were visualized with a fixed stage upright microscope (BX51WI, Olympus, Hamburg, Germany) using 40x and 60x water-immersion objectives (LUMplan FL/N 40x, 0.8 numerical aperture, 2 mm working distance; LUMplan FL/N 60x, 1.0 numerical aperture, 2 mm working distance, Olympus) with infrared differential interference contrast optics (Dodt and Zieglgansberger, 1990) and fluorescence optics. ZsGreen-expressing POMC neurons were identified by their anatomical location in the ARC and by their ZsGreen fluorescence that was visualized with an X-Cite 120 illumination system (EXFO Photonic Solutions, Ontario, Canada) in combination with a Chroma 41001 filter set (EX: HQ480/40x, BS: Q505LP, EM: HQ535/50m, Chroma, Rockingham, VT, USA). Electrodes with tip resistances between 4 and 6 M Ω were fashioned from borosilicate glass (0.86 mm inner diameter; 1.5 mm outer diameter; GB150-8P; Science Products) with a vertical pipette puller (PP-830; Narishige, London, UK). All recordings were performed with an EPC10 patch-clamp amplifier (HEKA, Lambrecht, Germany) controlled by the program PatchMaster (version 2.32; HEKA) running under Windows. In parallel, data were recorded using a micro1410 data acquisition interface and Spike 2 (version 7) (both from CED, Cambridge, UK). Current clamp recordings were sampled at 25 kHz and low-pass filtered at 2 kHz with a four-pole Bessel filter. Voltage clamp recordings were sampled at 5 kHz, smoothed ($\tau = 0.2$ s) and downsampled to 0.5 Hz. The calculated liquid junction potential of 14.6 mV between intracellular and extracellular solution was compensated or subtracted offline (calculated with Patcher's Power Tools plug-in from <http://www.mpibpc.mpg.de/groups/neher/index.php?page=software> for IGOR Pro 6 [Wavemetrics, Lake Oswego, OR, USA]).

Perforated patch experiments were conducted using protocols modified from (Horn and Marty, 1988) and (Akaike and Harata, 1994). Recordings were performed with pipette solution containing (in mM): 140 K-gluconate, 10 KCl, 10 HEPES, 0.1 EGTA, 2 MgCl₂ adjusted to pH 7.2 with KOH. ATP and GTP were omitted from the intracellular solution to prevent uncontrolled permeabilization of the cell membrane (Lindau and Fernandez, 1986). The patch pipette was tip filled with internal solution and backfilled with internal solution, which contained the ionophore to achieve perforated patch recordings and 0.02%

tetramethylrhodamine-dextran (3000 MW, D3308, Invitrogen, Eugene, OR, USA) to monitor the stability of the perforated membrane. Amphotericin B (A4888; Sigma) was dissolved in dimethyl sulfoxide to a concentration of $40 \mu\text{g} \cdot \mu\text{l}^{-1}$ (DMSO; D8418, Sigma) following the protocols of (Kyrozis, 1995; Rae et al., 1991). The used DMSO concentration (0.1–0.3%) had no obvious effect on the investigated neurons. The ionophore was added to the modified pipette solution shortly before use. The final concentration of amphotericin B was $\sim 120\text{--}160 \mu\text{g} \cdot \text{ml}^{-1}$. Amphotericin solutions were prepared from undissolved weighted samples (stored at 4°C protected from light) on every recoding day. During the perforation process, access resistance (R_a) was monitored continuously and experiments started after R_a had reached steady state ($\sim 15\text{--}20$ min), and the action potential amplitude was stable.

2.17.3 Intrinsic electrophysiological properties

To analyse in detail the intrinsic electrophysiological properties of ZsGreen-expressing POMC neurons, a set of current clamp protocols from a holding potential of -70 mV was applied. *Cell input resistance* was determined from a series of hyperpolarizing small current pulses (1 s, 2-10 pA increments) and the slope of the resulting I-V relations. *Whole-cell capacitances* were calculated from the membrane time constant (τ) and the input resistance (R): $C = \tau/R$. To analyse the I_H -dependent *sag-potentials*, the neurons were hyperpolarized with 5 consecutively incrementing current pulses. The increments were adjusted so that the last pulse hyperpolarized the membrane to -120 mV. The sag-potential was defined as the difference between the lowest voltage reached at the beginning of the pulse and the membrane potential reached at the end of hyperpolarization. To analyse post-inhibitory rebound excitation, we used an ‘enhanced rebound protocol’, where the same current-step amplitudes were applied as for the sag-potential analysis. This time as 2 s hyperpolarizing pre-pulses that were followed by a 1 s test pulse with the amplitude of a single increment. The maximum instantaneous frequencies during the rebound were determined and plotted over the membrane potentials of the pre-pulses. To analyse input-output relations, we applied a series of ascending and then descending current ramps (5 s each) where the ramp amplitudes were increased from 10 to 25 pA in 5 pA increments. Amplitudes were further increased if the 25 pA ramp did not elicit action potentials. Spike number ratios were calculated by dividing the number of action potentials during the ascending ramp by the number of action potentials

during the descending ramp. To further analyze excitability, i.e., evoked action potential firing, a series of depolarizing current pulses (1 s; 5–50 pA in 5 pA increments) was applied. For each current pulse, the number of action potentials was determined, plotted over the current amplitude, and linearly fit. Linear fits were performed for data points where action potentials were elicited. Only data points at which action potentials were triggered were considered for fit.

2.17.4 Peptide signaling

Leptin (100nM; L3772, Sigma-Aldrich, Taufkirchen, Germany), Glucagon-like peptide-1 Gp1 (300nM, Gpl1, H-5956, Bachem AG, Bubendorf Switzerland) were bath-applied for 15 or 30 min with a perfusion rate of 2.5 ml*s⁻¹.

2.18 Quantification and Statistical Analysis

2.19 Statistical analyses

Statistical significance for two groups was determined by unpaired two-tailed Student's t-test. In case of unequal variance between the two groups, the unpaired Welch's t test or unpaired Mann-Whitney rank test were used. For determining differences between more than two groups, one-way ANOVA was applied. Depending on the scientific question, the one-way ANOVA was followed by no post-hoc test, by Dunnett's post-hoc test (comparing all groups to one control) or by Tukey's post-hoc test (comparing all groups among each other), as indicated in the figure legends. All remaining data (more than 2 groups, more than one independent factor) were analysed with two-way ANOVA followed by Sidak's or Tukey's post-hoc analysis, as indicated in the figure legends. With exception of violin plots, data are represented as mean ± SEM. In violin plots solid lines represent median, dashed lines represent lower and upper quartile. Statistical analyses were performed using GraphPad Prism 8 Software. Statistical significance has been noted as following: * $p \leq 0.05$, ** $p \leq 0.01$, *** $p \leq 0.001$, **** $p \leq 0.0001$.

2.19.1 Statistical analysis of 3D data

The bounding box containing all the neuronal coordinates was divided into smaller cubes and to carry out a statistical assessment of the differences in distribution patterns for the two subpopulations, Student's t-test was calculated for each cube. Due to the variance in the total neuronal counts between the Lepr and Glp1r groups, the number of neurons in each cube was corrected by introducing a density factor (number of Glp1r neurons/number of Lepr neurons). This was done by multiplying the density factor to the total number of neurons in each group. Since the null distribution is two-sided, both null hypotheses are visualized within the same plot.

2.19.2 RNA-Sequencing Analysis Workflow

The RNA-sequencing results of Glp1r and Lepr samples were processed using the nf-core/rnaseq pipeline v1.4.2(Ewels et al., 2020). This involves (1) aligning the raw reads to the reference genome GRCm38.p6 using STAR 2.6.1d(Dobin et al., 2013) and (2) transcript abundance estimation using Salmon 0.14.1(Patro et al., 2017) using the reference transcriptome from Ensembl release 92(Yates et al., 2015). To normalize the ribosomal pulldown (IP) to the hypothalamic background (Input) per sample, we calculated a ratio of the Salmon gene counts (IP/Input). The differentially expressed genes between Glp1r and Lepr groups were derived using DESeq2 1.26.0(Love et al., 2014) . This yields genes that are regulated between the Glp1r and Lepr conditions and act as markers for these POMC populations.

Preface

All figures and content in the Results and Materials and Methods, as well as parts of the Discussion are directly taken or modified from the following manuscript:

Biglari, N., Gaziano, I., Schumacher, J. *et al.* Functionally distinct POMC-expressing neuron subpopulations in hypothalamus revealed by intersectional targeting. *Nat Neurosci* 24, 913–929 (2021). <https://doi.org/10.1038/s41593-021-00854-0>

Results displayed in Figures 3.1, 3.2 and 3.3 were outcomes from collaborations with Dr. Jonas Schumacher. Please refer to the thesis from Dr. Jonas Schumacher for details on cloning and verification of ROSA26^{lSlrSrM3Dq}-ZsGreen, ROSA26^{lSlrSrEGFP-L10a} mouse lines.

In section 3.3, Co-registration of the brain scans to the reference atlas were done by Michael Sue.

Data analysis of RNA sequencing in figures 3.16, 3.17 and 3.18 were carried out by Dr. Paul Klemm.

Experiments from figures 3.20, 3.21 and 3.22 were performed by Dr. Lars Paeger, Jan Radermacher and Svenja Corneliussen.

3 Results

3.1 Generation of POMC-Dre driver line

We generated a POMC-Dre transgenic line in order to target POMC neurons in a Dre-dependent manner. Thus, a POMC-Dre bacterial artificial chromosome (BAC) recombinase was generated (Dr. Tim Klöckener) in which the expression of the Dre recombinase is dependent on the regulating elements of the *Pomc* gene. Injection of the linearized BAC DNA into pronuclei prior to oocyte fertilization resulted in 15 transgenic founder animals, which were all bred to a Dre-dependent reporter line ROSA26rSrZsGreen. The stable single-site integration of the Dre transgene into the genome of the mouse line was also demonstrated. Figure 3.1 shows specific expression of the fluorophore *ZsGreen* in the ARC as well as the anterior and intermediate lobes of the pituitary in POMCDre ROSA26rSrZsGreen line. These results are in line with previous findings and the overall understanding of the anatomy and function of the pituitary gland (Emerald, 2016).

In situ hybridization methods showed that 97.6% of *ZsGreen*-labeled neurons in the ARC co-expressed *Pomc*, whereas only 1.9% co-expressed *Agrp* indicating high specificity in the Dre-mediated recombination POMC targeting (Fig. 3.1D, E). Consistent with this, 98.1% of *ZsGreen*-expressing neurons were non-*Agrp*-expressing and 2.4% of them did not express *Pomc*. This was an important finding since other reporters and recombinases targeting POMC neurons have also been shown to target AgRP neurons simultaneously. As introduced in Section 1.2.1, many progenitors of AgRP neurons express *Pomc* during development. It was shown that POMC-Cre line, commonly used to genetically target POMC neurons, also labels NPY-expressing neurons or show no expression of *Pomc* in adult mice. This indicated that, at least partially, functions attributed to POMC neurons could be due to non-*Pomc*-expressing neurons expressing the Cre recombinase (Padilla et al., 2010).

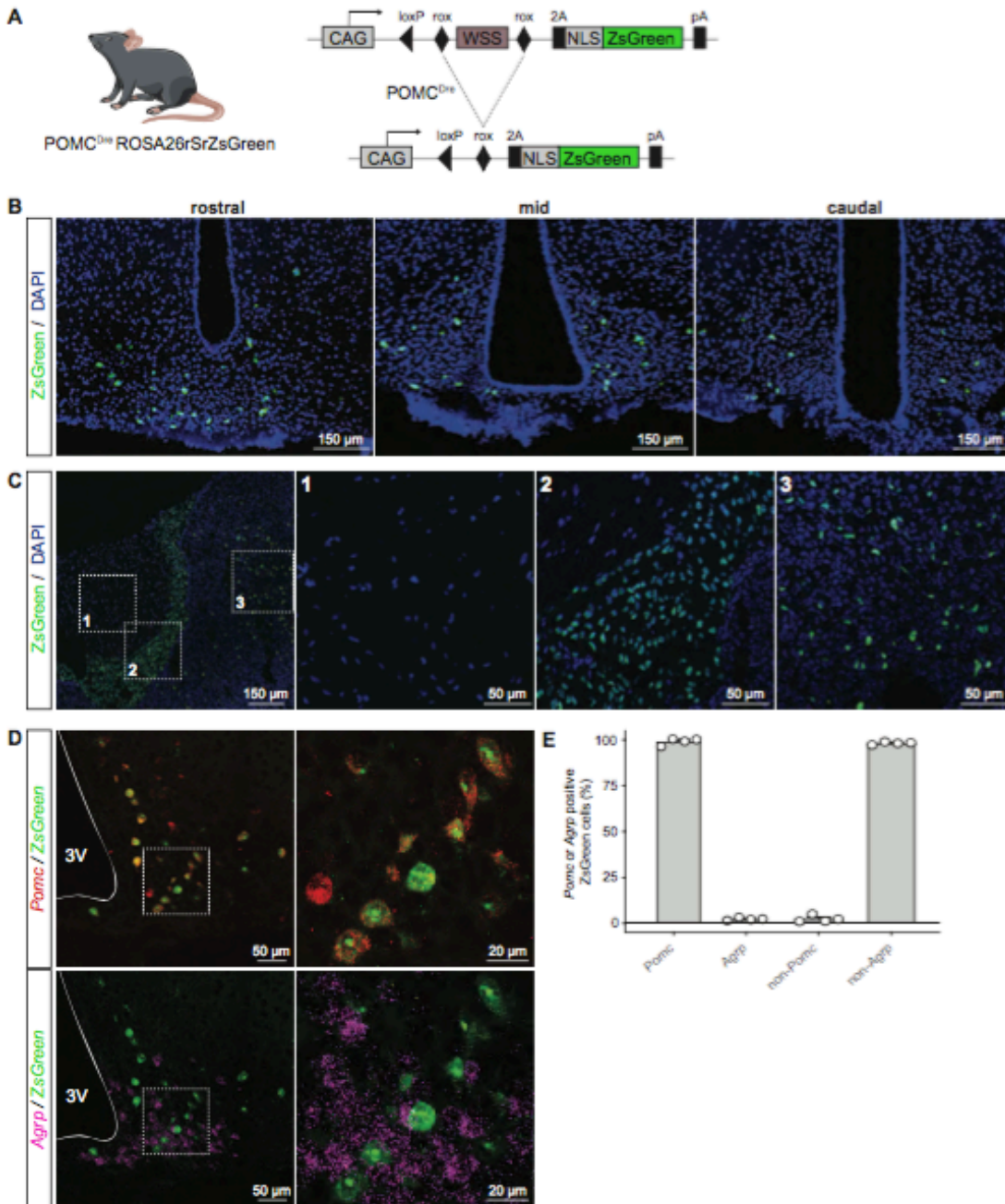


Figure 3.1 The POMC^{Dre} driver line successfully targets POMC neurons.

(A) Schematic diagram showing POMC^{Dre}-dependent recombination in the ROSA26rSrZsGreen reporter line. Excision of rox-flanked stop cassette leads to ZsGreen expression in POMC neurons. (B) ZsGreen expression across the rostral, mid and caudal sections of the ARC in POMC^{Dre} ROSA26rSrZsGreen at 15 weeks of age. (C) Dispersed ZsGreen expression in the intermediate and anterior lobes of the pituitary in POMC^{Dre} ROSA26rSrZsGreen mice. C1, C2 and C3 depict

magnifications of the posterior, intermediate and anterior pituitary, respectively. Scale bar represents 150 μm in the whole image and 50 μm in the magnifications. (D) RNA *in situ* hybridization against *Pomc/ZsGreen* (top) and *Agrp/ZsGreen* (bottom) in POMCDre ROSA26rSrZsGreen mice. Magnifications of the dashed boxes are displayed on the right of each image. Scale bars represent 50 μm in the whole image and 20 μm in the magnifications. 3V= Third ventricle. (E) Percentage of *ZsGreen*-positive cells co-expressing or lacking expression of either *Pomc* or *Agrp*, quantified from RNA *in situ* hybridization (D). Data are represented as mean \pm SEM, n=4.

The generated POMC-Dre recombinase line circumvents AgRP targeting through the temporal delay in recombination as shown in (Jonas Schumacher, Thesis). Importantly, analysis of the Dre-mediated recombination in POMC^{Dre} ROSA26rSrZsGreen mice between 3 and 30 weeks of age, demonstrated an increase in recombination before plateauing at 15 weeks (Jonas Schumacher, Thesis).

Previously published POMC-labeling recombinases and reporter lines (such as POMC-Cre) also show labeling in the NTS (Zhan et al., 2013). Therefore, we carried out *in situ* hybridization against *ZsGreen* in the NTS of a POMCDre ROSA26rSrZsGreen mouse. Interestingly, there was no *ZsGreen* expression detected in this area (Fig. 3.2A). To ensure that the random BAC integration into the mouse genome did not create any undesired metabolic phenotypes, we carried out standard phenotyping experiments on this line on NCD and HFD. Figure 3.2 shows no differences between the POMC-Dre^{tg/wt} and their littermates, POMC-Dre^{wt/wt} regarding food intake, energy expenditure (EE), locomotion in addition to glucose tolerance tests (Fig. 3.2B-K).

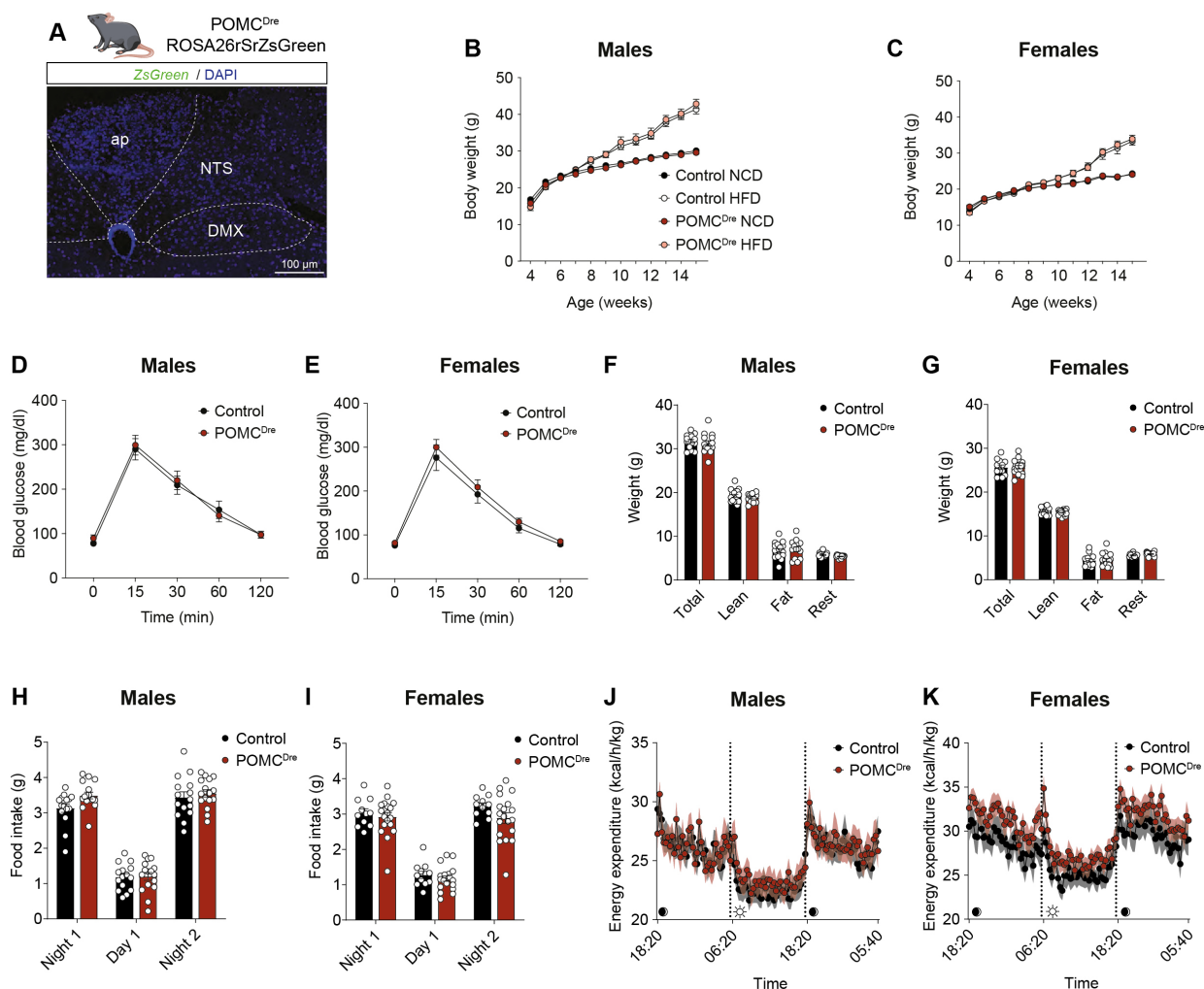


Figure 3.2 The POMC^{Dre} transgene does not cause any metabolic phenotypes compared to wildtype controls.

(A) RNA *in situ* hybridization against *ZsGreen* in POMC^{Dre} ROSA26rSrZsGreen mice. Scale bars represent 150 μ m. ap = area postrema, NTS = nucleus tractus solitarius, DMX = dorsal motor nucleus. (B-C) Body weight curve of POMC^{Dre} males (B, Control NCD n=19, Control HFD n=23, POMC^{Dre} NCD n=15, POMC^{Dre} HFD n=6) and females (C, Control NCD n=12, Control HFD n=15, POMC^{Dre} NCD n=19, POMC^{Dre} HFD n=15) versus control littermates on NCD and HFD. (D-E) Glucose tolerance test (F,G), body composition (H,I), food intake (J,K) and energy expenditure of POMC^{Dre} males and females on NCD. Data are represented as mean \pm SEM. *p*-values were calculated by one-way-ANOVA, two-way-ANOVA or unpaired two-tailed Student's *t* test followed by Holm-Sidak correction for multiple comparisons.

3.2 Combinatorial recombinase-dependent labeling of heterogeneous POMC neuron populations

POMC neurons can sense hormones leptin and Glp1 and express receptors specific to both hormones, introduced in the Section 1.4.1 and 1.4.2. Single cell sequencing of FACS-sorted EGFP-expressing POMC neurons demonstrated that within their sampling, POMC neurons expressing the *Lepr* and those expressing the *Glp1r* did not overlap (Lam et al., 2017). Thus, to investigate whether this holds true, we performed *in situ* hybridization in C57BL/6N mice across the rostrocaudal axis in the ARC. Having probed the sections for *Lepr*, *Glp1r* and *Pomc*, we could determine the percentage overlap of each receptor with *Pomc*. The results of this experiment showed that indeed the total percentage of neurons that expressed both *Lepr* and *Glp1r* was on average 15% across the rostrocaudal axis.

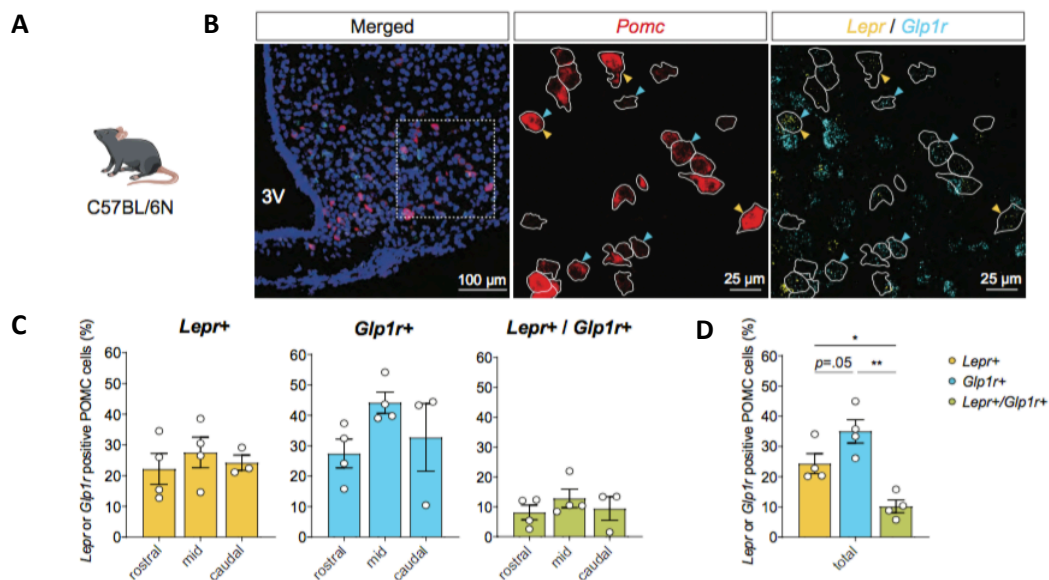


Figure 3.3 Co-expression of *Pomc* with either *Glp1r* or *Lepr* in the ARC.

(A) Icon of C57BL/6N mouse, experiments were carried out in these mice. (B) Representative micrograph of the *in situ* hybridization showing the merged image in the left panel, following magnifications of the co-expression of either *Glp1r* or *Lepr* with *Pomc* (middle panel) and the co-expression of *Lepr* and *Glp1r* (right panel). (C) Quantification of (B). (D) Total percentage overlap of *Lepr*⁺ and *Glp1r*⁺ POMC cells. Scale bars represent 100 μ m in the merged image and 25 μ m in the magnified images.

Based on these findings we decided to further investigate the functional roles of these two subpopulations of POMC neurons. Using a triple transgenic system, we used the aforementioned Dre line to target the whole POMC neuronal population and targeted the subpopulation of interest using either the Lepr Cre or Glp1r Cre lines. To achieve experimental mice, we bred homozygous ROSA26ISlrSrZsGreen mice to double transgenic POMC^{Dre} Lepr^{Cre} or POMC^{Dre} Glp1r^{Cre} mice that yielded four different genotypes. Using the Lepr-targeted line as an example, the resulting offspring carried the following genotypes; POMC^{Dre}+/- Lepr^{Cre}+/- ROSA26ISlrSrZsGreen^{+/-}, POMC^{Dre}-/- Lepr^{Cre}+/- ROSA26ISlrSrZsGreen^{+/-}, POMC^{Dre}+/- Lepr^{Cre}-/- ROSA26ISlrSrZsGreen^{+/-} and POMC^{Dre}-/- Lepr^{Cre}-/- ROSA26ISlrSrZsGreen^{+/-}. The breeding scheme used to yield the experimental mice is displayed in Figure 3.4.

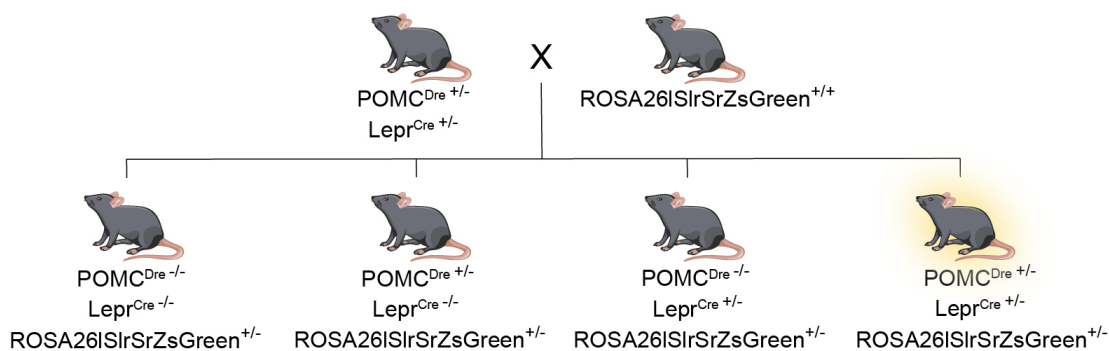


Figure 3.4 Breeding scheme used for generating experimental mice that shows the triple transgenic mice as well as their littermate controls.

Next, we analyzed *ZsGreen* expression in each of these genotypes, which was specific to the mice that carried both Cre and Dre transgenes but was not observed in any other genotypic combination. *In situ* hybridization analysis and quantification showed that 99.2% of *ZsGreen*-labelled neurons in triple transgenic POMC^{Dre} Lepr^{Cre} ROSA26ISlrSrZsGreen mice (from now on referred to as POMC^{Dre} Lepr^{Cre} ROSA26ISlrSrZsGreen) and 94.6% in POMC^{Dre} Glp1r^{Cre} ROSA26ISlrSrZsGreen mice co-expressed *Pomc* (Fig. 3.5C).

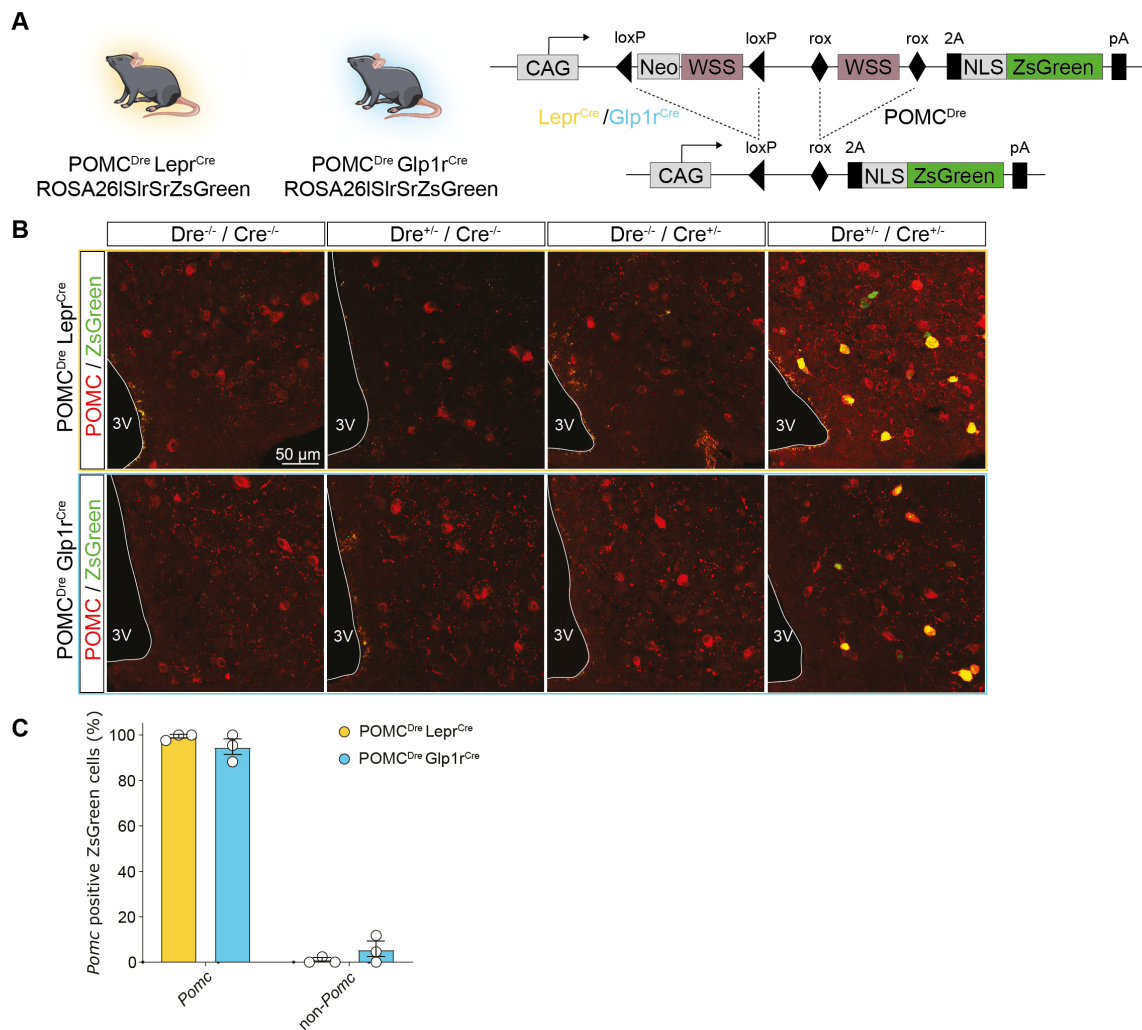


Figure 3.5 ZsGreen labeling of POMC^{Lepr+} and POMC^{Glp1r+} neurons using the Dre/Cre-dependent ROSA26ISrSrZsGreen reporter line.

(A) Illustrations of experimental mice and schematic diagram showing Dre- and Cre-dependent recombination of ROSA26ISrSrZsGreen reporter line. Excision of flox- or rox-flanked stop cassettes through recombination of both Dre and Cre drivers leads to ZsGreen expression in the targeted POMC population. (B) Representative microscopic images of immunohistochemical staining against POMC and ZsGreen in ARC of all resulting genotypes at 15 weeks of age. Scale bar represents 50 μ m. (C) Percentage of ZsGreen-positive cells co-expressing or lacking expression of *Pomc*, quantified from RNA *in situ* hybridization. Data are represented as mean \pm SEM, n=3. 3V= third ventricle.

3.3 Distinct anatomical distribution of POMC^{Lepr+} and POMC^{Glp1r+} neurons in the ARC

We were interested in the spatial and anatomical distribution of POMC^{Lepr+} and POMC^{Glp1r+} since differences in anatomical distribution could serve as an indication for different functional roles. Therefore, we specifically labeled POMC^{Lepr+} and POMC^{Glp1r+} in POMC Dre LeprCre ROSA26^{lSlrSrZsGreen} and POMC Dre Glp1rCre ROSA26^{lSlrSrZsGreen}, respectively. These mice were subjected to a whole-brain imaging technique. Differences in anatomical distribution of neurons could serve as an indication for different functional roles. Therefore, we aimed to create a three-dimensional representation of the anatomical distribution pattern of POMC^{ARC} neurons and our subpopulations of interest. We made use of tissue clearing techniques in combination with light-sheet fluorescence microscopy (LSFM) (Pan et al., 2016). To this end, I set up a pipeline for uDISCO clearing, LSFM-based imaging and subsequent data processing. POMC Dre ROSA26^{rSrZsGreen}, POMC Dre LeprCre ROSA26^{lSlrSrZsGreen} and POMC Dre Glp1rCre ROSA26^{lSlrSrZsGreen} mice were subjected to the aforementioned pipeline. The three-dimensional rendering of the distribution pattern of *ZsGreen*-labeled neurons is displayed in Figure 3-6A-C. The pre-requisite to any quantitative assessment on these datasets was a transformation into one coordinate system via image registration. Registration algorithms are categorized based on the transformation models they utilize. We opted for a linear transformation model built into the in-house developed registration VINCI software.

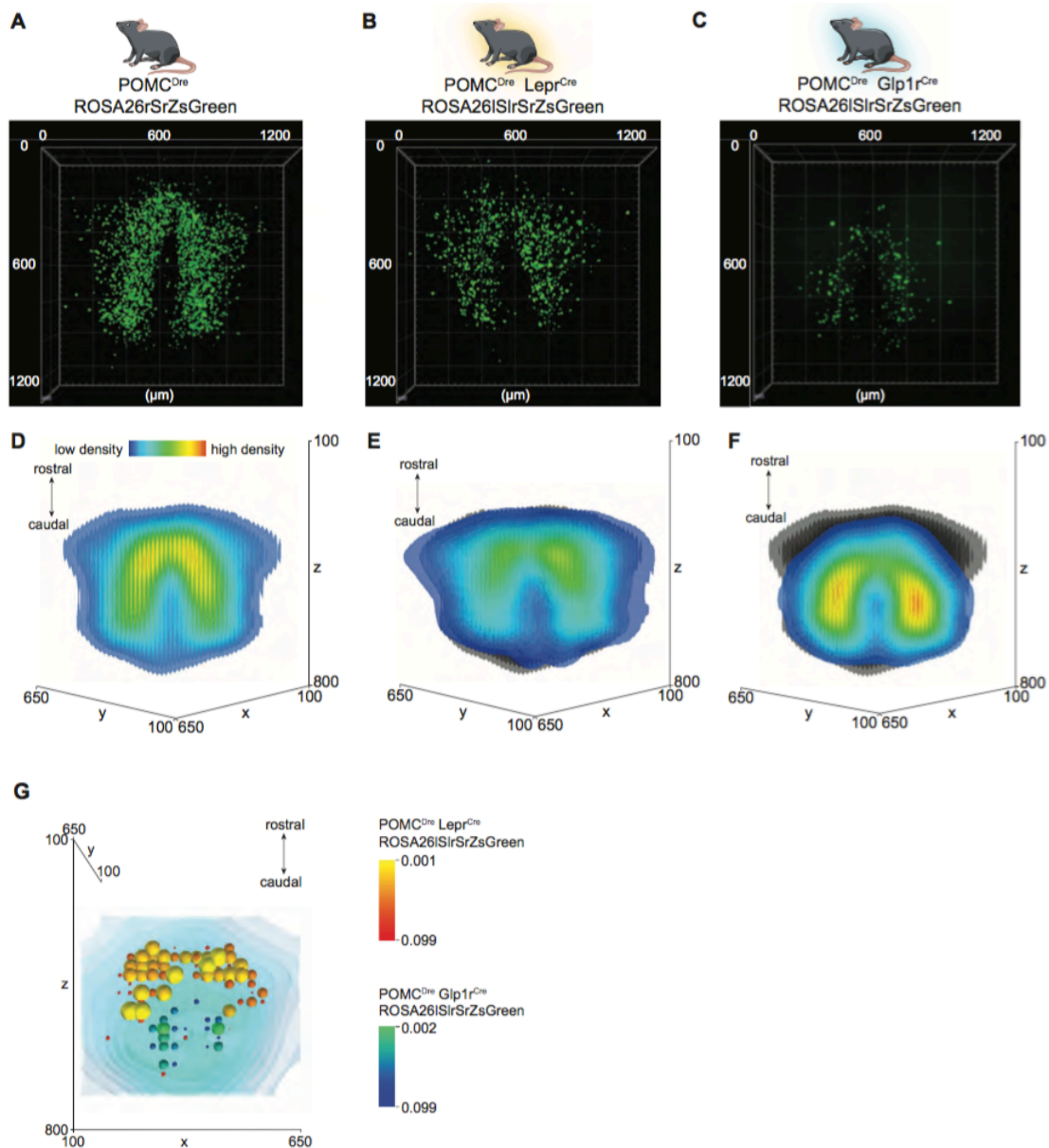


Figure 3.6 $POMC^{Lepr}$ and $POMC^{Glp1r}$ have different spatial distribution patterns in the ARC.

(A-C) Representative 3D reconstruction of the entire POMC population labeled in $POMC^{Dre}$ $ROSA26rSrZsGreen$ mice (A), or 3D reconstruction of subpopulations in $POMC^{Dre} Lepr^{Cre}$ $ROSA26lSlrSrZsGreen$ (B) or $POMC^{Dre} Glp1r^{Cre}$ $ROSA26lSlrSrZsGreen$ mice (C) at 15 weeks of age. Scans were obtained using the LSFM at 8X total magnification. $n=9$ (A), $n=7$ (B) and $n=8$ (C). (D-F) Isosurface density plots of the entire POMC population (D), the $POMC^{Lepr+}$ (E) and the $POMC^{Glp1r+}$ subpopulation (F). Grey shaded areas in (E and F) depict the entire POMC population. (G) Statistic representation of the differences in distribution between the $POMC^{Lepr+}$ and $POMC^{Glp1r+}$

subpopulations. P-values are plotted as spheres within the space occupied by the POMC neurons (depicted in the background). The size and color of the spheres indicates the significance values in ranges of yellow-orange (POMC^{Lepr+}) and cyan-blue (POMC^{Glp1r+}) as shown in the scale bars.

Linear transformations use rotation, scaling, translation, and other affine transforms to synchronize the target image space to the reference image space. In order to create a distribution pattern for each group and to carry out a statistical analysis, all acquired brain scans were co-registered onto a reference atlas that is a grayscale Nissl volume of reconstructed brain (Allen Brain 25 μ m reference Atlas) using VINCI. The next step was to extract the neuronal coordinates from the registered brain scans, which were subsequently plotted using a kernel density fit to create an isosurface density plot for each neuronal population (Fig. 3.6D-F). Finally, the distribution patterns were subjected to statistical analysis and displayed in Figure 5G. P-values calculated by Student's t-test, were plotted to show areas in which the number of neurons of one group were significantly higher in comparison to the other group. Interestingly, there were significant differences in the localization patterns of POMC^{Lepr+} versus POMC^{Glp1r+} neurons, revealing distinct distribution of each group in the ARC. To verify that the expression pattern of the ZsGreen-labelled cells observed in POMC Dre LeprCre ROSA26ISlrSrZsGreen and POMC Dre Glp1rCre ROSA26ISlrSrZsGreen transgenic mice corresponds with that of the *Lepr*- and *Glp1r*-expressing POMC neurons in wild type mice, we created anatomically matched coronal sections from the 3D coordinates. Figure 3.7A and B show that the coronal distribution pattern of POMC^{Lepr+} and POMC^{Glp1r+} neurons identified from the transgenic line and the wild type mice (from Fig. 3.3) were similar.

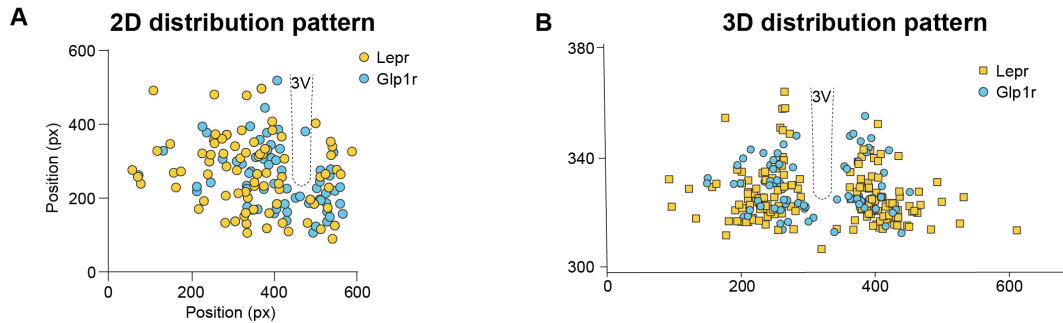


Figure 3.7 Similar coronal distribution pattern of transgenic-labeled and endogenously-expressed POMC^{Lepr+} and POMC^{Glp1r+} neurons.

(A) Bilateral, coronal view of the distribution pattern of POMC^{Lepr+} and POMC^{Glp1r+} neurons in POMC^{Dre} Lepr^{Cre} ROSA26ISlrSrZsGreen and POMC^{Dre} Glp1r^{Cre} ROSA26ISlrSrZsGreen mice. Coronal cross-sections were generated by extracting the 3D coordinates of transgenic-labelled POMC^{Lepr+} and POMC^{Glp1r+} neurons in the given section. Data was merged from n=3 mice/group. (B) Unilateral, coronal view of the distribution pattern of POMC^{Lepr+} and POMC^{Glp1r+} neurons labeled via RNA *in situ* hybridization. Data was merged from n=3 mice/group.

To ensure that the expression of the ZsGreen-labelled cells was specific to the ARC, whole brain clearing was carried out on samples from mice expressing the POMC^{Dre} transgene only, the Glp1r^{Cre} or Lepr^{Cre} transgene alone, or the combination of both, as displayed in Figure 3.8. Indeed, ZsGreen-positive cells could only be detected in triple transgenic mice within the ARC, ruling out leaky expression of the fluorophore in presence of only either Cre or Dre recombinase.

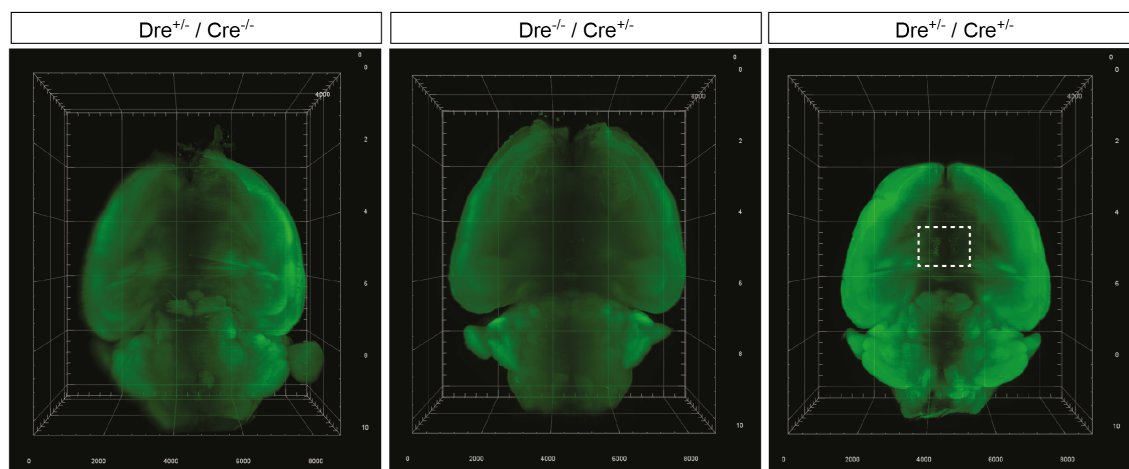


Figure 3.8 ZsGreen expression in ARC is only detected in mice expressing both Cre and Dre recombinases.

Left to right: Whole brain imaging of Pomc^{Dre+} Lepr^{Cre-} ROSA26rSrlSIZSGreen^{+/-}, Pomc^{Dre-} Glp1r^{Cre+} ROSA26rSrlSIZSGreen^{+/-}, Pomc^{Dre+} Lepr^{Cre+} ROSA26rSrlSIZSGreen^{+/-} 15-week-old mice, respectively. ZsGreen signal specific to the POMC^{Lepr+} in the ARC is displayed in the boxed area within the last image on the right. No ectopic expression was observed in only-Cre⁺ or only-Dre⁺ mice as depicted in the images on the left. Whole-brain scans were acquired using the LSFM with total magnification of 1.6X.

3.4 Similar projection patterns of POMC^{Lepr+} and POMC^{Glp1r+} neurons

Next, we investigated the projection sites of POMC^{Lepr+} and POMC^{Glp1r+} neurons using mice that express tdTomato in a Cre/Dre-dependent manner. In this manner we were able to label axonal projections and dendrites of these neurons that were subjected to whole-brain immunostaining and uDISCO-mediated tissue clearing. The samples were then imaged using LSFM and co-registered onto an annotated reference mouse brain atlas. Established projection areas of POMC neurons i.e., the bed nucleus of the striae terminalis (BNST), periaquiductal grey (PAG), dorsomedial nucleus of the hypothalamus (DMH) and the paraventricular nucleus of the hypothalamus (PVH) and NTS were identified via the annotated atlas and the three-dimensional projection densities were quantified using the VINCI software. Figure 3.9 displays representative images of 3D-rendering of the tdTomato-labeled projection densities of the POMC^{Lepr+} and POMC^{Glp1r+} neurons within the aforementioned brain regions. The quantified projection densities normalized to the number

of starter cells in each group, shown in Figure 3.9D, showed no differences in innervation densities between the different subpopulations.

This result is corroborated by the quantification of projection densities carried out in slices subsequent to immunostaining in the same mouse model. In the thesis of Dr. Jonas Schumacher, the projection patterns of the two subpopulations were analyzed by double immunolabeling against tdTomato and endogenous POMC. The results showed a higher tdTomato immunostained density in $Pomc^{DreLepr^{Cre}ROSA26rSrlSlttdTomato^{+/-}}$ mice in comparison to $Pomc^{DreGlp1r^{Cre}ROSA26rSrlSlttdTomato^{+/-}}$. This finding is likely attributable to the larger number of genetically-labeled $POMC^{Lepr+}$ neurons compared to $POMC^{Glp1r+}$ neurons.

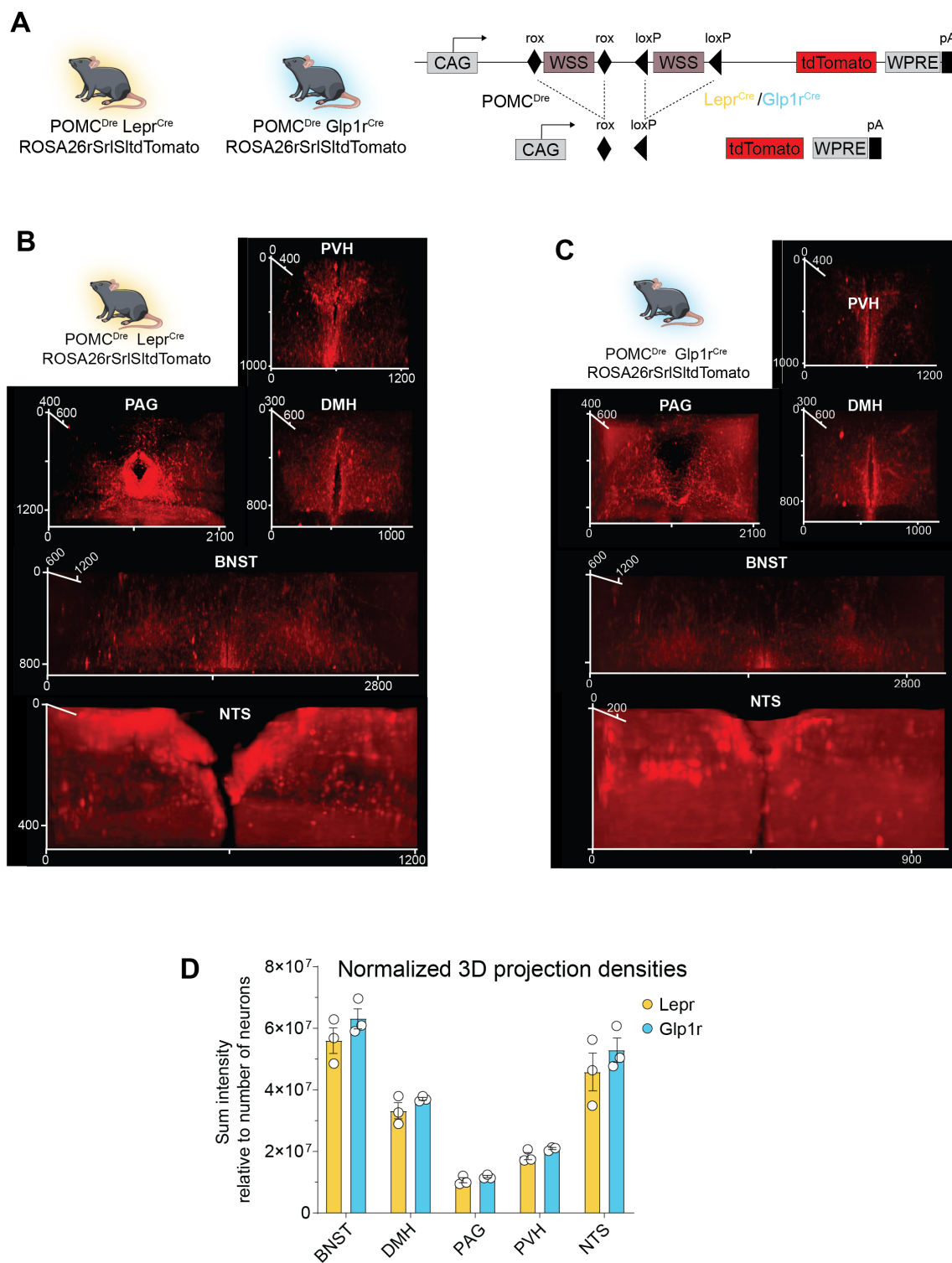


Figure 3.9 Three-dimensional analysis of the projections of POMC^{Lepr+} and POMC^{Glp1r+} neurons shows similar patterns.

(A) Scheme of POMCDre LeprCre ROSA26rSrlSltTomato and POMCDre Glp1rCre ROSA26rSrlSltTomato mice. Representative images of 3D projection densities in POMCDre LeprCre ROSA26rSrlSltTomato (B) and POMCDre Glp1rCre ROSA26rSrlSltTomato (C) in the paraventricular nucleus of the hypothalamus (PVH), the periaqueductal gray (PAG), the dorsomedial hypothalamic area (DMH), the anterior bed nucleus of the stria terminalis (BNST) and the nucleus tractus solitarius (NTS). (D) Quantification of 3D projection densities shown in A and B, normalized to the number of neurons. Data are represented as mean \pm SEM, n=3.

3.5 DREADD-dependent activation of POMC^{Lepr+} and POMC^{Glp1r+} neurons differentially regulates food intake

In order to investigate how different POMC neuron subpopulations regulate metabolic processes, we utilized mice that expressed the activatory DREADD receptor hM3Dq coupled to ZsGreen in a Cre/Dre-dependent manner. Cloning and verification of this line was performed by Dr. J Schumacher. A representation of the recombination resulting from breeding the mice to double recombinase positive mice is shown in Figure 3.10A. We assessed the functionality of this line by injecting POMC^{Dre}Lepr^{Cre}ROSA26lSlrSrhM3Dq males intraperitoneally (i.p.) with either saline or clozapine-N-oxide (CNO). *In situ* hybridization was performed against *Pomc*, *Lepr*, *ZsGreen* (in lieu of hM3Dq) and *Fos* as displayed in Figure 3.10C. The results show that 93.4% of POMC neurons expressing *ZsGreen* were positive for *Lepr* and no significant differences existed between *ZsGreen*-positive cells in saline (91.8%) vs CNO-injected (94.9%) mice (Fig. 3.10C). In addition, 47.3% of cells endogenously expressing *Lepr* and *Pomc* also express *ZsGreen* (Fig. 3.10D). While saline-injected mice expressed 6.9% *Fos* in *ZsGreen*-positive cells, 94.0% of them expressed *Fos* upon CNO administration (Fig. 3.10E).

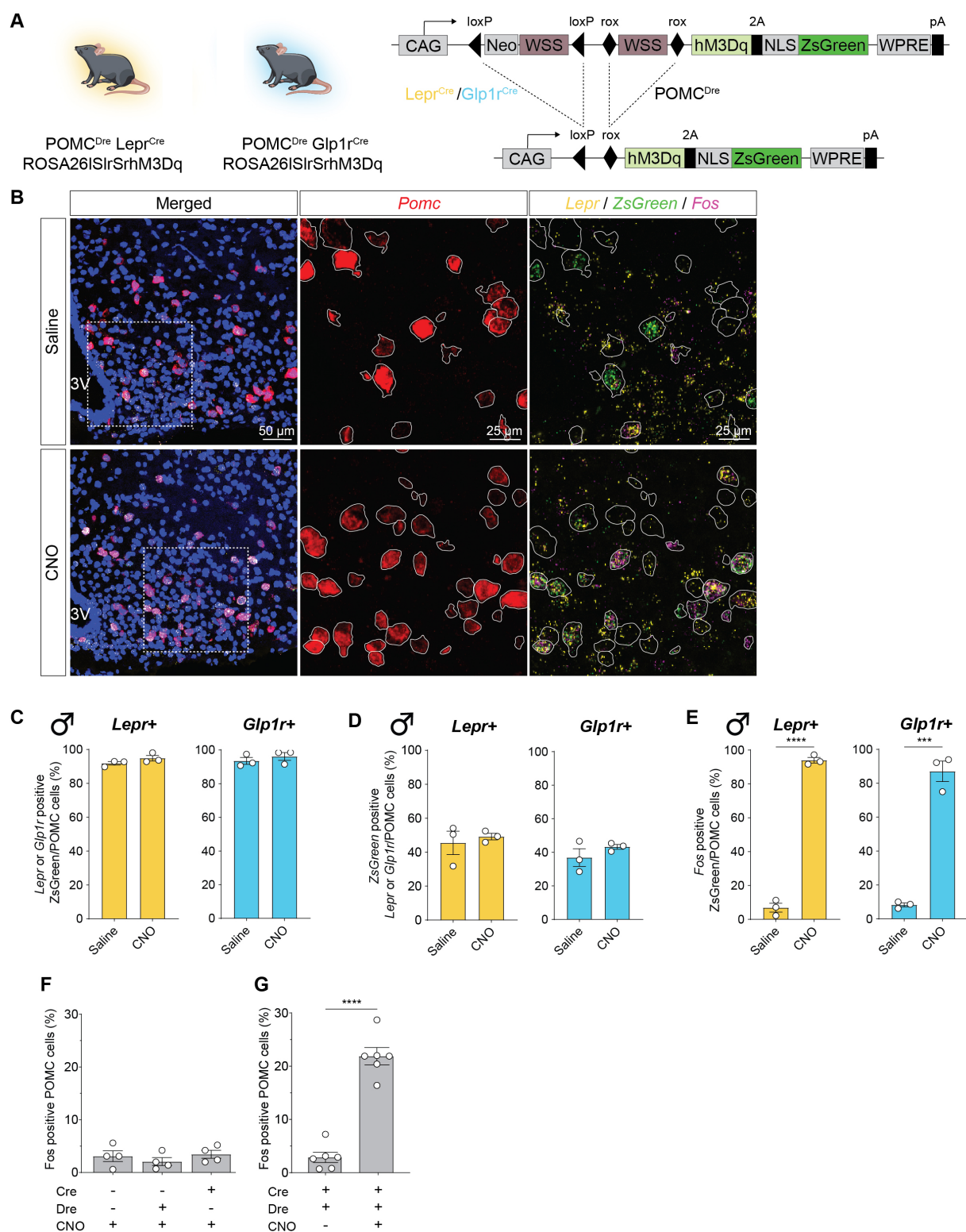


Figure 3.10 Cre/Dre-dependent hM3Dq transgenic lines allow for specific neuronal activation solely in triple transgenic mice.

(A) Illustrations of experimental mice and schematic diagram showing Dre- and Cre-dependent targeted expression of activatory hM3Dq in either POMC^{Lepr+} or POMC^{Glp1r+} neurons. Excision of flox

and rox-flanked stop cassettes through recombination of both Dre and Cre drivers leads to hM3Dq expression in the targeted subpopulation. (B) Representative microscopic images of RNA *in situ* hybridization against *Pomc*, *Lepr*, *ZsGreen* (in lieu of hM3Dq) and *Fos* in POMC^{Dre} Lepr^{Cre} ROSA26ISlrSrhM3Dq males injected with saline (top) or CNO (bottom). Images on the left show ISH in the ARC with nuclear counterstain (blue, DAPI). Magnifications of the dashed boxes are displayed on the right showing the indicated stainings. *Pomc*-positive neurons have been traced with a white outline. Scale bars represent 50 μ m in the merged image and 25 μ m in the magnifications. 3V=third ventricle. (C-E) Percentage of *ZsGreen-Pomc*-positive cells expressing *Lepr* or *Glp1r* (C), percentage of *Lepr/Glp1r-Pomc*-positive cells expressing *ZsGreen* (D) and percentage of *ZsGreen-Pomc*-positive cells expressing *Fos* (E) in POMC^{Dre} Lepr^{Cre} ROSA26ISlrSrhM3Dq or POMC^{Dre} Glp1r^{Cre} ROSA26ISlrSrhM3Dq male mice (22-26 weeks old) injected with saline or CNO. n=3. (F-G) Percentage of *Pomc*-positive cells expressing *Fos* in the different CNO-injected genotype controls (F) and triple transgenic animals injected with saline or CNO (G) of POMC^{Dre} Lepr^{Cre} ROSA26ISlrSrhM3Dq and POMC^{Dre} Glp1r^{Cre} ROSA26ISlrSrhM3Dq mice. n=4-6. CNO= 3 mg/kg.

The same procedure was followed in order to specifically express the activatory hM3Dq in POMC^{Glp1r+} neurons (representative image not shown). Homozygous ROSA26ISlrSrhM3Dq^{+/+} mice were bred with double positive POMC^{Dre} Glp1r^{Cre} mice. Assessment of *Fos* expression in these mice showed upon CNO injection increased *Fos* expression to 90% in comparison to a 6% expression detected with saline (Fig. 3.10E). Importantly, *Fos* expression did not increase upon CNO injection in any of the control groups for either subpopulation meaning that the combination of ROSA26ISlrSrhM3Dq with either the Dre, Cre recombinase alone and also in the absence of both could not activate the hM3Dq receptor (Fig. 3.10F-G). These experiments demonstrate that the ROSA26ISlrSrhM3Dq mouse line serves as a useful tool for activation of specific subpopulations of neurons upon combinatorial Cre/Dre-based recombination.

After having verified the functionality of the Cre/Dre-dependent DREADD mouse line, we carried out experiments to investigate the physiological effects of activating either the POMC^{Lepr+} or POMC^{Glp1r+} neuronal populations. To monitor food intake, we injected POMC^{Dre} Lepr^{Cre} ROSA26ISlrSrhM3Dq^{+/-} or POMC^{Dre} Glp1r^{Cre} ROSA26ISlrSrhM3Dq^{+/-} animals and their respective controls with either saline or CNO at two time points i.e., one hour before the onset of dark and once again 4 hours into the dark cycle. Saline or CNO treatment did not alter food intake in the genotype controls in male mice (Fig 3.11A-B).

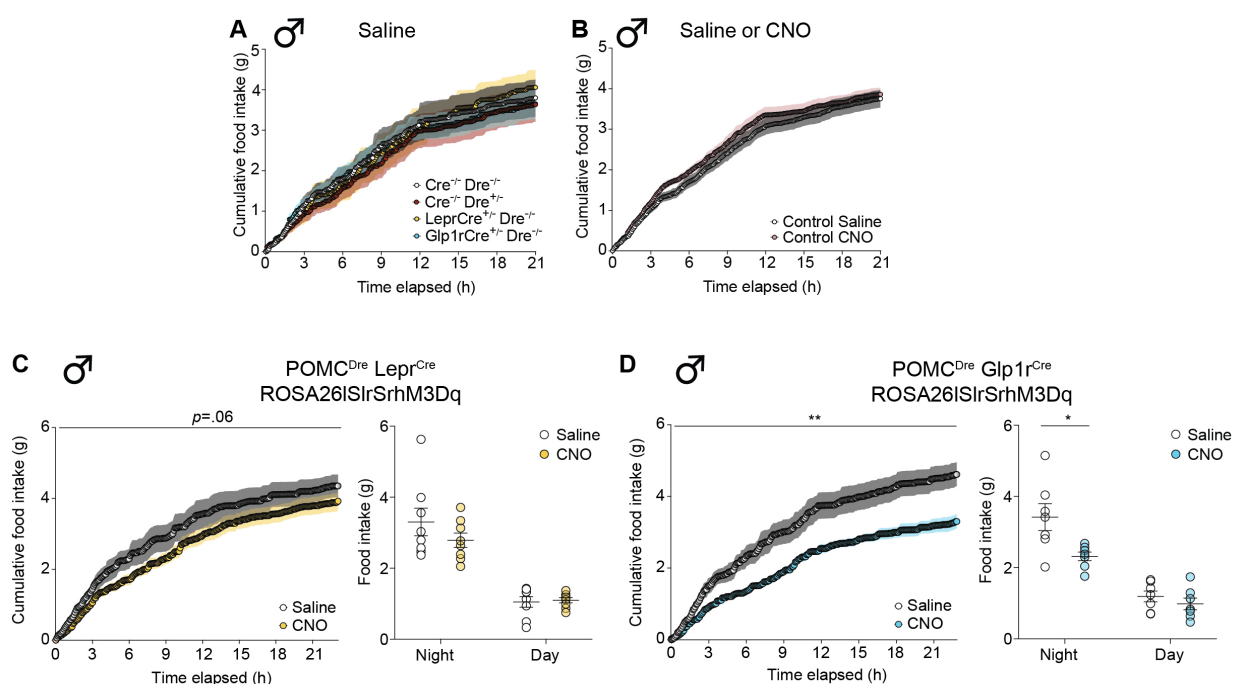


Figure 3.11 Chemogenetic activation of POMC^{Lepr+} and POMC^{Glp1r+} neurons differentially suppresses food intake in male mice without eliciting a response in genotype controls.

(A) Cumulative food intake of the various control groups. (B) Control groups pooled to show food intake after treatment with either saline or CNO. (C and D) Food intake over a time course of 24 hours in POMC^{Dre} Lepr^{Cre} ROSA26ISlrSrhM3Dq (C) and POMC^{Dre} Glp1r^{Cre} ROSA26ISlrSrhM3Dq male mice (D) starting with the night cycle. Mice were injected with saline at 18:00 and 23:00, followed by one day gap and subsequent CNO injections at 18:00 and 23:00 on the next day. Left: Cumulative food intake in mice injected with saline vs. CNO. Right: Total food intake during night and day. n=8 (C), n=7 (D). CNO= 3 mg/kg.

CNO injections of male POMC^{Dre} Lepr^{Cre} ROSA26ISlrSrhM3Dq^{+/-} mice reduced food intake 3 hours after injection. The cumulative food intake showed 15.6% suppression of food intake. On the other hand, injecting CNO into POMC^{Dre} Glp1r^{Cre} ROSA26ISlrSrhM3Dq^{+/-} male mice resulted in an earlier (2.5 h after CNO injection) and stronger suppression of feeding, culminating into an overall 32.3% reduction in food intake over the duration of the dark cycle. In contrast, activating POMC^{Lepr+} and POMC^{Glp1r+} neurons in female mice via chemogenetics had no effect on feeding behavior, despite an elevation in *Fos* induced upon injection of CNO in female POMC^{Dre} Lepr^{Cre} ROSA26ISlrSrhM3Dq and POMC^{Dre} Glp1r^{Cre} ROSA26ISlrSrhM3Dq mice as displayed in Figure 3.12.

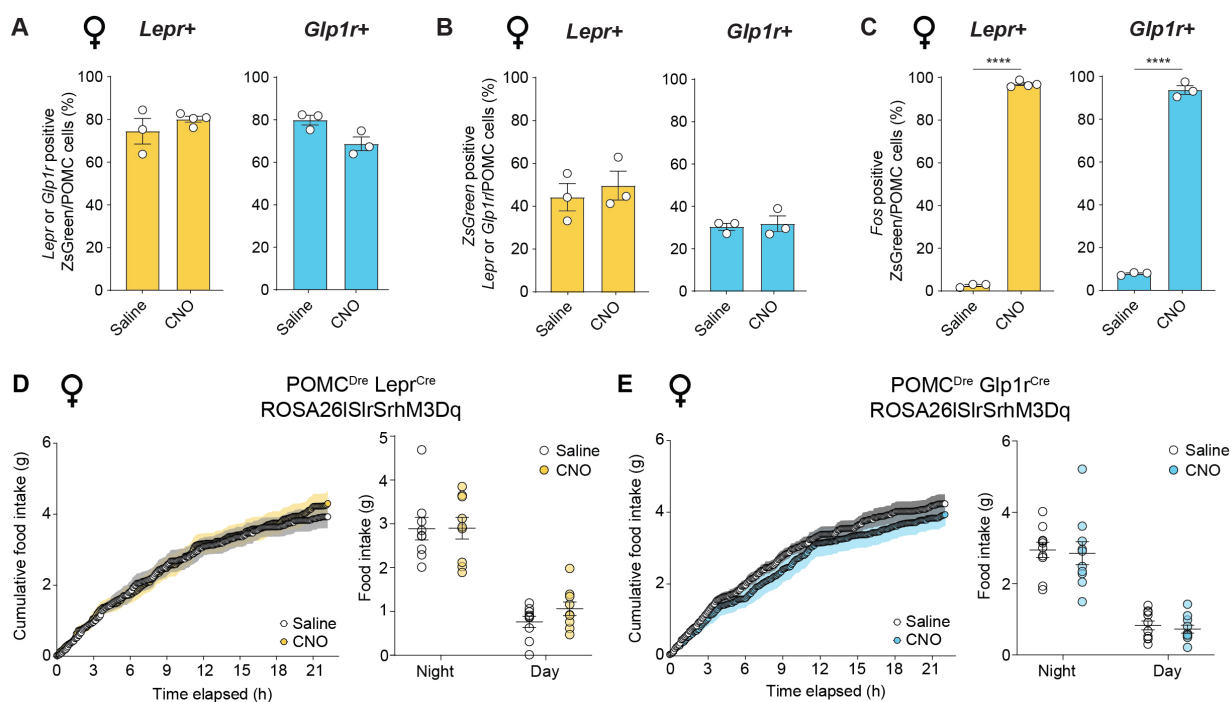


Figure 3.12 Chemogenetic activation of POMC^{Lepr+} and POMC^{Glp1r+} neurons does not affect food intake in female mice.

(A-C) Percentage of *ZsGreen-Pomc*-positive cells expressing *Lepr* or *Glp1r* (A), percentage of *Lepr/Glp1r-Pomc*-positive cells expressing *ZsGreen* (B) and percentage of *ZsGreen-Pomc*-positive cells expressing *Fos* (C) in POMC^{Dre} Lepr^{Cre} ROSA26ISlrSrhM3Dq or POMC^{Dre} Glp1r^{Cre} ROSA26ISlrSrhM3Dq females (22-26 weeks old) injected with saline or CNO. n=3. (D-E) Food intake over a time course of 24 hours in POMC^{Dre} Lepr^{Cre} ROSA26ISlrSrhM3Dq (D) and POMC^{Dre} Glp1r^{Cre} ROSA26ISlrSrhM3Dq female mice (E) starting with the night cycle. Mice were injected with saline or CNO as described for males. Left: Cumulative food intake in mice injected with saline vs. CNO. Right: Total food intake during night and day. n=9 mice/group (D), n=10 mice/group (E). CNO= 3 mg/kg.

Metabolic assessment was carried out on these mice by indirect calorimetry methods. In this instance, the mice were injected with either saline or CNO for a total of three times i.e., one hour before the onset of dark and once again 4 hours into the dark cycle and two hours after the onset of the light cycle. The results in Figure 3.13 demonstrate that chemogenetic activation of POMC^{Lepr+} or POMC^{Glp1r+} neurons in male mice had no impact on energy expenditure or locomotor activity. Although a reduction in respiratory exchange ratio (RER) was observed that indicates a switch to utilization of fatty acids in both triple transgenic models (Fig. 3.13C-D).

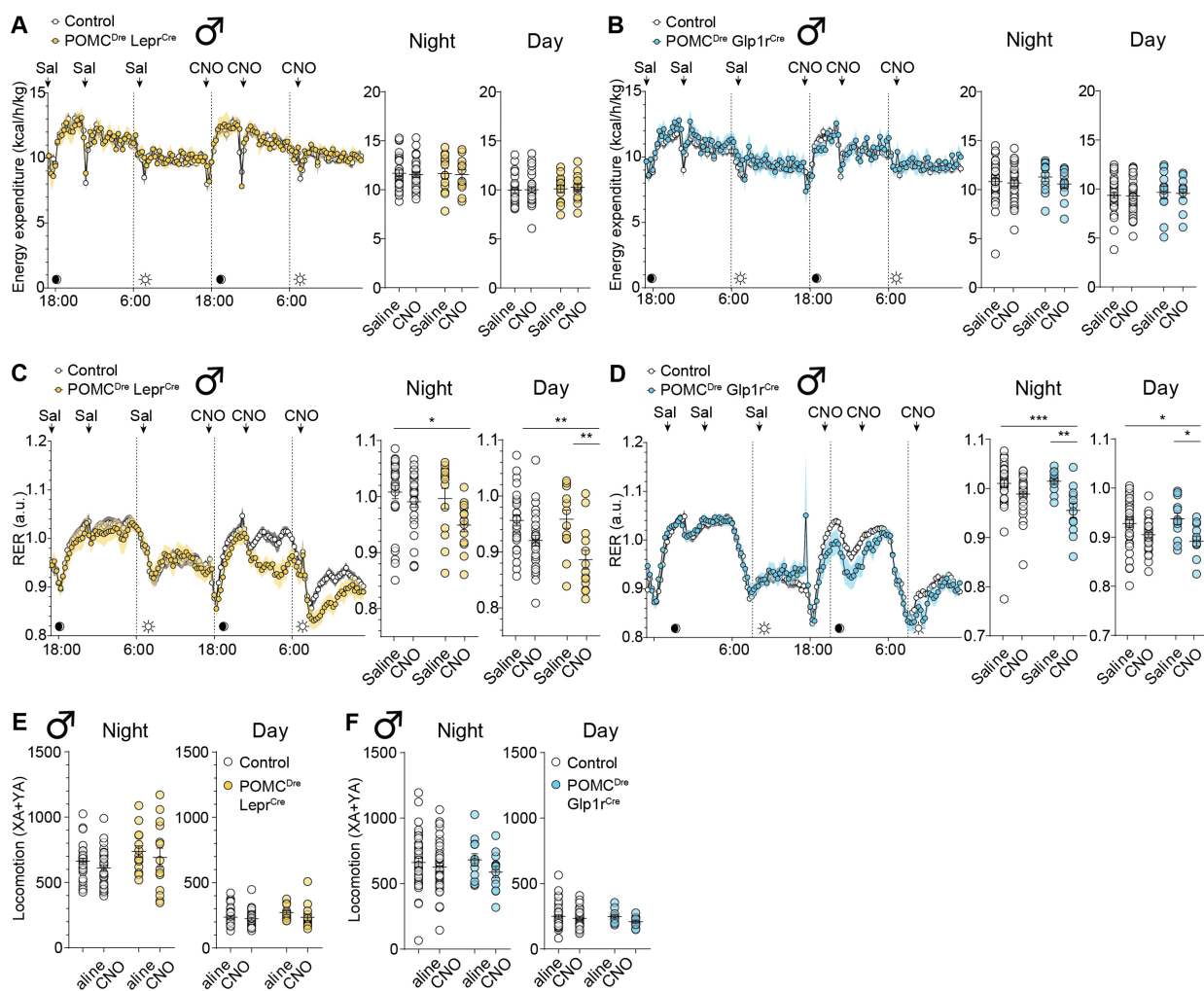


Figure 3.13 Chemogenetic activation of POMC^{Lepr+} and POMC^{Glp1r+} neurons leads to reduced RER.

(A-B) Energy expenditure (C,D), RER and (E,F) locomotion in (A,C,E) POMC^{Dre} Lepr^{Cre} ROSA26|SlrSrhM3Dq (B,D,F) and POMC^{Dre} Glp1r^{Cre} ROSA26|SlrSrhM3Dq male mice vs. controls at 12-14 weeks of age. Mice were injected with saline at 17:00, 22:00 and 07:00 followed by CNO at 17:00, 22:00 and 07:00 on the next day. Scatter plots on the right show the average values during night and day as averaged from left graph. Values of control animals were pooled from all corresponding genotype controls.

Due to the differential regulation of food intake observed in activating POMC^{Glp1r+} neurons compared to POMC^{Lepr+} neurons in male mice, we were interested in the neurotransmitter properties of the two POMC neuron subpopulations. We thus compared the

expression of vesicular GABA transporter (*Vgat*, *Slc32a1*) and that of the vesicular glutamate transporter (*Vglut2*, *Slc17a6*) in POMC^{Dre} Lepr^{Cre} ROSA26ISlrSrhM3Dq^{+/-} or POMC^{Dre} Glp1r^{Cre} ROSA26ISlrSrhM3Dq^{+/-} animals by *in situ* hybridization (Fig. 3.14A). Quantification of the proportion of this analysis in both mouse lines revealed a higher expression of *Vglut2* in POMC^{Lepr+} neurons in comparison to POMC^{Glp1r+} neurons (Fig. 3.14B).

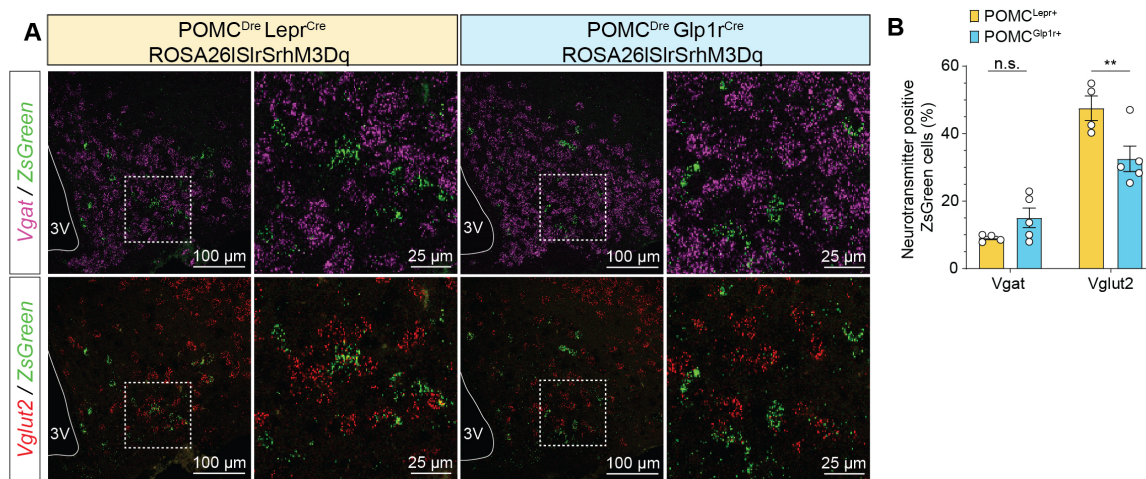


Figure 3.14 *Vgat* or *Vglut2* expression in POMC^{Lepr+} and POMC^{Glp1r+} neurons.

A) Representative microscopic images of RNA *in situ* hybridization against *ZsGreen* and *Vgat* or *Vglut2* in POMC^{Dre} Lepr^{Cre} ROSA26ISlrSrhM3Dq (left) and POMC^{Dre} Glp1r^{Cre} ROSA26ISlrSrhM3Dq (right) male mice. Scale bars represent 100 μ m in the merged image and 25 μ m in the magnifications. (B) Quantification of the percentage overlap of *Vgat* or *Vglut2* with *ZsGreen*-expressing cells. n=4-5 mice. Data are represented as mean \pm SEM. Statistical analyses on B were performed by two-way-ANOVA with Sidak's post-hoc test. * $p \leq 0.05$, ** $p \leq 0.01$, *** $p \leq 0.001$, **** $p \leq 0.0001$.

As mentioned previously (Section 3.1), POMC is also expressed in the anterior and intermediate lobe of the pituitary. Thus, *ZsGreen* expression was assessed in the pituitary of POMC^{Dre} Lepr^{Cre} ROSA26ISlrSrZsGreen^{+/-} or POMC^{Dre} Glp1r^{Cre} ROSA26ISlrSrZsGreen^{+/-} mice. Figures 3.15A and B shows *ZsGreen* expression in the intermediate lobe of both mouse lines. Subsequently, we measured serum concentrations of corticosterone in hM3Dq-expressing triple transgenic mice injected with either saline or CNO, one hour post injection. Figures 3.15 C and D demonstrates that no differences were observed in circulating corticosterone levels in

saline versus CNO-injected mice indicating that the regulation of feeding cannot be attributed to the function of the pituitary.

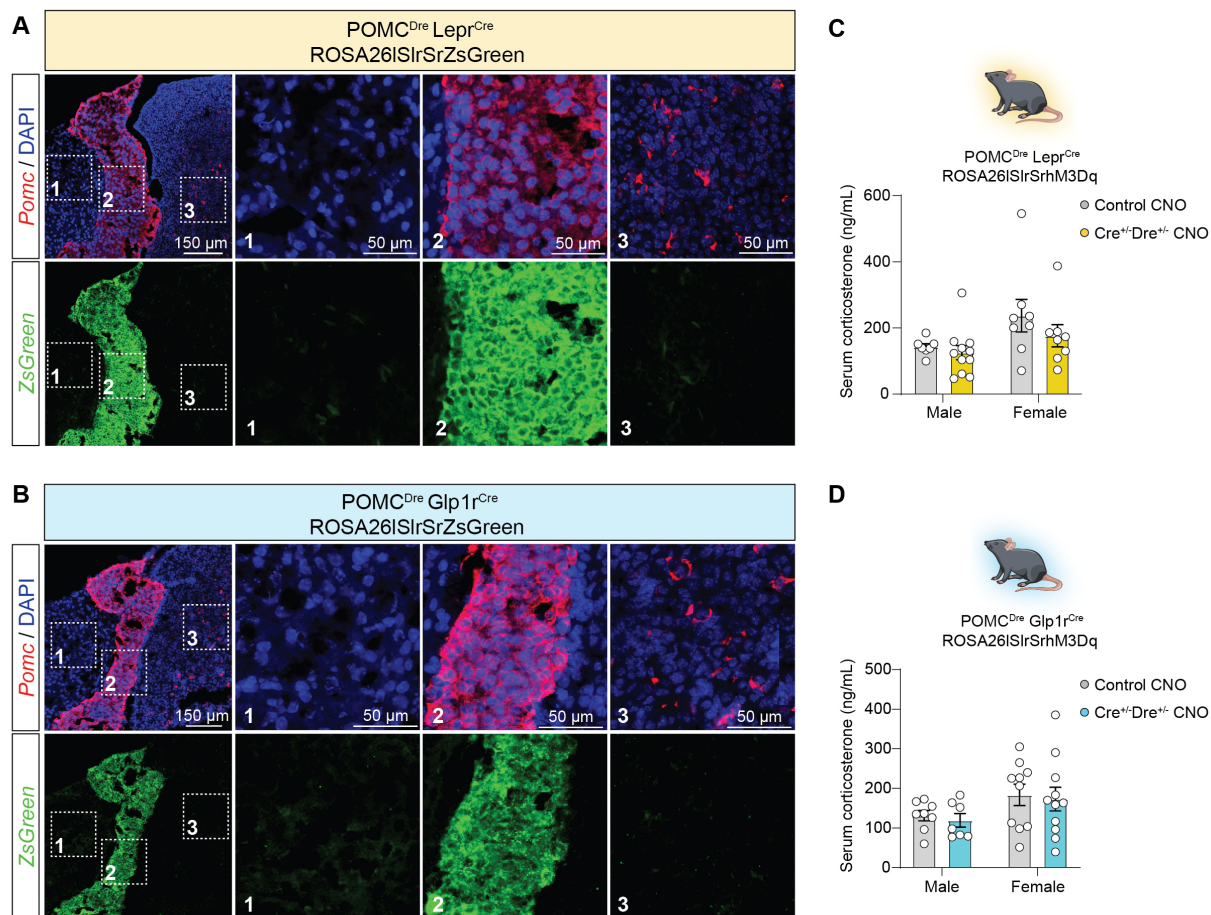


Figure 3.15 No effects observed on circulating corticosterone levels upon chemogenetic activation of POMC^{Lepr+} and POMC^{Glp1r+} neurons.

(A-B) Representative microscopic images of RNA *in situ* hybridization against ZsGreen in pituitary of POMC^{Dre} Lepr^{Cre} ROSA26ISrSrZsGreen (A) and POMC^{Dre} Glp1r^{Cre} ROSA26ISrSrZsGreen (B) mice, respectively. Scale bars represent 150 μm in the merged image and 50 μm in the magnifications. (C-D) Concentration of corticosterone in sera of CNO-treated POMC^{Dre} Lepr^{Cre} ROSA26ISrSrM3Dq (C) and POMC^{Dre} Glp1r^{Cre} ROSA26ISrSrM3Dq (D) male and female mice. n=7-10 mice /group. Mice were fasted for 2 hours and injected with CNO 1 hour into the fast, prior to serum collection. CNO= 3 mg/kg. Data are represented as mean ± SEM. Statistical analyses on (C-D) were performed by unpaired two-tailed Student's t test with Holm-Sidak correction for multiple comparisons.

3.6 Distinct translational signatures of POMC^{Lepr+} and POMC^{Glp1r+} neurons

At this point the heterogeneous nature of POMC^{Lepr+} and POMC^{Glp1r+} neurons was established on the basis of anatomical and functional characteristics and we aimed to understand more regarding the molecular features of these subpopulations. We used mice that express the L10a ribosomal protein fused to EGFP dependent on combinatorial Cre/Dre excision that would enable us to immunoprecipitate ribosomal subunits and bound mRNA in a cell-type specific manner. Triple transgenic EGFPL10-expressing mice were obtained by breeding homozygous ROSA26ISlrSrEGFPL10a^{+/+} mice to POMC^{Dre} Lepr^{Cre} or POMC^{Dre} Glp1r^{Cre} animals and the respective hypothalamic were pooled to create samples with extractable amounts of RNA. Due to the differences in neuronal numbers between genetically targeted POMC^{Lepr+} and POMC^{Glp1r+} neurons, hypothalami of 6 and 12 mice from POMC^{Dre} Lepr^{Cre} ROSA26ISlrSrEGFPL10a^{+/-} and POMC^{Dre} Glp1r^{Cre} ROSA26ISlrSrEGFPL10a^{+/-} transgenic lines were pooled. The pooled samples contained the same number of male and female hypothalamic. Pooled hypothalamic extracts from each transgenic line (biological replicates) served as input RNA samples that were subjected to anti-EGFP immunopurification of EGFP-tagged ribosomes of POMC^{Lepr+} or POMC^{Glp1r+} neurons, resulting in respective immunoprecipitate (IP) samples. Quality assessment of input and IP samples via automated gel-electrophoresis followed by RNA integrity number (RIN) computation confirmed successful and efficient pull down of that RNA from POMC neuronal subpopulations (approximately 500-1000 cells). Specificity of the pull down was verified by subjecting equivalent amounts of hypothalami from the genotype controls (ROSA26ISlrSrEGFPL10a^{+/-}, POMC^{Dre} ROSA26ISlrSrEGFPL10a^{+/-}, Lepr^{Cre} ROSA26ISlrSrEGFPL10a^{+/-}, or Glp1r^{Cre} ROSA26ISlrSrEGFPL10a^{+/-}), in which case no RNA was immunopurified. The expression of the EGFPL10a fusion in the ARC of the triple transgenic mouse lines was verified using immunohistochemistry against EGFP. After carrying out the necessary verification steps of the specificity of the double recombinase-dependent of EGFPL10a expression, the extracted RNA from IP and input samples of POMC^{Dre} Lepr^{Cre} ROSA26ISlrSrEGFPL10a^{+/-} and POMC^{Dre} Glp1r^{Cre} ROSA26ISlrSrEGFPL10a^{+/-} were sequenced. Once the reads were mapped, 17239 genes were identified which were subjected to principal component analyses (PCA). The resulting PCA of the highest expressed genes in each population, showed a clear separation of input (IN) from IP samples, as well as for POMC^{Dre} Lepr^{Cre} ROSA26ISlrSrEGFPL10a^{+/-} IP from POMC^{Dre} Glp1r^{Cre}

ROSA26ISlrSrEGFPL10a^{+/-} IP samples, confirming the similarity between the input samples and highlighting differences between IP and input (data not shown). We analyzed the enrichment or depletion levels of individual reads obtained from each neuronal group by normalizing each IP to its respective input. Subsequent to a statistical analysis of the normalized expression levels of identified genes within samples of each group, the resulting p-values were plotted to create a volcano plot (Fig. 3.16B).

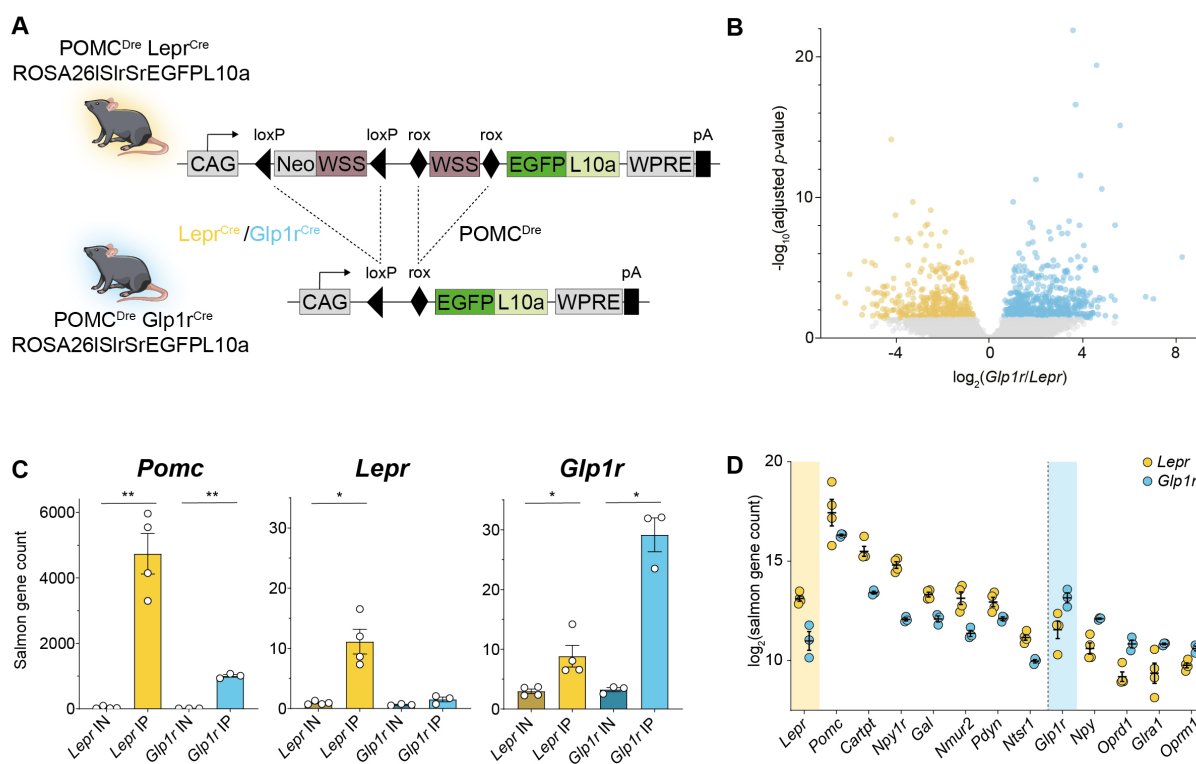


Figure 3.16 Transcriptomic profiling of POMC^{Lepr+} or POMC^{Glp1r+} neurons via targeted EGFPL10a expression.

(A) Illustration of experimental mice and schematic diagram showing Dre- and Cre-dependent targeted expression of EGFPL10a in either POMC^{Lepr+} or POMC^{Glp1r+} neurons. Excision of flox and rox-flanked stop cassettes through recombination of both Dre and Cre drivers leads to EGFPL10a expression in the targeted subpopulation. (B) Volcano plot of differentially ribotag-enriched transcripts in POMC^{Lepr+} and POMC^{Glp1r+} neurons. Significantly differentially enriched transcripts ($p < 0.05$) are indicated in the coloured region. Yellow and cyan depict a significantly higher enrichment in POMC^{Lepr+} and POMC^{Glp1r+} neurons, respectively. (C) Expression of *Pomc*, *Lepr* and *Glp1r* in input and IPs of each subpopulation. (D) Significantly differentially enriched genes ($p < 0.05$) of POMC^{Lepr+} and POMC^{Glp1r+} neurons, belonging to the GO-term "neuropeptide-signaling pathways". Vertical dashed line

separates higher enrichment in POMC^{Lepr+} neurons (left) from higher enrichment in POMC^{Glp1r+} neurons (right).

This plot demonstrates that a similar number of enriched transcripts were identified in the POMC^{Lepr+} neurons in comparison to POMC^{Glp1r+} neurons and vice versa. It was expected that both neuronal populations express high levels of *Pomc* mRNA and IPs from POMC^{Lepr+} neurons exhibited a stronger enrichment for *Pomc* mRNA compared to IPs from POMC^{Glp1r+} neurons, indicating that the two POMC subpopulations may exhibit a differential *Pomc* mRNA expression (Fig. 3.16C). Similarly, we also determined the enrichment of *Lepr*- and *Glp1r*-expression in these samples and found clear overrepresentation for the reads of the *Lepr* in IPs from POMC^{Lepr+} neurons and an enrichment of *Glp1r*-expression in IPs from POMC^{Glp1r+} neurons (Fig. 3.16C). Together these findings indicate the successful and specific isolation and sequencing of RNA isolated from tagged ribosomes from the genetically, differentially targeted POMC subpopulations.

The next step was to distinguish the categories of transcripts that differ between the differentially enriched genes in POMC^{Lepr+} and POMC^{Glp1r+} neurons. A GO-term analysis on the basis of molecular function, biological processes, and cellular component was carried out on the previously analyzed profiles. It is noteworthy that transcripts categorized within GO-terms of neuropeptide signaling, regulation of response to nutrient levels, and dendrite cytoplasm were significantly different in both neuronal groups. This analysis sparked interest in identifying the neuropeptides and neuropeptide receptors differentially expressed by POMC^{Lepr+} and POMC^{Glp1r+} neurons. The plotted relative expression levels (*gene count IP / gene count input* for each individual sample) of selected genes listed in the GO-term “neuropeptide signaling pathway” (GO-ID: 0007218) is shown in Figure 3.17. For instance, opioid-receptors (*Oprd1* and *Oprm1*) and NPY-enrichments were higher in IPs from POMC^{Glp1r+} neurons, enrichment for Prodynorphin (*Pdyn*), galanin (*Gal*), Cocaine and amphetamine regulated transcript protein (*Cartpt*), Neuromedin-U receptor 2 (*Nmur2*), and NPY-receptor (*Npy1r*) was higher in IPs from POMC^{Lepr+} neurons (Fig. 3.16D).

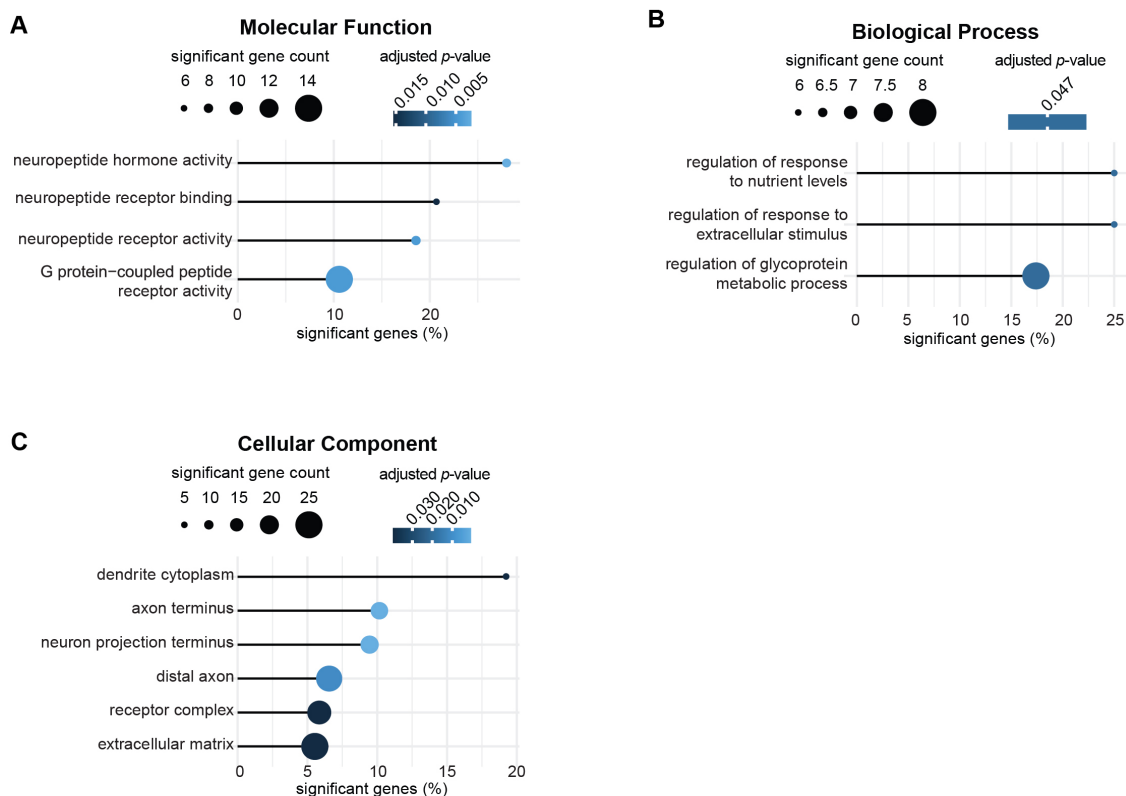


Figure 3.17 GO-term analysis on of the differently expressed genes between the POMC^{Lepr+} and POMC^{Glp1r+}.

(A-C) GO term representations of the differently expressed genes between the Lepr⁺ and Glp1r⁺ clusters mapping the percentage of regulated genes to the total GO term gene count against significant gene count and adjusted p-value per term. *p*-values were calculated using the DESeq2 1.26.0 pipeline.

We were next interested in comparing the translational profiles obtained within the current study from POMC^{Lepr+} and POMC^{Glp1r+} neurons to publicly available datasets of single-cell mRNA sequencing and the identified clusters. Two source datasets were used: the droplet single-cell mRNA sequencing (RNA-Seq) of 20,921 cells from the ARC and ME and a single-cell mRNA-sequencing dataset of 163 EGFP-expressing POMC neurons for which four clusters were identified. In order to limit the data from the ARC/ME single sequencing to *Pomc*-expressing cells only, the data was filtered for *Pomc* using the R Seurat package and 11 clusters were found (4,248/20,921 cells). Following this, the volcano plot from Figure 3.16B was filtered for markers of the clusters defined in the source datasets. The log-ratio of the marker genes expressed differentially between POMC^{Lepr+} and POMC^{Glp1r+} neurons in our

ribosomal profiling were calculated ($\log\text{Ratio}=\log_2 (n_{\text{Glp1r}}/n_{\text{Lepr}})$). A cluster was considered enriched for POMC^{Glp1r+} marker genes with $\text{rlogRatio}\geq 2$ and *vice-versa* enriched for POMC^{Lepr+} marker genes with $\text{rlogRatio}\leq -2$. When we employ this threshold on the 11 POMC-positive neurons from the ARC/median eminence data set, clusters 2 and 10 are classified as enriched for POMC^{Lepr+}-marker genes and cluster 3 for POMC^{Glp1r+}-marker genes. With the same basis, clusters 3 and 4 of the EGFP-expressing POMC neurons were identified as enriched for POMC^{Lepr+} and cluster 1 and 2 enriched for POMC^{Glp1r+}-marker genes. The representation of the results of this analysis is displayed in Figure 3.18.

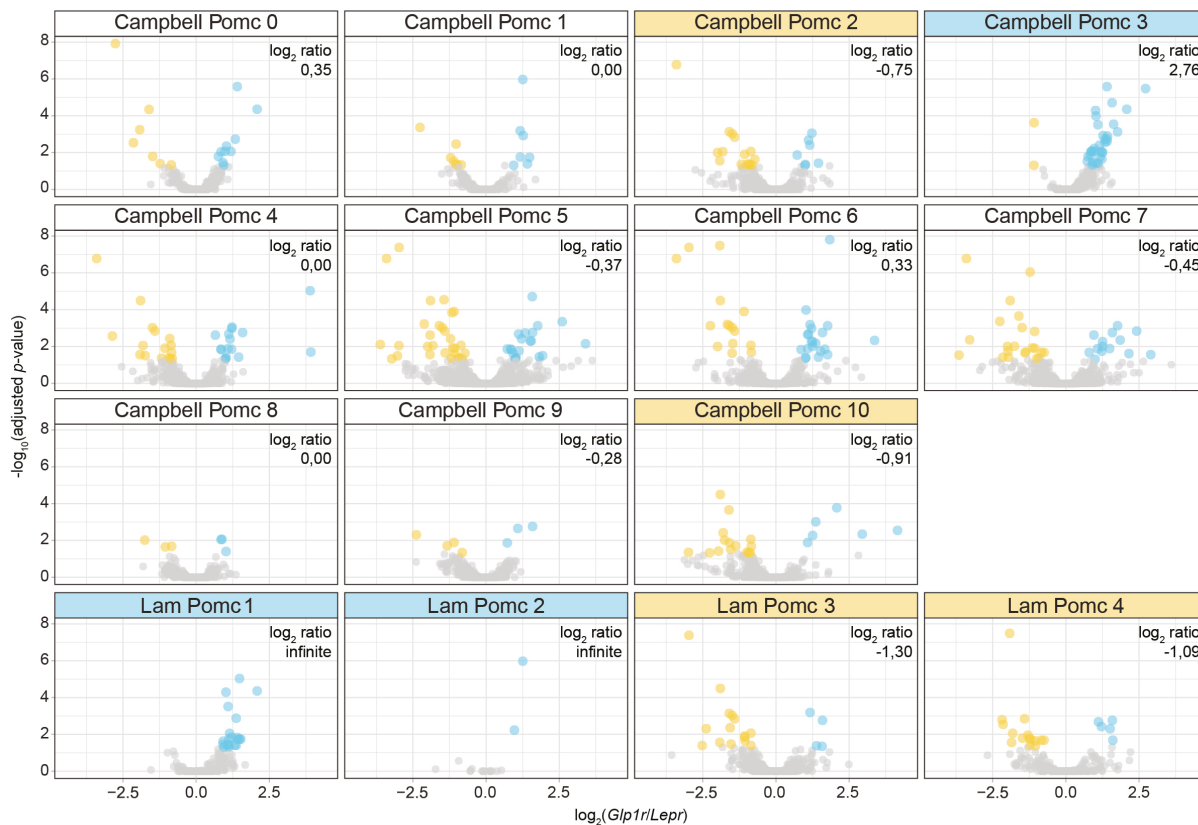


Figure 3.18 Overlap analysis of the publicly available single-cell RNA-sequencing data from mouse hypothalamic with our dataset.

Collectively, our translational profiles of POMC^{Lepr+} and POMC^{Glp1r+} neurons allowed for successful independent identification of molecularly defined POMC clusters, which had been defined based on single cell mRNA sequencing, further supporting the notion that *Glp1r* and *Lepr* expression defines specific POMC neuron populations. Moreover, it highlights the complementary potential to further define heterogeneous neuronal populations based on the

integration of single cell mRNA sequencing results with in depth translational profiles via combinatorial recombinase-based ribosomal profiling of molecularly defined neuronal populations in general.

3.7 Verification of endogenously expressed, differentially regulated genes in POMC^{Lepr+} and POMC^{Glp1r+} neurons

We carried out RNA *in situ* hybridization to validate the mRNA expression of genes identified as differentially enriched in the genetically labeled POMC^{Lepr+} and POMC^{Glp1r+} neurons. We probed against *Pomc*, *Lepr*- and *Glp1r*-mRNA in wildtype mice and checked for co-expression with *Cartpt*, *Npy1r*, *Oprm1* and *Nmur2*.

Quantification of these results primarily confirmed the enrichment of *Pomc* mRNA in POMC^{Lepr+} compared to POMC^{Glp1r+} neurons as detected in the sequencing experiments. In accordance with this observation, *Cartpt* expression was higher in POMC neurons expressing *Lepr* than those expressing *Glp1r*. The differential enrichment of genes encoding neuropeptide receptors such as *Npy1r*, *Oprm1* and *Nmur2* were found to have the same directionality as identified in the RNA-sequencing experiments within the two subpopulations. Collectively, ribotrap-based profiling of heterogeneous POMC populations allowed for reliably identifying distinct signatures predictive of differential neuropeptide release and responses to neuropeptides in these two populations of POMC neurons (Fig. 3.19).

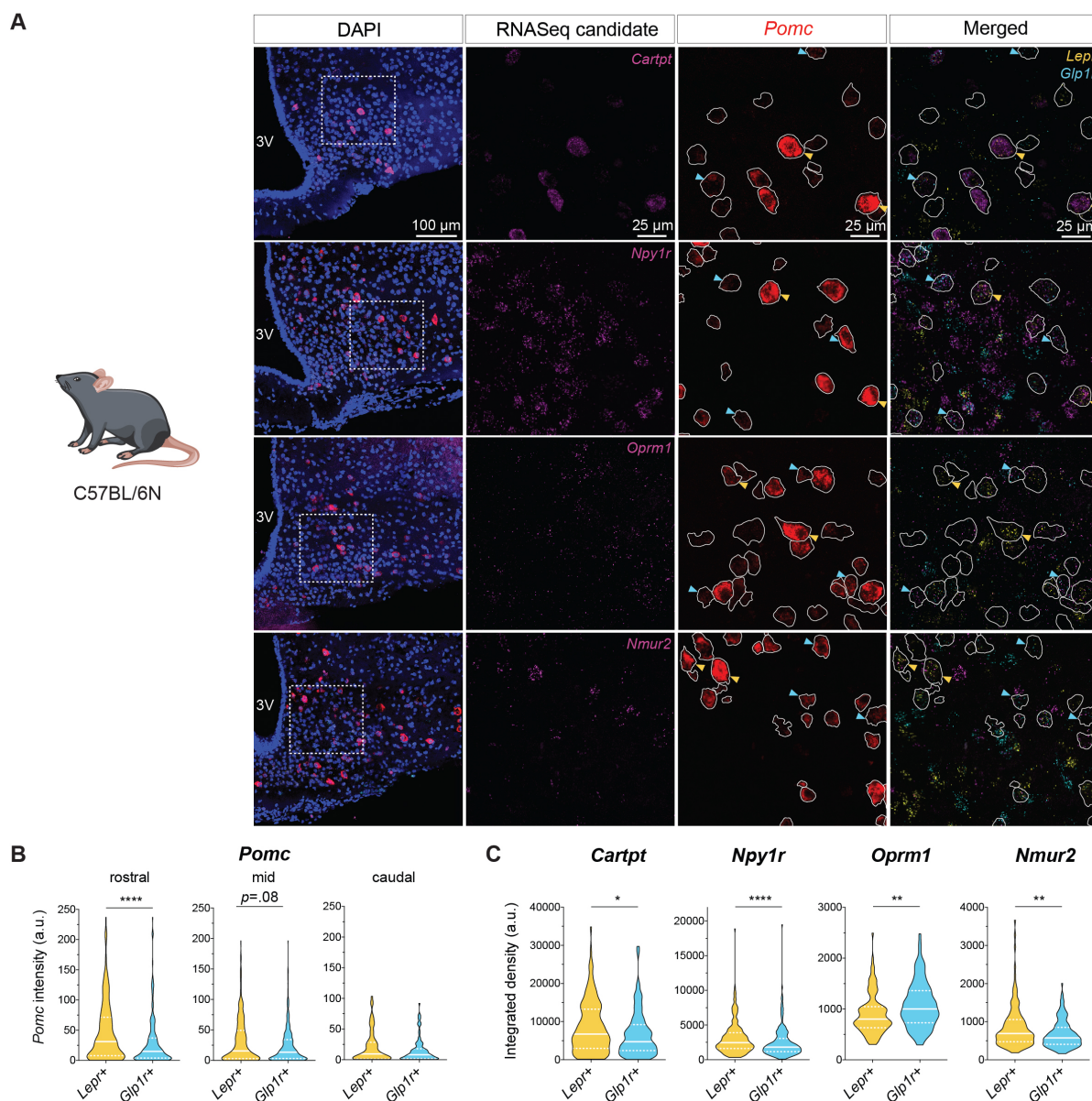


Figure 3.19 Differential expression of endogenous mRNA for identified candidates in $POMC^{Lepr+}$ and $POMC^{Glp1r+}$ neurons.

(A) Representative microscopic images of RNA *in situ* hybridization against *Pomc*, *Glp1r*, *Lepr* together with differentially expressed neuropeptidergic signaling candidate RNAs, identified in the ribotag-experiments, *Cartpt*, *Npy1r*, *Oprm1* and *Nmur2* in C57BL/6N mice at 12 weeks of age. First image shows ISH in the ARC with nuclear counterstain (blue, DAPI). Magnifications of the dashed boxes are displayed on the right showing the indicated stainings. *Pomc*-positive neurons have been traced with a white outline. Yellow and cyan arrows indicate *Lepr* or *Glp1r*-positive POMC neurons, respectively. Scale bars represent 100 μm in the merged image and 25 μm in the magnifications. (B) Violin plots showing the quantified intensity (a.u.) of *Pomc* mRNA across the rostro-caudal axis of the ARC in

POMC^{Lepr+} or POMC^{Glp1r+} neurons. n=4 mice. (C) Violin plots showing quantified expression of the RNASeq candidates measured as integrated density in POMC^{Lepr+} or POMC^{Glp1r+} neurons as assessed from RNA *in situ* hybridization (A). n=4 mice. In B-C solid white lines represent median, dashed white lines represent lower and upper quartile. *p*-values were calculated using the unpaired Mann-Whitney rank test.

3.8 POMC^{Lepr+} and POMC^{Glp1r+} neurons have distinct intrinsic electrophysiological properties

The electrophysiological properties of POMC^{Lepr+} and POMC^{Glp1r+} neurons were investigated using perforated patch-clamp recordings on the genetically targeted neurons in POMC^{Dre} Lepr^{Cre} ROSA26|SlrSrZsGreen^{+/-} or POMC^{Dre} Glp1r^{Cre} ROSA26|SlrSrZsGreen^{+/-} mice (Performed by Jan Radermacher and Dr. Lars Paeger). As displayed in Figure 3.20 POMC^{Glp1r+} neurons depolarized more and had higher cell input resistance and were more excitable in comparison to POMC^{Lepr+} neurons.

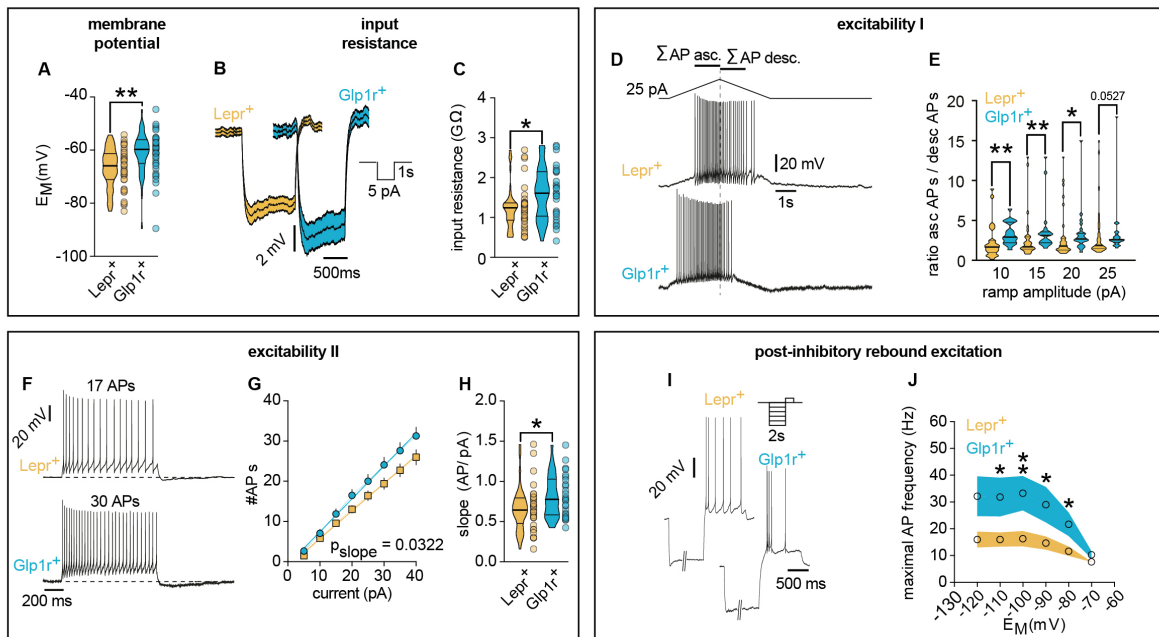


Figure 3.20 POMC^{Lepr} and POMC^{Glp1r} neurons exhibit different intrinsic properties.

Representative electrophysiological recordings of (A) Membrane potential of POMC^{Lepr+} and POMC^{Glp1r+} neurons (POMC^{Lepr+} n=38; POMC^{Glp1r+} n=39). (B, C) Input resistance. Mean response to 5pA hyperpolarizing current pulses (B) and violin plots (C) showing the input resistance of POMC^{Lepr+} and POMC^{Glp1r+} neurons (POMC^{Lepr+} n=37; POMC^{Glp1r+} n=28). (D, E) Excitability I. Original recording

illustrating a depolarizing ascending and descending current ramp protocol in POMC^{Lep^r+} and POMC^{Glp1^r+} neurons (D) and respective spike number ratios of the ascending and descending phase of the protocol in POMC^{Lep^r+} and POMC^{Glp1^r+} neurons (E; POMC^{Lep^r+} n=34; POMC^{Glp1^r+} n=24). (F-H) Excitability II. Example responses to 30 pA pulses (F). Number of action potentials as a function of current pulse amplitude. (G) in POMC^{Lep^r+} and POMC^{Glp1^r+} neurons and the respective slopes (H). (POMC^{Lep^r+} n=32; POMC^{Glp1^r+} n=26). (I, J) Post-inhibitory rebound excitation. Original recordings illustrating the responses to a depolarizing current pulse that followed a pro-longed (2s) hyperpolarizing pre-pulse (I). Mean maximal instantaneous frequency as function of the pre-pulse potential for POMC^{Lep^r+} and POMC^{Glp1^r+} neurons (J, n=19-32). Data generated by Jan Radermacher and Dr. Lars Paeger.

Prolonged depolarization experiments revealed phasic activity in POMC^{Glp1^r+} neurons and tonic activity in response to sustained excitatory output. Application of ascending and subsequent descending current ramps resulted in a higher number of action potentials in POMC^{Glp1^r+} during ascending ramps compared to their counterparts while the opposite effect was observed during descending ramps i.e., higher action potentials in POMC^{Lep^r+} neurons. Thus, the spike number ratio between the ascending and descending ramp in POMC^{Glp1^r+} neurons was significantly higher that implies a voltage-dependent adaptation of neuronal activity in these neurons. To summarize, it is likely that POMC^{Glp1^r+} neurons respond to sustained excitatory input with phasic, adaptive excitability.

In addition, the frequency-current relationships, post-inhibitory rebound, spike frequency adaptation, and sag potentials during hyperpolarization from both POMC^{Glp1^r+} and POMC^{Lep^r+} neurons were measured. Once again, a higher excitability was observed in POMC^{Glp1^r+} neurons, verified by a “steeper” frequency-current relationship. The post-inhibitory rebound excitation in POMC^{Glp1^r+} neurons was more pronounced, despite smaller sag potentials during prolonged hyperpolarization.

3.8.1 Specific regulation of POMC^{Lepr+} and POMC^{Glp1r+} neurons by energy state sensing signals

To investigate the response of each neuronal population to stimulation with their respective ligands i.e., leptin and Glp1. POMC^{Dre} Lepr^{Cre} ROSA26ISrSrZsGreen^{+/-} or POMC^{Dre} Glp1r^{Cre} ROSA26ISrSrZsGreen^{+/-} mice were used for electrophysiological recordings. In the presence of blockers for glutamatergic and GABAergic synaptic input, leptin (100 nM) depolarized 40% and hyperpolarized 20% of POMC^{Lepr+} neurons and 40% did not respond (Fig. 3.21A-D). On the other hand, 60% of POMC^{Glp1r+} neurons were non-responsive to leptin and surprisingly, 40% of the cells were inhibited (Fig. 3.22 D-E).

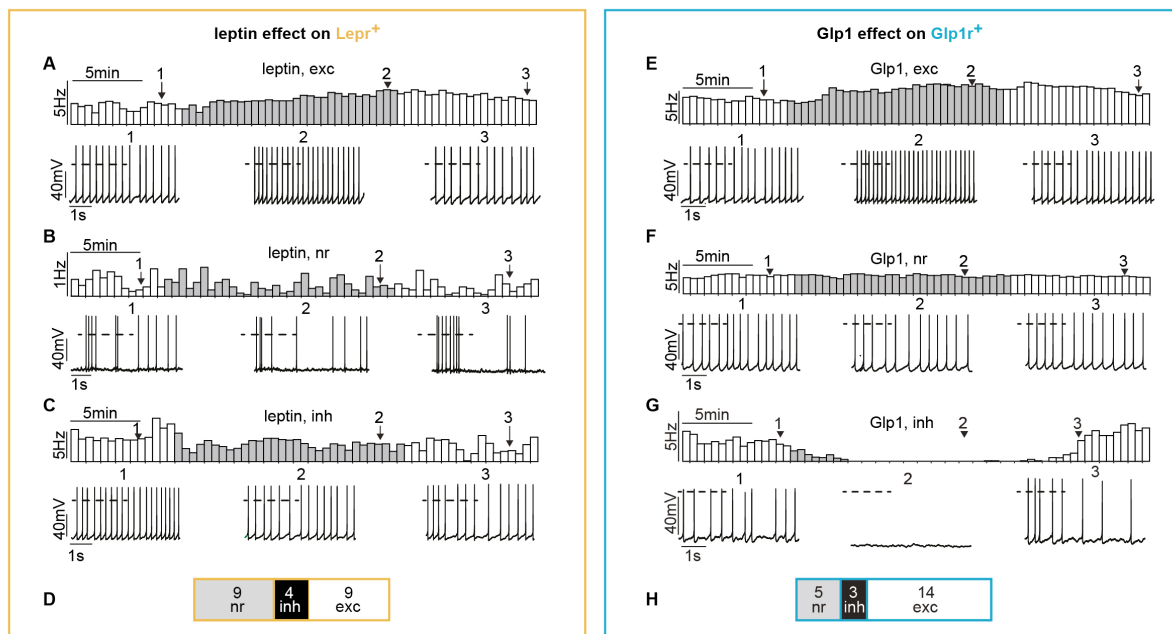


Figure 3.21 Electrophysiological recordings of the effect of leptin and Glp1 on transgenic labeled POMC^{Lepr} and POMC^{Glp1r} neurons, respectively.

(A-C) Example electrophysiological recordings of the effect of leptin in POMC^{Dre} Lepr^{Cre} ROSA26ISrSrZsGreen and (E-G) Glp1 in POMC^{Dre} Glp1r^{Cre} ROSA26ISrSrZsGreen mice. A and E display representations of excited, B and F, non-responsive and C and G, inhibited traces. D and H show the total number of neurons grouped according to their response type. The population responses were compared by using ANOVA with post-hoc Tukey tests (POMC^{Lepr+} n = 14; POMC^{Glp1r+} n = 12. **p<0.01. Data generated by Jan Radermacher and Svenja Corneliussen.

Glp1 (300nM) treatment on POMC^{Glp1r+} excited 63% of these neurons and inhibited 13% while 22% remained unaffected (Fig. 3.21E-H). When POMC^{Lepr+} neurons were treated with Glp1, 18% were hyperpolarized and the remaining 81%, non-responsive (Fig. 3.22D-E). To rule out effects interactions within the network of neurons responsive to these hormonal stimuli, recordings were carried out in the presence of tetrodotoxin (TTX) (1 μ M) to block action-potential-dependent signaling in addition to glutamatergic and GABAergic synaptic transmission blockage. These experimental conditions resulted in 14% of POMC^{Lepr+} neurons excited by Glp1, 6% were inhibited and the majority (80%) were not affected (Fig. 3.22C). When treated with leptin, 91% of POMC^{Glp1r+} neurons were hyperpolarized in a reversible manner and only 9% were non-responsive (Fig. 3.22F) which is an overall interesting yet unexpected finding due to the lack of receptor in question on these cells indicating a possibility of spontaneous release from these neurons (Kavalali, 2015).

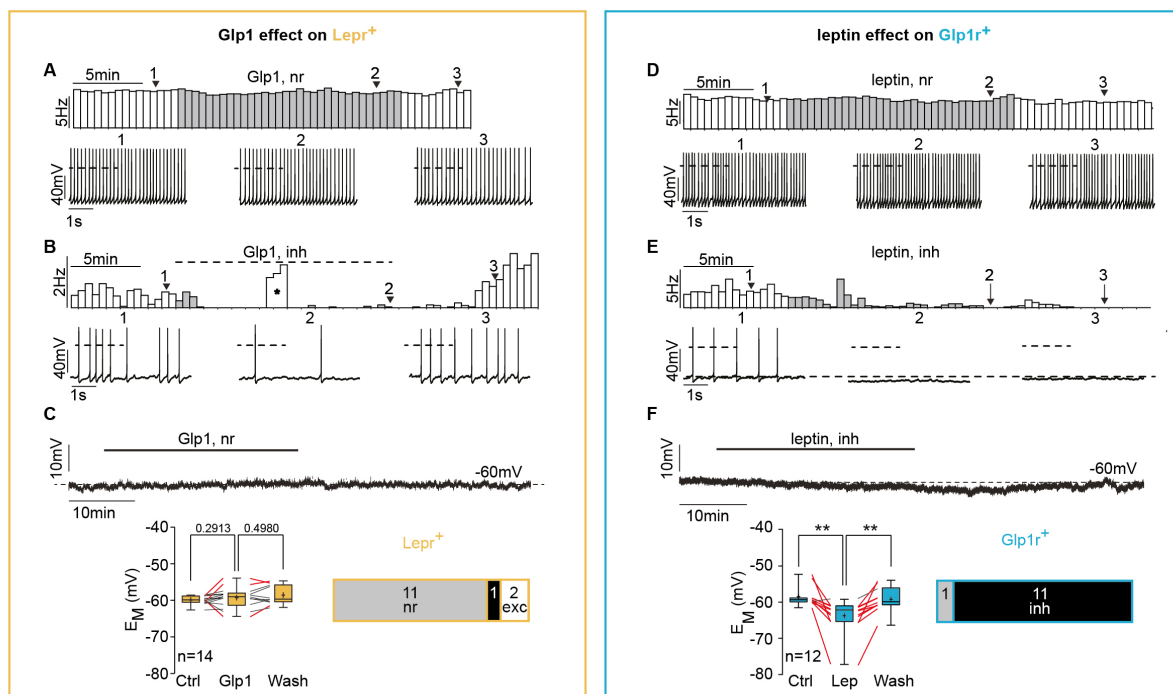


Figure 3.22 Representative traces showing the effect of Glp1 and leptin on transgenic labeled POMC^{Lepr} and POMC^{Glp1r} neurons, respectively.

(A-C) Example traces of the effect of Glp1 in POMC^{Dre LeprCre ROSA26lSlrSrZsGreen} and (D-F) leptin in POMC^{Dre Glp1rCre ROSA26lSlrSrZsGreen} mice. A and D display recordings of non-responsive and B and E, inhibited neurons. C and F demonstrate current clamp recordings in the presence of TTX (1 μ M) as well as the total number of neurons grouped according to their response type. Exemplary trace

(top) and summary and histogram of all recordings. Red lines indicate significance in membrane potential changes due to treatment. TTX suppresses synaptic release induced by action potentials. Data generated by Jan Radermacher and Svenja Corneliussen.

4 Discussion

In the recent decades, great advances in the understanding of POMC neurons and their role in energy metabolism regulation have been made. Developments in single cell RNA sequencing have given us insight into the heterogeneity of circuits that were previously well defined, including systems involved in the regulation of energy homeostasis. Insights into the heterogeneous nature of POMC neurons were corroborated by the electrophysiological studies demonstrating distinct responses to energy state-sensing hormones. Thus, we aimed to gain understanding into the molecular heterogeneity and functional implications.

4.1 The POMC-Dre driver mouse is a versatile tool for studying POMC neurons

To be able to investigate the heterogeneity of POMC neurons using the generated combinatorial Cre/Dre system together with the already established and available Cre driver lines, we generated and characterized a POMC-Dre driver line. Validation of this line showed a high specificity for POMC neurons and that incorporation of the BAC into the mouse genome was stable. Moreover, BAC integration did not influence whole body metabolism or glucose metabolism (Fig. 3.2). An important feature identified in the characterization of this line was that almost no AgRP neurons were targeted via POMC-Dre recombination. This observation was likely due to the age-dependent increase in Dre-based recombination that reached a maximum at 15 weeks. It has been reported that 25% of NPY/AgRP neurons are derived from Pomc-expressing progenitor cells (Padilla et al., 2010). Thus, it is possible that the delayed recombinase activity of the POMC-Dre line circumvented this proportion of AgRP/NPY neurons. Up until now, the POMC-Cre BAC line has been widely used for targeting and functional assessment of POMC neurons (Balthasar et al., 2004). This driver lines have been used in a multitude of studies that have contributed greatly to gaining understanding of the involvement of POMC neurons in various physiological processes (Huo et al., 2006; Wang et al., 2019; Zhan et al., 2013). However, some functions assigned to POMC neurons might be mediated by non-POMC neurons that also express the Cre transgene. An example of this can be observed in a study that carried out CRISPR-mediated deletion of the *Lepr* on POMC neurons, which was shown to have no physiological effects. Interestingly, it was also shown

that the glucose impairment phenotype seen in the POMC-Cre-based deletion of the *Lepr* is due to partial targeting of AgRP neurons through ectopic Cre activity in the developmental stages (Xu et al., 2018). This pinpoints the importance of using appropriate targeting strategies for functional studies. Within this scope, new driver lines have been developed for specific targeting of POMC neurons such as the tamoxifen-inducible POMC-Cre ERT2 transgenic mouse model or a POMC-IRES-Cre mouse line (Berglund et al., 2013; Fenselau et al., 2017). A factor to take into account is that the recombination efficiency of the POMC-Dre line peaks at around 50% (Thesis of Dr. J. Schumacher). It would be of interest to investigate whether the different POMC neuron subpopulations are equally represented within the 50% targeted cells. It is noteworthy that comparing endogenous *Lepr*- and *Glp1r*-expressing POMC neurons to the genetically targeted subpopulations using the Dre/Cre dependent system, both neuronal groups appear to be represented proportionately. We can therefore conclude that the POMC-Dre driver line is a valuable tool for functional investigations in to POMC neurons and their subpopulations.

4.2 The Cre/Dre combinatorial recombinase system for studying heterogeneity

The groundbreaking innovations in the field of neuroscience have revolutionized the scope at which we can investigate the mechanism within neuronal systems. Calcium imaging, sequencing techniques including TRAP and phospho-riboTRAP and single cell techniques, chemo- and optogenetic as well as virus-based tools were all developed in the past two decades and have brought us closer to unraveling the complexity of neurocircuits (Emery and Barres, 2008). Targeting of specific cell types has mostly been carried out through the use of the Cre-loxP system (Sternson et al., 2016). The yeast-derived FLP/FRT system has been developed as an alternative to the Cre-loxP system, however, FLP functions optimally at 30 °C, rendering it inefficient in mammalian cells. Improved versions of the FLP have been produced through mutagenesis that includes FLPe and FLPo (Buchholz et al., 1998). The Cre/FLPo system has been used to study the heterogeneity of the dopaminergic neurons of the VTA but in general, only a few examples employing FLP-based recombination for intersectional targeting in transgenic mice exist (Poulin et al., 2018). The Dre-rox recombinase system was later identified in bacteriophages and was incorporated to create a combinatorial

recombinase system for subpopulation targeting (Anastassiadis et al., 2009). Although the Dre recombinase has been reported to be slightly less efficient in comparison to the Cre, it is considered complementary to Cre for the use in an intersectional system.

In this study we made use of newly generated transgenic mouse lines that allow for specific targeting of subsets of cells based on double recombinase activity of Dre and Cre recombinases. In the framework of this project, tools facilitating neuronal manipulation and circuit analysis were integrated into the double Cre/Dre recombinase system (Thesis of Jonas Schumacher and unpublished data). Previous reports show that the activity of the Dre recombinase can target the loxP-flanked DNA in a ROSA26|S|Tomato reporter line, yet our results show that Dre-dependent recombination is specific for rox-flanked DNA segments since we did not find cross-reactivity with loxP-flanked alleles in ROSA26|S|Sr-ZsGreen, -hM3Dq/ZsGreen or -EGFPL10a. The expression of either recombinase alone shows no ZsGreen labeling in cleared brains (Fig. 3.8). Functionally, the presence of either Cre or Dre recombinase had no aberrant or unexpected effects as displayed in food intake of saline and CNO-treated genotype control mice (Fig. 3.11). In addition, the transgenes in the transgenic mice were not expressed in the presence of only Cre or Dre recombinase. These experiments together with the functional verification of each tool validate the usage of Cre/Dre-mediated combinatorial recombinases for analyses of heterogeneous populations. Integration of novel neuroscience tools such as calcium sensor GCaMP6s, optogenetic tools like channelrhodopsin or halorhodopsin or the virus receptor protein TVA into this double recombinase system is ongoing and will provide a great repertoire for understanding selected cellular or neuronal populations.

4.3 Anatomical localization of POMC^{Lepr+} and POMC^{Glp1r+} neurons

For the first time, we carried out a comprehensive spatial analysis of the anatomical localization of POMC neurons and two subpopulations within the ARC. uDISCO-based clearing techniques coupled with LSFM image acquisition allowed us to create 3D-rendered representations of neuronal distribution. Statistical evaluation of the distribution patterns showed that these neurons were largely non-overlapping. Pre-existing evidence on the distribution of POMC subpopulations are limited and mostly based on samplings carried out in two-dimensional sections obtained from rats or mice. Despite this, there are parallels

between the results obtained in our experiments and previous published data. Sandoval and colleagues demonstrated the involvement of central Glp1 receptors in glucose homeostasis regulation (Sandoval et al., 2008). In order to narrow down the effects to a particular set of neurons, the co-expression of *Glp1r* with *Pomc* and *Npy* mRNA was analyzed in the two strains Long-Evans and Sprague-Dawley rats. Almost no co-localization with *Npy* was detected whereas 40% of POMC neurons in the retrochiasmatic nucleus (RCA) and 68% of POMC^{ARC} neurons co-expressed *Glp1r*. The anatomical distribution of this co-expression analysis in serial sections was reconstructed in a three-dimensional manner in this study. In general, Glp1 receptor-expressing cells were found more in the caudal ARC (Sandoval et al., 2008). This 3D representation allowed for the identification of two distinct populations of POMC neurons based on the expression of the *Glp1r*. POMC neurons expressing the receptor were mainly found in the medio-lateral part of the ARC and those located more laterally within the ARC mostly did not co-express Glp1 receptors. This pattern was quite similar to that observed in our study where the POMC^{Glp1r+} neurons are situated more medially and the POMC^{Lepr+} neurons are more lateral (Fig. 3.6). The difference in detected co-expression levels to our study could be due to the fact that they were carried out in rats whereas we used mice for the analysis. Interestingly, the distribution pattern of POMC^{Glp1r+} neurons looks quite similar to the 3D reconstruction created in our study, which suggests that the anatomical distribution pattern could be conserved in closely related species. In addition to this, observation of 40% and 68% co-expression in RTN and ARC, respectively indicates that most POMC^{Glp1r+} neurons are located in the caudal regions of the ARC, a pattern also observed in our experiments (Sandoval et al., 2008). With regards to *Lepr*-expressing POMC neurons, Lam and colleagues observed that 50%–80% of POMC^{ARC} neurons express *Lepr* depending on the methodologies used for detection (Lam et al., 2015). Some studies have found differences in *Lepr* expression or responsiveness to leptin across the rostral-caudal axis amongst POMC neurons. A study focusing on the reactivity of POMC neurons to either insulin or leptin in rats showed that 34% of POMC cells in the RCA and up to 25% in the ARC displayed higher FOS levels in response to leptin (Williams et al., 2010). An overall 35% were depolarized with leptin application while some were non-responsive and very few were inhibited by leptin. The assessment of the anatomical localization pattern of these neurons showed that the leptin-activated neurons within rostral sections were found to be more lateral while in more caudal areas they

bordered the third ventricle (Williams et al., 2010). This description is quite similar to the pattern observed in our distribution experiments (Fig. 3.6).

4.4 Similar projection patterns of POMC^{Lepr+} and POMC^{Glp1r+} neurons

POMC^{Lepr+} and POMC^{Glp1r+} neurons exhibit different localization in the ARC, a differential molecular profile and distinct electrophysiological properties. Since our DREADD-dependent experiments demonstrate a differential ability between POMC^{Lepr+} or POMC^{Lepr-} neurons in regulation of food intake, one plausible explanation would be due that these neurons mediate their functions via different brain regions. Interestingly, whole-brain immunostaining and three-dimensional analysis of the projection patterns in Cre/Dre-dependent tdTomato mice showed no differences in fiber densities innervating BNST, PVH, DMH, PAG and NTS from POMC^{Lepr+} and POMC^{Glp1r+} neurons (Fig. 3.9). Primarily, the analysis of the projection pattern carried out in slices (2D) using the same mouse models shows that these neuronal groups have similar projection patterns (Thesis of Dr. J. Schumacher). Despite some discrepancies between the 2D and 3D analyses, the overall conclusion from both techniques was the same. A report in 2016 analyzed projection originating from POMC^{Lepr+} or POMC^{Lepr-} neurons. They labeled all Lepr-expressing neurons and their axonal projections using a LeprCre-dependent tdTomato line, while POMC neurons were identified with α -MSH or β -endorphin immunostaining. Analysis of co-localization of tdTomato with α -MSH/ β -endorphin showed an overall similar projection pattern between the two groups (Lima et al., 2016). Although Glp1r-expressing POMC neurons do not account for all other non-Lepr-expressing POMC neurons, it could indicate that POMC subpopulations do not differ with respect to projection patterns. Still, it is unclear whether axonal fibers from these two neuronal subpopulations converge onto the same cell types or if they exert their function through separate circuits within the same nuclei. Further studies are required to investigate the downstream circuits and the functional implications with more details. Moreover, the neuronal inputs into POMC^{Lepr+} or POMC^{Lepr-} neurons have not yet been described. Through incorporation of rabies virus tracing methods into the developed Cre/Dre-dependent expression system, the inputs into these neurons could be analyzed.

4.5 Physiological effects of POMC^{Lepr+} and POMC^{Glp1r+} neuron activation

Specific activation of POMC^{Lepr+} neurons using the double recombinase-dependent DREADD system elicited minor suppressive effects on food intake in male mice (Fig. 3.11). While energy expenditure and locomotor activity were not affected, RER was reduced indicating switch to lipid metabolism (Fig. 3.13). Many studies have been performed with the aim of understanding the role of leptin in the metabolism-regulatory effects of POMC neurons. In general, findings of these studies have been controversial. The POMC-specific knockout of the *Lepr* using POMC-Cre, *Lepr*^{flox/flox} mice led to a slight increase in body weight, 18% of the weight gain observed in mice with complete deficiency of LEPRs. This suggests a crucial role for LEPRs on other cell typed in the regulation of body weight (Balthasar et al., 2004). Despite an increase in adipose mass and serum leptin levels, no effect was observed on daily food intake or Oxygen consumption in these mice. A more recent study was conducted to assess the consequences of deleting the *Lepr* on POMC neurons in adult mice using an inducible Pomc^{CreERT2} transgenic mouse model. One week after deletion of the receptor, impairment in hepatic glucose production in addition to a reduction in fasting-induced reduction in leptin levels was observable without alterations in food intake, body weight, and energy expenditure or RER. This suggested a role for the *Lepr*-expressing POMC neurons in regulation of leptin levels upon food deprivation (Caron et al., 2018). It would be interesting to investigate this effect using the double-recombinase activatory and inhibitory DREADD systems. In addition, both studies show no direct effect on food intake upon deletion of the leptin receptor from POMC neurons, which suggest that POMC^{Lepr+} neurons are not direct regulators of food intake. As more sophisticated tools are developed, the crude phenotypes described previously are narrowed down to specific cell types and the refined molecular mechanisms involved in metabolism are uncovered. For instance, CRISPR-mediated deletion of *Lepr* on the POMC^{ARC} neurons and did not affect body weight or blood glucose, suggesting a dispensable role of *Lepr* on POMC neurons (Xu et al., 2018). In contrast, POMC-deficiency or selective ablation of hypothalamic POMC neurons in mice and humans leads to severe obesity and re-expression of POMC in the *Lepr*-positive subpopulation of POMC neurons is sufficient for normal energy homeostasis (Lam et al., 2015). Taken together, it is likely that POMC^{Lepr+} neurons have a developmental role in control of energy homeostasis and that other regulators might contribute to the role of leptin. Recent experiments using Ca²⁺ imaging of POMC neuron

activity in freely behaving mice, revealed that POMC neurons rapidly change their activity in response to sensory food perception independent of changes in circulating energy state sensing hormones. Thus, it is likely that POMC^{Lepr+} neurons exert control through synaptic inputs.

In an example investigation, to study the involvement of melanocortin neurons on mediating the effect of leptin on the autonomic system, the *Lepr* was deleted in POMC or AgRP neurons. The results illustrated a divergent effect of POMC and AgRP neurons mediating the leptin-dependent regional activity of the autonomic system. POMC was involved in leptin controlled sympathetic nerve activity (SNA) of brown adipose tissue (BAT), hepatic parasympathetic activity in addition to lumbar, splanchnic and renal SNA. The data showed that the leptin-stimulated elevation in BAT sympathetic activity was in part attenuated by a lack of *Lepr* on both AgRP and POMC neurons (Bell et al., 2018). It would be interesting to investigate the effect of POMC^{Lepr+} activation on BAT activity and thermogenesis using the tools developed in our study.

On the other hand, chemogenetic activation of POMC^{Glp1r+} neurons in male mice reduces food intake more potently (Fig. 3.11) compared to previous studies where POMC^{Cre}-expressing neurons have been activated either chemo- or optogenetically (Zhan et al., 2013). This is particularly remarkable in light of the fact that the transgenic-targeted POMC^{Glp1r+} neurons represent a significantly smaller population than the POMC^{Lepr+} neurons (data not shown). In a study carried out in 2014, rats fed with normal and high fat diet were injected chronically with EX-4. This led to a reduction in food intake and bodyweight as well as inducing an increase in *Pomc* and decreased *Npy* in ARC of both diet groups supporting the notion that EX-4 alters signaling in these neurons toward an anorexigenic profile (Yang et al., 2014). To analyze which hypothalamic areas and neuronal types could mediate the anorectic effects of Glp1r agonists, the expression of Glp1r was knocked down in the hypothalamus, PVN and POMC neurons using Glp1r-flox mice in combination with *Nkx2.1-Cre*, *Sim1-Cre* and *POMC-Cre*, respectively (Burmeister et al., 2017). Knockdown of Glp1r in the PVN had no effect on food intake though a decrease in EE was observed in these mice. However, knockdown of this receptor in POMC neurons had no effect on food intake or EE, RER, locomotor activity or glucose homeostasis in normal chow diet fed mice. Knocking down of the Glp1r in *Nkx2.1*-expressing neurons, POMC neurons, or the PVN does not prevent the food

intake suppression by peripheral administrated EX-4. Overall, the results demonstrated that the Glp1r expression in the ARC and PVN, is sufficient but not necessary for the effects of Glp1 and its agonists on energy balance and points to the role of extra-hypothalamic sites (Burmeister et al., 2017).

POMC neurons have been previously reported to be both GABAergic or glutamatergic, this might indicate, that POMC^{Glp1r+} neurons are primarily glutamatergic. However, our gene expression analysis indicates that POMC^{Glp1r+} do not exhibit a greater proportion of *Slc17a6* (*Vglut2*) expression in comparison to POMC^{Lep^r+} neurons. Thus, differential neurotransmitter content likely does not account for the differential ability of both neuronal subtypes to acutely regulate feeding in male mice.

Surprisingly, specific activation of POMC^{Lep^r+} and POMC^{Glp1r+} neurons in female mice using the double recombinase-dependent hm3Dq system had no effect on food intake (Fig. 3.12). Analysis of *Fos* via *in situ* hybridization showed that these neurons were activated in an efficient manner verified by an increase in expression. Thus, it is likely that the regulation of food intake in males and females is regulated differently. Previous studies have reported a higher expression of *Pomc* mRNA and associated bioactive peptides such as β -endorphin in female mice in comparison to males (Nohara et al., 2011; Wang et al., 2018). It was shown that female POMC neurons have a higher firing rate in comparison to neurons from males, a pattern, which was not observed in AgRP/NPY, SF1, or SIM1 neurons. Thus, the general lower body weight in females could at least partially be due to this characteristic. Susceptibility to DIO in female mice was enhanced by deletion of TAp63 though these effects were not seen in males displaying a clear instance of sexual dimorphism in energy balance. TAp63 deletion caused a reduction in POMC firing frequency in females only and likely contributed to increased food intake and higher DIO susceptibility (Wang et al., 2018). Other examples of sexual dimorphism with regard to POMC neuronal function have been reported. LKB1 knockout in POMC neurons impairs hepatic glucose metabolism and reduces α MSH levels by half in female mice with no effect on body weight (Claret et al., 2011). In another study, SIRT1 deletion in POMC neurons led to greater body weight gain in HFD-fed females than in males (Ramadori et al., 2011). The primary contributor to sexual dimorphism in energy homeostasis is the female sex hormone; estrogen, and differences in feeding behavior between genders also largely can be attributed to it (reviewed in (Asarian and Geary, 2013). On the other hand,

a study investigating the role of leptin signaling on POMC neurons in reproduction and gender-dependent regulation of energy balance showed that the sexual dichotomy observed in glucose homeostasis control was likely independent of ovarian hormones (Shi et al., 2010).

It is worth noting that the anorectic effects of estrogen are simultaneous with reductions in expression of *Npy* and *Agrp*, but not *Pomc* in female mice. AgRP/NPY neurons were found to be essential in mediating the cyclic alterations in feeding (Olofsson et al., 2009). Although these effects are not mediated through POMC neurons, it is an example of gender-based variation in the regulation of food intake. It is apparent that food intake control in females, factors in different determinants and further studies are required to fully grasp the mechanisms and circuitry involved. It is thus crucial to carry out experiments in both genders, particularly when investigating the effects of potential therapeutics.

In summary, the experiments presented here indicate functional diversification of POMC neuron subpopulations in the regulation of feeding and possibly even other POMC neuron mediated responses.

4.6 Molecular and electrophysiological differences between POMC^{Lepr+} and POMC^{Glp1r+} neurons

After identifying anatomical and functional differences in the two POMC neuron populations, we aimed to characterize both populations molecularly and the Cre/Dre-dependent ROSA26^{IslrSrEGFP}L10a mouse line was used. Sequencing of RNA isolated from each subpopulation gave rise to an extensive dataset describing the molecular profile of both Glp1r-expressing and Lepr-expressing POMC subpopulations. The successful application of this technique to such small neuronal subpopulations allowed deeper insight into the molecular heterogeneity of POMC neurons. Currently published data suggested a segregation of Lepr and Glp1r expressing POMC neurons, which was confirmed in our reported dataset at a molecular level. This dataset resulted in a library of cell-type specific cell surface receptors, based on which, we can develop new hypotheses for experimental interrogation. The translational profiling of POMC^{Lepr+} and POMC^{Glp1r+} neurons in this study has enabled the identification of possible regulators of these neuronal types, other than leptin and Glp1.

As expected, *Pomc* expression in both neuronal sets were high in comparison to the hypothalamic input; however, the detected levels of *Pomc* and *Cartpt* were higher in the Lepr-

expressing POMC neurons compared to *Glp1r*-expressing POMC neurons (Fig. 3.16). In turn, expression of opioid receptors on *Glp1r*-expressing POMC neurons was higher compared to *Lepr*-expressing POMC neurons (Fig. 3.16). CARTPT is involved in the regulation of a wide range of physiological functions including food intake and energy homeostasis, which also majorly colocalizes with POMC neurons in the ARC (Farzi et al. 2018). In the ARC it is known to be mainly expressed in the majority of POMC neurons (Lam et al. 2017; Campbell et al. 2017). Galanin has been described to have orexigenic effects on food intake when administered into the PVH (Lang et al. 2015). In single cell sequencing data *Gal* was found in 50% of ARC POMC neurons (Lam et al. 2017). This seems rather contradictory since POMC neurons have been known to have anorexigenic effects and possible release of GAL by POMC neurons requires further experimentation. It is noteworthy that orexigenic effects of POMC neurons have previously been described through the activation of CB1R and via a shift from α -MSH to β -endorphin release in the terminals at the PVN (Koch et al. 2015). As mentioned previously (Section 1.3.2) processing of the POMC precursor protein also produces the opioid peptide β -endorphin. Another classical opioid precursor gene is prodynorphin (*Pdyn*), also significantly higher expressed in *Lepr*-expressing POMC neurons compared to *Glp1r*-expressing POMC neurons. It is known that activation of opioid receptors on POMC neurons leads to hyperpolarization (Fox and Hentges 2017).

Neuromedin-U (NMU) receptor 2 (*Nmur2*) was also identified as differentially regulated between the two groups. NMU is a neuropeptide with a range of physiological effects and it also affects feeding behavior (Kaisho et al. 2017). Studies in mice could show that NMUR2 agonists can decrease food intake and reduce body weight (Kaisho et al. 2017; Sampson et al. 2018). In addition, administration of an NMUR2 agonist in combination with liraglutide reduced body weight in DIO mice in an additive manner (Kaisho et al. 2017). Interestingly, *Nmur2* expression is significantly higher in *Lepr*-expressing POMC neurons in the current study. However, specific activation of *Lepr*-expressing POMC neurons had little effect on food intake (Fig. 3.11). Thus, it is likely that the anorectic effect of the NMUR2 agonist is mediated through other neurons. Interestingly, *Glp1r*-expressing POMC neurons express higher levels of NPY compared to *Lepr*-expressing POMC neurons suggesting a release of NPY by *Glp1r*-expressing POMC neurons. The implications of this require further research to elucidate if *Glp1r*-expressing POMC neurons could be a source of NPY.

Taken together, further experiments on the neuropeptide profiles of POMC subpopulations might reveal a greater level of functional heterogeneity of POMC neurons than previously anticipated.

Electrophysiological recordings from genetically labeled POMC^{Lepr+} and POMC^{Glp1r+} neurons demonstrated differences in their basic intrinsic properties. While POMC^{Glp1r+} exhibit phasic, low threshold excitability, POMC^{Lepr+} have tonic activity (Fig. 3.20). Treatment of these neurons with leptin or Glp1 resulted in distinct responses. Surprisingly, POMC^{Glp1r+} neurons were hyperpolarized upon leptin treatment despite blockage of glutamate and GABA receptor and suppression of action-potential-dependent synaptic release. Seeing as the majority of this neuronal group do not express the receptor in question, it is possible that leptin provokes the release of inhibiting mediators from presynaptic neurons in a manner that is not dependent on action potentials. Based on the enrichment of opioid receptors in POMC^{Glp1r+} neurons, β -endorphins might be responsible for this inhibitory effect, released through modulation of spontaneous release (Kavalali, 2015). Spontaneous release is one of three modes of neurotransmitter release that in contrast to the other two types (synchronous and asynchronous release) occurs in the absence of presynaptic depolarization (Kaesler and Regehr, 2014). Further experiments are required for the investigation of this hypothesis as well as possible cross-interaction amongst POMC neuronal subsets.

A very recent study from the Williams group carried out electrophysiological recordings on Lepr-expressing POMC neurons treated with liraglutide (He et al. 2019). Due to the contradictory existing evidence on the physiological role of Glp1 and leptin mediated by the central melanocortin system, the study investigated whether these hormones have a synergistic effect on POMC and AgRP/NPY neurons. It was observed that liraglutide directly excited POMC^{Lepr+} neurons and that this effect was potentiated by leptin through TRPC5 channels. In contrast, liraglutide inhibited AgRP/NPY neurons via post-synaptic GABA_A receptors. Taken together, the study identified molecular mechanisms of the mode of action of Glp1r agonists within the melanocortin system. It is noteworthy, that in the mentioned study liraglutide depolarized 10 out of 27 Lepr-expressing POMC neurons suggesting heterogeneous responses within POMC activity even within a subset of targeted neurons. This is similar to the findings in our study (Fig. 3.21 and 3.22) where electrophysiological recordings from both POMC^{Lepr+} and POMC^{Glp1r+} neurons upon treatment

with either leptin or Glp1 elicited non-uniform responses. In the mentioned study, all 5 Lepr-expressing POMC neurons depolarize upon Glp1 treatment whereas we found 2/14 POMC^{Lepr+} neurons to be directly excited by Glp1. This discrepancy could be attributed to the differences in concentrations of Glp1 used (100 nm vs 1 μ M). In our experiments, 11/14 targeted Lepr-expressing POMC were non-responsive to Glp1 and may elicit responses with higher doses of the peptide (He et al. 2019).

In summary, the molecular profiling and electrophysiological differences identified in POMC subpopulations open new avenues for new research on possible functional relevance and in unraveling potential divergent downstream pathways of these neurons.

4.7 Conclusion

Obesity and its associated comorbidities are major concerns for today's world population. The CNS plays an important role in regulating energy homeostasis, food intake and glucose homeostasis. POMC and AgRP neurons have been the focus of research for some years now and first clinical success was reported exploiting the gained knowledge about hypothalamic neurocircuits of both of these neuronal populations. However, the heterogeneity within those populations remains to be elucidated. Thus, we developed and utilized transgenic mouse models to successfully identify POMC subpopulations in an intersectional Cre/Dre-dependent manner. The results reveal that these two subpopulations are mainly non-overlapping with distinct electrophysiological properties. They also exhibit differential expression of neuropeptide or hormone receptors and vary in their ability to suppress feeding. Further experiments are required to understand the functionality of the identified heterogeneity.

5 Bibliography

- Abbott, C.R., Monteiro, M., Small, C.J., Sajedi, A., Smith, K.L., Parkinson, J.R., Ghatei, M.A., and Bloom, S.R. (2005). The inhibitory effects of peripheral administration of peptide YY(3-36) and glucagon-like peptide-1 on food intake are attenuated by ablation of the vagal-brainstem-hypothalamic pathway. *Brain Res* 1044, 127-131.
- Akaike, N., and Harata, N. (1994). Nystatin perforated patch recording and its applications to analyses of intracellular mechanisms. *Jpn J Physiol* 44, 433-473.
- Anand, B.K., and Brobeck, J.R. (1951). Localization of a "feeding center" in the hypothalamus of the rat. *Proc Soc Exp Biol Med* 77, 323-324.
- Anastassiadis, K., Fu, J., Patsch, C., Hu, S., Weidlich, S., Duerschke, K., Buchholz, F., Edenhofer, F., and Stewart, A.F. (2009). Dre recombinase, like Cre, is a highly efficient site-specific recombinase in *E. coli*, mammalian cells and mice. *Dis Model Mech* 2, 508-515.
- Aponte, Y., Atasoy, D., and Sternson, S.M. (2011). AGRP neurons are sufficient to orchestrate feeding behavior rapidly and without training. *Nat Neurosci* 14, 351-355.
- Apovian, C.M. (2016). Obesity: definition, comorbidities, causes, and burden. *Am J Manag Care* 22, s176-185.
- Armbruster, B.N., Li, X., Pausch, M.H., Herlitze, S., and Roth, B.L. (2007). Evolving the lock to fit the key to create a family of G protein-coupled receptors potently activated by an inert ligand. *Proc Natl Acad Sci U S A* 104, 5163-5168.
- Asarian, L., and Geary, N. (2013). Sex differences in the physiology of eating. *Am J Physiol Regul Integr Comp Physiol* 305, R1215-1267.
- Ashburner, M., Ball, C.A., Blake, J.A., Botstein, D., Butler, H., Cherry, J.M., Davis, A.P., Dolinski, K., Dwight, S.S., Eppig, J.T., *et al.* (2000). Gene ontology: tool for the unification of biology. The Gene Ontology Consortium. *Nat Genet* 25, 25-29.
- Atasoy, D., Betley, J.N., Su, H.H., and Sternson, S.M. (2012). Deconstruction of a neural circuit for hunger. *Nature* 488, 172-177.
- Bacart, J., Leloire, A., Levoye, A., Froguel, P., Jockers, R., and Couturier, C. (2010). Evidence for leptin receptor isoforms heteromerization at the cell surface. *FEBS Lett* 584, 2213-2217.
- Baggio, L.L., and Drucker, D.J. (2014). Glucagon-like peptide-1 receptors in the brain: controlling food intake and body weight. *J Clin Invest* 124, 4223-4226.
- Bagnol, D., Lu, X.Y., Kaelin, C.B., Day, H.E., Ollmann, M., Gantz, I., Akil, H., Barsh, G.S., and Watson, S.J. (1999). Anatomy of an endogenous antagonist: relationship between Agouti-related protein and proopiomelanocortin in brain. *J Neurosci* 19, RC26.
- Baker, R.A., and Herkenham, M. (1995). Arcuate nucleus neurons that project to the hypothalamic paraventricular nucleus: neuropeptidergic identity and consequences of adrenalectomy on mRNA levels in the rat. *J Comp Neurol* 358, 518-530.
- Balthasar, N., Coppari, R., McMinn, J., Liu, S.M., Lee, C.E., Tang, V., Kenny, C.D., McGovern, R.A., Chua, S.C., Jr., Elmquist, J.K., *et al.* (2004). Leptin receptor signaling in POMC neurons is required for normal body weight homeostasis. *Neuron* 42, 983-991.
- Barrera, J.G., Sandoval, D.A., D'Alessio, D.A., and Seeley, R.J. (2011). GLP-1 and energy balance: an integrated model of short-term and long-term control. *Nat Rev Endocrinol* 7, 507-516.

- Barrios-Correa, A.A., Estrada, J.A., and Contreras, I. (2018). Leptin Signaling in the Control of Metabolism and Appetite: Lessons from Animal Models. *J Mol Neurosci* 66, 390-402.
- Beiroa, D., Imbernon, M., Gallego, R., Senra, A., Herranz, D., Villarroya, F., Serrano, M., Ferno, J., Salvador, J., Escalada, J., *et al.* (2014). GLP-1 agonism stimulates brown adipose tissue thermogenesis and browning through hypothalamic AMPK. *Diabetes* 63, 3346-3358.
- Belgardt, B.F., Okamura, T., and Bruning, J.C. (2009). Hormone and glucose signalling in POMC and AgRP neurons. *J Physiol* 587, 5305-5314.
- Bell, G.I., Santerre, R.F., and Mullenbach, G.T. (1983). Hamster preproglucagon contains the sequence of glucagon and two related peptides. *Nature* 302, 716-718.
- Belteki, G., Gertsenstein, M., Ow, D.W., and Nagy, A. (2003). Site-specific cassette exchange and germline transmission with mouse ES cells expressing phiC31 integrase. *Nat Biotechnol* 21, 321-324.
- Bergendahl, M., Wiemann, J.N., Clifton, D.K., Huhtaniemi, I., and Steiner, R.A. (1992). Short-term starvation decreases POMC mRNA but does not alter GnRH mRNA in the brain of adult male rats. *Neuroendocrinology* 56, 913-920.
- Berglund, E.D., Liu, C., Sohn, J.W., Liu, T., Kim, M.H., Lee, C.E., Vianna, C.R., Williams, K.W., Xu, Y., and Elmquist, J.K. (2013). Serotonin 2C receptors in pro-opiomelanocortin neurons regulate energy and glucose homeostasis. *J Clin Invest* 123, 5061-5070.
- Bergman, R.N., Kim, S.P., Catalano, K.J., Hsu, I.R., Chiu, J.D., Kabir, M., Hucking, K., and Ader, M. (2006). Why visceral fat is bad: mechanisms of the metabolic syndrome. *Obesity (Silver Spring)* 14 Suppl 1, 16S-19S.
- Bernard, C. (1855). *Leçons de physiologie expérimentale appliquée à la médecine: faites au Collège de France* (JB Baillière et fils).
- Berthoud, H.R., Munzberg, H., and Morrison, C.D. (2017). Blaming the Brain for Obesity: Integration of Hedonic and Homeostatic Mechanisms. *Gastroenterology* 152, 1728-1738.
- Betley, J.N., Cao, Z.F., Ritola, K.D., and Sternson, S.M. (2013). Parallel, redundant circuit organization for homeostatic control of feeding behavior. *Cell* 155, 1337-1350.
- Beverly, J.L., Beverly, M.F., and Meguid, M.M. (1995). Alterations in extracellular GABA in the ventral hypothalamus of rats in response to acute glucoprivation. *Am J Physiol* 269, R1174-1178.
- Biddinger, S.B., and Kahn, C.R. (2006). FROM MICE TO MEN: Insights into the Insulin Resistance Syndromes. *Annual Review of Physiology* 68, 123-158.
- Brady, L.S., Smith, M.A., Gold, P.W., and Herkenham, M. (1990). Altered expression of hypothalamic neuropeptide mRNAs in food-restricted and food-deprived rats. *Neuroendocrinology* 52, 441-447.
- Brion, M.J., Lawlor, D.A., Matijasevich, A., Horta, B., Anselmi, L., Araujo, C.L., Menezes, A.M., Victora, C.G., and Smith, G.D. (2011). What are the causal effects of breastfeeding on IQ, obesity and blood pressure? Evidence from comparing high-income with middle-income cohorts. *Int J Epidemiol* 40, 670-680.
- Brobeck, J.R. (1946a). Mechanism of the development of obesity in animals with hypothalamic lesions. *Physiological reviews* 26, 541-559.
- Brobeck, J.R. (1946b). Mechanism of the development of obesity in animals with hypothalamic lesions. *Physiol Rev* 26, 541-559.
- Buchholz, F., Angrand, P.O., and Stewart, A.F. (1998). Improved properties of FLP recombinase evolved by cycling mutagenesis. *Nat Biotechnol* 16, 657-662.
- Buggy, J.J. (1998). Binding of alpha-melanocyte-stimulating hormone to its G-protein-coupled receptor on B-lymphocytes activates the Jak/STAT pathway. *Biochem J* 331 (Pt 1), 211-216.

- Burmeister, M.A., Ayala, J.E., Smouse, H., Landivar-Rocha, A., Brown, J.D., Drucker, D.J., Stoffers, D.A., Sandoval, D.A., Seeley, R.J., and Ayala, J.E. (2017). The Hypothalamic Glucagon-Like Peptide 1 Receptor Is Sufficient but Not Necessary for the Regulation of Energy Balance and Glucose Homeostasis in Mice. *Diabetes* 66, 372-384.
- Butler, A., Hoffman, P., Smibert, P., Papalexi, E., and Satija, R. (2018). Integrating single-cell transcriptomic data across different conditions, technologies, and species. *Nat Biotechnol* 36, 411-420.
- Butler, A.A., Girardet, C., Mavrikaki, M., Trevaskis, J.L., Macarthur, H., Marks, D.L., and Farr, S.A. (2017). A Life without Hunger: The Ups (and Downs) to Modulating Melanocortin-3 Receptor Signaling. *Frontiers in Neuroscience* 11.
- Campbell, J.N., Macosko, E.Z., Fenselau, H., Pers, T.H., Lyubetskaya, A., Tenen, D., Goldman, M., Verstegen, A.M., Resch, J.M., McCarroll, S.A., *et al.* (2017). A molecular census of arcuate hypothalamus and median eminence cell types. *Nat Neurosci* 20, 484-496.
- Cannon, W.B. (1932). *Homeostasis. The wisdom of the body* Norton, Newyork.
- Caron, A., Dungan Lemko, H.M., Castorena, C.M., Fujikawa, T., Lee, S., Lord, C.C., Ahmed, N., Lee, C.E., Holland, W.L., Liu, C., *et al.* (2018). POMC neurons expressing leptin receptors coordinate metabolic responses to fasting via suppression of leptin levels. *Elife* 7.
- Cawley, N.X., Li, Z., and Loh, Y.P. (2016). 60 YEARS OF POMC: Biosynthesis, trafficking, and secretion of pro-opiomelanocortin-derived peptides. *J Mol Endocrinol* 56, T77-97.
- Challis, B.G., Coll, A.P., Yeo, G.S., Pinnock, S.B., Dickson, S.L., Thresher, R.R., Dixon, J., Zahn, D., Rochford, J.J., White, A., *et al.* (2004). Mice lacking pro-opiomelanocortin are sensitive to high-fat feeding but respond normally to the acute anorectic effects of peptide-YY(3-36). *Proc Natl Acad Sci U S A* 101, 4695-4700.
- Challis, B.G., Pritchard, L.E., Creemers, J.W., Delplanque, J., Keogh, J.M., Luan, J., Wareham, N.J., Yeo, G.S., Bhattacharyya, S., Froguel, P., *et al.* (2002). A missense mutation disrupting a dibasic prohormone processing site in pro-opiomelanocortin (POMC) increases susceptibility to early-onset obesity through a novel molecular mechanism. *Hum Mol Genet* 11, 1997-2004.
- Chao, P.T., Yang, L., Aja, S., Moran, T.H., and Bi, S. (2011). Knockdown of NPY expression in the dorsomedial hypothalamus promotes development of brown adipocytes and prevents diet-induced obesity. *Cell Metab* 13, 573-583.
- Chehab, F.F. (2014). 20 years of leptin: leptin and reproduction: past milestones, present undertakings, and future endeavors. *J Endocrinol* 223, T37-48.
- Chen, A.S., Metzger, J.M., Trumbauer, M.E., Guan, X.M., Yu, H., Frazier, E.G., Marsh, D.J., Forrest, M.J., Gopal-Truter, S., Fisher, J., *et al.* (2000). Role of the melanocortin-4 receptor in metabolic rate and food intake in mice. *Transgenic Res* 9, 145-154.
- Chen, H., Charlat, O., Tartaglia, L.A., Woolf, E.A., Weng, X., Ellis, S.J., Lakey, N.D., Culpepper, J., Moore, K.J., Breitbart, R.E., *et al.* (1996). Evidence that the diabetes gene encodes the leptin receptor: identification of a mutation in the leptin receptor gene in db/db mice. *Cell* 84, 491-495.
- Chen, K.Y., Muniyappa, R., Abel, B.S., Mullins, K.P., Staker, P., Brychta, R.J., Zhao, X., Ring, M., Psota, T.L., Cone, R.D., *et al.* (2015). RM-493, a melanocortin-4 receptor (MC4R) agonist, increases resting energy expenditure in obese individuals. *J Clin Endocrinol Metab* 100, 1639-1645.
- Chen, M., Mema, E., Kelleher, J., Nemechek, N., Berger, A., Wang, J., Xie, T., Gavrilova, O., Drucker, D.J., and Weinstein, L.S. (2011). Absence of the glucagon-like peptide-1 receptor does not affect the metabolic phenotype of mice with liver-specific G(s)alpha deficiency. *Endocrinology* 152, 3343-3350.

- Cheung, C.C., Clifton, D.K., and Steiner, R.A. (1997). Proopiomelanocortin neurons are direct targets for leptin in the hypothalamus. *Endocrinology* *138*, 4489-4492.
- Cho, Y.M., Fujita, Y., and Kieffer, T.J. (2014). Glucagon-like peptide-1: glucose homeostasis and beyond. *Annu Rev Physiol* *76*, 535-559.
- Ciofi, P., Garret, M., Lapirot, O., Lafon, P., Loyens, A., Prevot, V., and Levine, J.E. (2009). Brain-endocrine interactions: a microvascular route in the mediobasal hypothalamus. *Endocrinology* *150*, 5509-5519.
- Cizek, J., Herholz, K., Vollmar, S., Schrader, R., Klein, J., and Heiss, W.D. (2004). Fast and robust registration of PET and MR images of human brain. *Neuroimage* *22*, 434-442.
- Claret, M., Smith, M.A., Knauf, C., Al-Qassab, H., Woods, A., Heslegrave, A., Piipari, K., Emmanuel, J.J., Colom, A., Valet, P., *et al.* (2011). Deletion of *Lkb1* in pro-opiomelanocortin neurons impairs peripheral glucose homeostasis in mice. *Diabetes* *60*, 735-745.
- Clark, J.T., Kalra, P.S., Crowley, W.R., and Kalra, S.P. (1984). Neuropeptide Y and human pancreatic polypeptide stimulate feeding behavior in rats. *Endocrinology* *115*, 427-429.
- Collet, T.H., Dubern, B., Mokrosinski, J., Connors, H., Keogh, J.M., Mendes de Oliveira, E., Henning, E., Poitou-Bernert, C., Oppert, J.M., Tounian, P., *et al.* (2017). Evaluation of a melanocortin-4 receptor (MC4R) agonist (Setmelanotide) in MC4R deficiency. *Mol Metab* *6*, 1321-1329.
- Comuzzie, A.G., Hixson, J.E., Almasy, L., Mitchell, B.D., Mahaney, M.C., Dyer, T.D., Stern, M.P., MacCluer, J.W., and Blangero, J. (1997). A major quantitative trait locus determining serum leptin levels and fat mass is located on human chromosome 2. *Nat Genet* *15*, 273-276.
- Cone, R.D. (2005). Anatomy and regulation of the central melanocortin system. *Nat Neurosci* *8*, 571-578.
- Cooper, S.J. (2008). From Claude Bernard to Walter Cannon. Emergence of the concept of homeostasis. *Appetite* *51*, 419-427.
- Cowley, M.A., Smart, J.L., Rubinstein, M., Cerdan, M.G., Diano, S., Horvath, T.L., Cone, R.D., and Low, M.J. (2001). Leptin activates anorexigenic POMC neurons through a neural network in the arcuate nucleus. *Nature* *411*, 480-484.
- Dalvi, P.S., Nazarians-Armavil, A., Purser, M.J., and Belsham, D.D. (2012). Glucagon-like peptide-1 receptor agonist, exendin-4, regulates feeding-associated neuropeptides in hypothalamic neurons in vivo and in vitro. *Endocrinology* *153*, 2208-2222.
- De Souza, C.T., Araujo, E.P., Bordin, S., Ashimine, R., Zollner, R.L., Boschero, A.C., Saad, M.J., and Velloso, L.A. (2005). Consumption of a fat-rich diet activates a proinflammatory response and induces insulin resistance in the hypothalamus. *Endocrinology* *146*, 4192-4199.
- Dennison, C.S., King, C.M., Dicken, M.S., and Hentges, S.T. (2016). Age-dependent changes in amino acid phenotype and the role of glutamate release from hypothalamic proopiomelanocortin neurons. *J Comp Neurol* *524*, 1222-1235.
- Dobin, A., Davis, C.A., Schlesinger, F., Drenkow, J., Zaleski, C., Jha, S., Batut, P., Chaisson, M., and Gingeras, T.R. (2013). STAR: ultrafast universal RNA-seq aligner. *Bioinformatics* *29*, 15-21.
- Dodd, G.T., Decherf, S., Loh, K., Simonds, S.E., Wiede, F., Balland, E., Merry, T.L., Munzberg, H., Zhang, Z.Y., Kahn, B.B., *et al.* (2015). Leptin and insulin act on POMC neurons to promote the browning of white fat. *Cell* *160*, 88-104.
- Dodt, H.U., and Zieglgansberger, W. (1990). Visualizing unstained neurons in living brain slices by infrared DIC-videomicroscopy. *Brain Res* *537*, 333-336.
- Dunbar, J.C., and Lu, H. (2000). Proopiomelanocortin (POMC) products in the central regulation of sympathetic and cardiovascular dynamics: studies on melanocortin and opioid interactions. *Peptides* *21*, 211-217.

- Edition, I. International Diabetes Federation. IDF Diabetes Atlas, 8th edn. Brussels, Belgium: International Diabetes Federation, 2017.
- Elias, C.F., Aschkenasi, C., Lee, C., Kelly, J., Ahima, R.S., Bjorbaek, C., Flier, J.S., Saper, C.B., and Elmquist, J.K. (1999). Leptin differentially regulates NPY and POMC neurons projecting to the lateral hypothalamic area. *Neuron* *23*, 775-786.
- Elias, C.F., Lee, C., Kelly, J., Aschkenasi, C., Ahima, R.S., Couceyro, P.R., Kuhar, M.J., Saper, C.B., and Elmquist, J.K. (1998). Leptin activates hypothalamic CART neurons projecting to the spinal cord. *Neuron* *21*, 1375-1385.
- Emery, B., and Barres, B.A. (2008). Unlocking CNS cell type heterogeneity. *Cell* *135*, 596-598.
- Erdheim, J. (1904). Über hypophysengeschwülste und hirncholesteatome (Gerold).
- Ewels, P.A., Peltzer, A., Fillinger, S., Patel, H., Alneberg, J., Wilm, A., Garcia, M.U., Di Tommaso, P., and Nahnsen, S. (2020). The nf-core framework for community-curated bioinformatics pipelines. *Nat Biotechnol* *38*, 276-278.
- Fei, H., Okano, H.J., Li, C., Lee, G.H., Zhao, C., Darnell, R., and Friedman, J.M. (1997). Anatomic localization of alternatively spliced leptin receptors (Ob-R) in mouse brain and other tissues. *Proc Natl Acad Sci U S A* *94*, 7001-7005.
- Fenselau, H., Campbell, J.N., Versteegen, A.M., Madara, J.C., Xu, J., Shah, B.P., Resch, J.M., Yang, Z., Mandelblat-Cerf, Y., Livneh, Y., *et al.* (2017). A rapidly acting glutamatergic ARC-->PVH satiety circuit postsynaptically regulated by alpha-MSH. *Nat Neurosci* *20*, 42-51.
- Ferguson, A.V., Latchford, K.J., and Samson, W.K. (2008). The paraventricular nucleus of the hypothalamus - a potential target for integrative treatment of autonomic dysfunction. *Expert Opin Ther Targets* *12*, 717-727.
- Flak, J.N., and Myers, M.G., Jr. (2016). Minireview: CNS Mechanisms of Leptin Action. *Mol Endocrinol* *30*, 3-12.
- Friedman, J.M. (2004). Modern science versus the stigma of obesity. *Nat Med* *10*, 563-569.
- Fröhlich, A. (1901). Ein fall von tumor der hypophysis cerebri ohne akromegalie.
- Furuta, M., Yano, H., Zhou, A., Rouille, Y., Holst, J.J., Carroll, R., Ravazzola, M., Orci, L., Furuta, H., and Steiner, D.F. (1997). Defective prohormone processing and altered pancreatic islet morphology in mice lacking active SPC2. *Proc Natl Acad Sci U S A* *94*, 6646-6651.
- Gamber, K.M., Huo, L., Ha, S., Hairston, J.E., Greeley, S., and Bjorbaek, C. (2012). Over-expression of leptin receptors in hypothalamic POMC neurons increases susceptibility to diet-induced obesity. *PLoS One* *7*, e30485.
- Garfield, A.S., Lam, D.D., Marston, O.J., Przydzial, M.J., and Heisler, L.K. (2009). Role of central melanocortin pathways in energy homeostasis. *Trends Endocrinol Metab* *20*, 203-215.
- Getting, S.J. (2006). Targeting melanocortin receptors as potential novel therapeutics. *Pharmacol Ther* *111*, 1-15.
- Gong, S., Doughty, M., Harbaugh, C.R., Cummins, A., Hatten, M.E., Heintz, N., and Gerfen, C.R. (2007). Targeting Cre recombinase to specific neuron populations with bacterial artificial chromosome constructs. *J Neurosci* *27*, 9817-9823.
- Graaf, C., Donnelly, D., Wootten, D., Lau, J., Sexton, P.M., Miller, L.J., Ahn, J.M., Liao, J., Fletcher, M.M., Yang, D., *et al.* (2016). Glucagon-Like Peptide-1 and Its Class B G Protein-Coupled Receptors: A Long March to Therapeutic Successes. *Pharmacol Rev* *68*, 954-1013.
- Gropp, E., Shanabrough, M., Borok, E., Xu, A.W., Janoschek, R., Buch, T., Plum, L., Balthasar, N., Hampel, B., Waisman, A., *et al.* (2005). Agouti-related peptide-expressing neurons are mandatory for feeding. *Nat Neurosci* *8*, 1289-1291.
- Grundy, S.M. (2008). Metabolic syndrome pandemic. *Arterioscler Thromb Vasc Biol* *28*, 629-636.

- Hagan, M.M., Rushing, P.A., Schwartz, M.W., Yagaloff, K.A., Burn, P., Woods, S.C., and Seeley, R.J. (1999). Role of the CNS melanocortin system in the response to overfeeding. *J Neurosci* *19*, 2362-2367.
- Hakansson, M.L., and Meister, B. (1998). Transcription factor STAT3 in leptin target neurons of the rat hypothalamus. *Neuroendocrinology* *68*, 420-427.
- Hansen, L., Deacon, C.F., Orskov, C., and Holst, J.J. (1999). Glucagon-like peptide-1-(7-36)amide is transformed to glucagon-like peptide-1-(9-36)amide by dipeptidyl peptidase IV in the capillaries supplying the L cells of the porcine intestine. *Endocrinology* *140*, 5356-5363.
- Hanson, M., Gluckman, P., and Bustreo, F. (2016). Obesity and the health of future generations. *Lancet Diabetes Endocrinol* *4*, 966-967.
- Harno, E., Gali Ramamoorthy, T., Coll, A.P., and White, A. (2018). POMC: The Physiological Power of Hormone Processing. *Physiol Rev* *98*, 2381-2430.
- Heiman, M., Schaefer, A., Gong, S., Peterson, J.D., Day, M., Ramsey, K.E., Suarez-Farinas, M., Schwarz, C., Stephan, D.A., Surmeier, D.J., *et al.* (2008). A translational profiling approach for the molecular characterization of CNS cell types. *Cell* *135*, 738-748.
- Hess, W. (1949). *Das Zwischenhirn: Syndrome Lokalisationen Funktionen (The Diencephalon: Syndrome Localization Function)*(ed. 2).
- Hetherington, A., and Ranson, S. (1942). Effect of early hypophysectomy on hypothalamic obesity. *Endocrinology* *31*, 30-34.
- Holst, J.J. (2007). The physiology of glucagon-like peptide 1. *Physiol Rev* *87*, 1409-1439.
- Horn, R., and Marty, A. (1988). Muscarinic activation of ionic currents measured by a new whole-cell recording method. *J Gen Physiol* *92*, 145-159.
- Horvath, T.L., Bechmann, I., Naftolin, F., Kalra, S.P., and Leranth, C. (1997). Heterogeneity in the neuropeptide Y-containing neurons of the rat arcuate nucleus: GABAergic and non-GABAergic subpopulations. *Brain Res* *756*, 283-286.
- Huang, Z.J., and Zeng, H. (2013). Genetic approaches to neural circuits in the mouse. *Annu Rev Neurosci* *36*, 183-215.
- Huo, L., Grill, H.J., and Bjorbaek, C. (2006). Divergent regulation of proopiomelanocortin neurons by leptin in the nucleus of the solitary tract and in the arcuate hypothalamic nucleus. *Diabetes* *55*, 567-573.
- Huszar, D., Lynch, C.A., Fairchild-Huntress, V., Dunmore, J.H., Fang, Q., Berkemeier, L.R., Gu, W., Kesterson, R.A., Boston, B.A., Cone, R.D., *et al.* (1997). Targeted disruption of the melanocortin-4 receptor results in obesity in mice. *Cell* *88*, 131-141.
- Jackson, R.S., Creemers, J.W., Ohagi, S., Raffin-Sanson, M.L., Sanders, L., Montague, C.T., Hutton, J.C., and O'Rahilly, S. (1997). Obesity and impaired prohormone processing associated with mutations in the human prohormone convertase 1 gene. *Nat Genet* *16*, 303-306.
- Jarvie, B.C., and Hentges, S.T. (2012). Expression of GABAergic and glutamatergic phenotypic markers in hypothalamic proopiomelanocortin neurons. *J Comp Neurol* *520*, 3863-3876.
- Kaesler, P.S., and Regehr, W.G. (2014). Molecular mechanisms for synchronous, asynchronous, and spontaneous neurotransmitter release. *Annu Rev Physiol* *76*, 333-363.
- Kastin, A.J., Akerstrom, V., and Pan, W. (2002). Interactions of glucagon-like peptide-1 (GLP-1) with the blood-brain barrier. *J Mol Neurosci* *18*, 7-14.
- Kavalali, E.T. (2015). The mechanisms and functions of spontaneous neurotransmitter release. *Nat Rev Neurosci* *16*, 5-16.
- Kelley, A.E., Baldo, B.A., Pratt, W.E., and Will, M.J. (2005). Corticostriatal-hypothalamic circuitry and food motivation: integration of energy, action and reward. *Physiol Behav* *86*, 773-795.

- Kieffer, T.J., and Francis Habener, J. (1999). The Glucagon-Like Peptides. *Endocrine Reviews* 20, 876-913.
- Kievit, P., Halem, H., Marks, D.L., Dong, J.Z., Glavas, M.M., Sinnayah, P., Pranger, L., Cowley, M.A., Grove, K.L., and Culler, M.D. (2013). Chronic treatment with a melanocortin-4 receptor agonist causes weight loss, reduces insulin resistance, and improves cardiovascular function in diet-induced obese rhesus macaques. *Diabetes* 62, 490-497.
- Kim, E.M., Grace, M.K., Welch, C.C., Billington, C.J., and Levine, A.S. (1999). STZ-induced diabetes decreases and insulin normalizes POMC mRNA in arcuate nucleus and pituitary in rats. *Am J Physiol* 276, R1320-1326.
- Koch, M., Varela, L., Kim, J.G., Kim, J.D., Hernandez-Nuno, F., Simonds, S.E., Castorena, C.M., Vianna, C.R., Elmquist, J.K., Morozov, Y.M., *et al.* (2015). Hypothalamic POMC neurons promote cannabinoid-induced feeding. *Nature* 519, 45-50.
- Konda, Y., Gantz, I., DelValle, J., Shimoto, Y., Miwa, H., and Yamada, T. (1994). Interaction of dual intracellular signaling pathways activated by the melanocortin-3 receptor. *J Biol Chem* 269, 13162-13166.
- Krashes, M.J. (2017). Untangling Appetite Circuits with Optogenetics and Chemogenetics. In *Appetite and Food Intake: Central Control*, nd, and R.B.S. Harris, eds. (Boca Raton (FL)), pp. 91-116.
- Krashes, M.J., Koda, S., Ye, C., Rogan, S.C., Adams, A.C., Cusher, D.S., Maratos-Flier, E., Roth, B.L., and Lowell, B.B. (2011). Rapid, reversible activation of AgRP neurons drives feeding behavior in mice. *J Clin Invest* 121, 1424-1428.
- Krude, H., Biebermann, H., Luck, W., Horn, R., Brabant, G., and Gruters, A. (1998). Severe early-onset obesity, adrenal insufficiency and red hair pigmentation caused by POMC mutations in humans. *Nat Genet* 19, 155-157.
- Kyrozis, A., and Reichling, D.B. (1995). Perforated-patch recording with gramicidin avoids artifactual changes in intracellular chloride concentration. *Journal of Neuroscience Methods*, 27-35.
- Lam, B.Y.H., Cimino, I., Poley-Wolf, J., Nicole Kohnke, S., Rimmington, D., Iyemere, V., Heeley, N., Cossetti, C., Schulte, R., Saraiva, L.R., *et al.* (2017). Heterogeneity of hypothalamic pro-opiomelanocortin-expressing neurons revealed by single-cell RNA sequencing. *Mol Metab* 6, 383-392.
- Lam, D.D., Attard, C.A., Mercer, A.J., Myers, M.G., Jr., Rubinstein, M., and Low, M.J. (2015). Conditional expression of *Pomc* in the *Lepr*-positive subpopulation of POMC neurons is sufficient for normal energy homeostasis and metabolism. *Endocrinology* 156, 1292-1302.
- Lee, E.J., Martinson, F., Kotlar, T., Thimmapaya, B., and Jameson, J.L. (2001). Adenovirus-mediated targeted expression of toxic genes to adrenocorticotropin-producing pituitary tumors using the proopiomelanocortin promoter. *J Clin Endocrinol Metab* 86, 3400-3409.
- Lee, S., and Lee, D.Y. (2017). Glucagon-like peptide-1 and glucagon-like peptide-1 receptor agonists in the treatment of type 2 diabetes. *Ann Pediatr Endocrinol Metab* 22, 15-26.
- Leshan, R.L., Bjornholm, M., Munzberg, H., and Myers, M.G., Jr. (2006). Leptin receptor signaling and action in the central nervous system. *Obesity (Silver Spring)* 14 Suppl 5, 208S-212S.
- Levin, B.E., Becker, T.C., Eiki, J., Zhang, B.B., and Dunn-Meynell, A.A. (2008). Ventromedial hypothalamic glucokinase is an important mediator of the counterregulatory response to insulin-induced hypoglycemia. *Diabetes* 57, 1371-1379.

- Lima, L.B., Metzger, M., Furigo, I.C., and Donato, J., Jr. (2016). Leptin receptor-positive and leptin receptor-negative proopiomelanocortin neurons innervate an identical set of brain structures. *Brain Res* 1646, 366-376.
- Lindau, M., and Fernandez, J.M. (1986). IgE-mediated degranulation of mast cells does not require opening of ion channels. *Nature* 319, 150-153.
- Lippert, R.N., Cremer, A.L., Edwin Thanarajah, S., Korn, C., Jahans-Price, T., Burgeno, L.M., Tittgemeyer, M., Bruning, J.C., Walton, M.E., and Backes, H. (2019). Time-dependent assessment of stimulus-evoked regional dopamine release. *Nat Commun* 10, 336.
- Liu, T., Kong, D., Shah, B.P., Ye, C., Koda, S., Saunders, A., Ding, J.B., Yang, Z., Sabatini, B.L., and Lowell, B.B. (2012). Fasting activation of AgRP neurons requires NMDA receptors and involves spinogenesis and increased excitatory tone. *Neuron* 73, 511-522.
- Locke, A.E., Kahali, B., Berndt, S.I., Justice, A.E., Pers, T.H., Day, F.R., Powell, C., Vedantam, S., Buchkovich, M.L., Yang, J., *et al.* (2015). Genetic studies of body mass index yield new insights for obesity biology. *Nature* 518, 197-206.
- Lohr, H., Hess, S., Pereira, M.M.A., Reinoss, P., Leibold, S., Schenkel, C., Wunderlich, C.M., Kloppenburg, P., Bruning, J.C., and Hammerschmidt, M. (2018). Diet-Induced Growth Is Regulated via Acquired Leptin Resistance and Engages a Pomc-Somatostatin-Growth Hormone Circuit. *Cell Rep* 23, 1728-1741.
- Love, M.I., Huber, W., and Anders, S. (2014). Moderated estimation of fold change and dispersion for RNA-seq data with DESeq2. *Genome Biol* 15, 550.
- Lu, D., Willard, D., Patel, I.R., Kadwell, S., Overton, L., Kost, T., Luther, M., Chen, W., Woychik, R.P., Wilkison, W.O., *et al.* (1994). Agouti protein is an antagonist of the melanocyte-stimulating-hormone receptor. *Nature* 371, 799-802.
- Luquet, S., Perez, F.A., Hnasko, T.S., and Palmiter, R.D. (2005). NPY/AgRP neurons are essential for feeding in adult mice but can be ablated in neonates. *Science* 310, 683-685.
- Madisen, L., Garner, A.R., Shimaoka, D., Chuong, A.S., Klapoetke, N.C., Li, L., van der Bourg, A., Niino, Y., Egolf, L., Monetti, C., *et al.* (2015). Transgenic mice for intersectional targeting of neural sensors and effectors with high specificity and performance. *Neuron* 85, 942-958.
- Meeran, K., O'Shea, D., Edwards, C.M., Turton, M.D., Heath, M.M., Gunn, I., Abusnana, S., Rossi, M., Small, C.J., Goldstone, A.P., *et al.* (1999). Repeated intracerebroventricular administration of glucagon-like peptide-1-(7-36) amide or exendin-(9-39) alters body weight in the rat. *Endocrinology* 140, 244-250.
- Millington, G., and Buckingham, J.C. (1992). Thymic peptides and neuroendocrine-immune communication. *J Endocrinol* 133, 163-168.
- Millington, G.W. (2006). Proopiomelanocortin (POMC): the cutaneous roles of its melanocortin products and receptors. *Clin Exp Dermatol* 31, 407-412.
- Millington, G.W. (2007). The role of proopiomelanocortin (POMC) neurones in feeding behaviour. *Nutr Metab (Lond)* 4, 18.
- Millington, G.W., Tung, Y.C., Hewson, A.K., O'Rahilly, S., and Dickson, S.L. (2001). Differential effects of alpha-, beta- and gamma(2)-melanocyte-stimulating hormones on hypothalamic neuronal activation and feeding in the fasted rat. *Neuroscience* 108, 437-445.
- Mizuno, T.M., Kleopoulos, S.P., Bergen, H.T., Roberts, J.L., Priest, C.A., and Mobbs, C.V. (1998). Hypothalamic pro-opiomelanocortin mRNA is reduced by fasting and [corrected] in ob/ob and db/db mice, but is stimulated by leptin. *Diabetes* 47, 294-297.
- Muscogiuri, G., DeFronzo, R.A., Gastaldelli, A., and Holst, J.J. (2017). Glucagon-like Peptide-1 and the Central/Peripheral Nervous System: Crosstalk in Diabetes. *Trends Endocrinol Metab* 28, 88-103.

- Navarro, S., Soletto, L., Puchol, S., Rotllant, J., Soengas, J.L., and Cerda-Reverter, J.M. (2016). 60 YEARS OF POMC: POMC: an evolutionary perspective. *J Mol Endocrinol* *56*, T113-118.
- Nishizawa, M., Nakabayashi, H., Uchida, K., Nakagaw, A., and Nijima, A. (1996). The hepatic vagal nerve is receptive to incretin hormone glucagon-like peptide-I, but not to glucose-dependent insulinotropic polypeptide, in the portal vein. *Journal of the autonomic nervous system* *61*, 149-154.
- Nohara, M., Momoeda, M., Kubota, T., and Nakabayashi, M. (2011). Menstrual cycle and menstrual pain problems and related risk factors among Japanese female workers. *Ind Health* *49*, 228-234.
- O'Rahilly, S., Farooqi, I.S., Yeo, G.S., and Challis, B.G. (2003). Minireview: human obesity-lessons from monogenic disorders. *Endocrinology* *144*, 3757-3764.
- Ollmann, M.M., Wilson, B.D., Yang, Y.K., Kerns, J.A., Chen, Y., Gantz, I., and Barsh, G.S. (1997). Antagonism of central melanocortin receptors in vitro and in vivo by agouti-related protein. *Science* *278*, 135-138.
- Olofsson, L.E., Pierce, A.A., and Xu, A.W. (2009). Functional requirement of AgRP and NPY neurons in ovarian cycle-dependent regulation of food intake. *Proc Natl Acad Sci U S A* *106*, 15932-15937.
- Organization, W.H. (2018). *World Health Statistics 2018: Monitoring Health for the SDGs Sustainable Development Goals* (World Health Organization).
- Orskov, C., Poulsen, S.S., Moller, M., and Holst, J.J. (1996). Glucagon-like peptide I receptors in the subfornical organ and the area postrema are accessible to circulating glucagon-like peptide I. *Diabetes* *45*, 832-835.
- Padilla, S.L., Carmody, J.S., and Zeltser, L.M. (2010). Pomc-expressing progenitors give rise to antagonistic neuronal populations in hypothalamic feeding circuits. *Nat Med* *16*, 403-405.
- Pan, C., Cai, R., Quacquarelli, F.P., Ghasemigharagoz, A., Loubopoulos, A., Matryba, P., Plesnila, N., Dichgans, M., Hellal, F., and Erturk, A. (2016). Shrinkage-mediated imaging of entire organs and organisms using uDISCO. *Nat Methods* *13*, 859-867.
- Parton, L.E., Ye, C.P., Coppari, R., Enriori, P.J., Choi, B., Zhang, C.Y., Xu, C., Vianna, C.R., Balthasar, N., Lee, C.E., *et al.* (2007). Glucose sensing by POMC neurons regulates glucose homeostasis and is impaired in obesity. *Nature* *449*, 228-232.
- Patro, R., Duggal, G., Love, M.I., Irizarry, R.A., and Kingsford, C. (2017). Salmon provides fast and bias-aware quantification of transcript expression. *Nat Methods* *14*, 417-419.
- Pinto, S., Roseberry, A.G., Liu, H., Diano, S., Shanabrough, M., Cai, X., Friedman, J.M., and Horvath, T.L. (2004). Rapid rewiring of arcuate nucleus feeding circuits by leptin. *Science* *304*, 110-115.
- Pop, M.G., Crivii, C., and Opincariu, I. (2018). *Anatomy and Function of the Hypothalamus. Hypothalamus in Health and Diseases.*
- Poulin, J.F., Caronia, G., Hofer, C., Cui, Q., Helm, B., Ramakrishnan, C., Chan, C.S., Dombeck, D.A., Deisseroth, K., and Awatramani, R. (2018). Mapping projections of molecularly defined dopamine neuron subtypes using intersectional genetic approaches. *Nat Neurosci* *21*, 1260-1271.
- Pritchard, L.E., Turnbull, A.V., and White, A. (2002). Pro-opiomelanocortin processing in the hypothalamus: impact on melanocortin signalling and obesity. *J Endocrinol* *172*, 411-421.
- Rae, J., Cooper, K., Gates, P., and Watsky, M. (1991). Low access resistance perforated patch recordings using amphotericin B. *J Neurosci Methods* *37*, 15-26.

- Ramadori, G., Fujikawa, T., Anderson, J., Berglund, E.D., Frazao, R., Michan, S., Vianna, C.R., Sinclair, D.A., Elias, C.F., and Coppari, R. (2011). SIRT1 deacetylase in SF1 neurons protects against metabolic imbalance. *Cell Metab* *14*, 301-312.
- Richards, P., Parker, H.E., Adriaenssens, A.E., Hodgson, J.M., Cork, S.C., Trapp, S., Gribble, F.M., and Reimann, F. (2014). Identification and characterization of GLP-1 receptor-expressing cells using a new transgenic mouse model. *Diabetes* *63*, 1224-1233.
- Ring, L.E., and Zeltser, L.M. (2010). Disruption of hypothalamic leptin signaling in mice leads to early-onset obesity, but physiological adaptations in mature animals stabilize adiposity levels. *J Clin Invest* *120*, 2931-2941.
- Roberts, C.K., Hevener, A.L., and Barnard, R.J. (2013). Metabolic syndrome and insulin resistance: underlying causes and modification by exercise training. *Compr Physiol* *3*, 1-58.
- Rodriguez, E.M., Blazquez, J.L., and Guerra, M. (2010). The design of barriers in the hypothalamus allows the median eminence and the arcuate nucleus to enjoy private milieus: the former opens to the portal blood and the latter to the cerebrospinal fluid. *Peptides* *31*, 757-776.
- Rogan, S.C., and Roth, B.L. (2011). Remote control of neuronal signaling. *Pharmacol Rev* *63*, 291-315.
- Roselli-Reh fuss, L., Mountjoy, K.G., Robbins, L.S., Mortrud, M.T., Low, M.J., Tatro, J.B., Entwistle, M.L., Simerly, R.B., and Cone, R.D. (1993). Identification of a receptor for gamma melanotropin and other proopiomelanocortin peptides in the hypothalamus and limbic system. *Proc Natl Acad Sci U S A* *90*, 8856-8860.
- Rouille, Y., Martin, S., and Steiner, D.F. (1995). Differential processing of proglucagon by the subtilisin-like prohormone convertases PC2 and PC3 to generate either glucagon or glucagon-like peptide. *J Biol Chem* *270*, 26488-26496.
- Sandoval, D.A., Bagnol, D., Woods, S.C., D'Alessio, D.A., and Seeley, R.J. (2008). Arcuate glucagon-like peptide 1 receptors regulate glucose homeostasis but not food intake. *Diabetes* *57*, 2046-2054.
- Sawchenko, P.E., Brown, E.R., Chan, R.K., Ericsson, A., Li, H.Y., Roland, B.L., and Kovacs, K.J. (1996). The paraventricular nucleus of the hypothalamus and the functional neuroanatomy of visceromotor responses to stress. *Prog Brain Res* *107*, 201-222.
- Schioth, H.B., Chhajlani, V., Muceniece, R., Klusa, V., and Wikberg, J.E. (1996). Major pharmacological distinction of the ACTH receptor from other melanocortin receptors. *Life Sci* *59*, 797-801.
- Schwartz, G.J. (2000). The role of gastrointestinal vagal afferents in the control of food intake: current prospects. *Nutrition* *16*, 866-873.
- Schwartz, M.W., Seeley, R.J., Zeltser, L.M., Drewnowski, A., Ravussin, E., Redman, L.M., and Leibel, R.L. (2017). Obesity Pathogenesis: An Endocrine Society Scientific Statement. *Endocr Rev* *38*, 267-296.
- Secher, A., Jelsing, J., Baquero, A.F., Hecksher-Sorensen, J., Cowley, M.A., Dalboge, L.S., Hansen, G., Grove, K.L., Pyke, C., Raun, K., *et al.* (2014). The arcuate nucleus mediates GLP-1 receptor agonist liraglutide-dependent weight loss. *J Clin Invest* *124*, 4473-4488.
- Shi, H., Sorrell, J.E., Clegg, D.J., Woods, S.C., and Seeley, R.J. (2010). The roles of leptin receptors on POMC neurons in the regulation of sex-specific energy homeostasis. *Physiol Behav* *100*, 165-172.
- Simerley, R. (1995). Anatomical substrates of hypothalamic integration. The rat nervous system.

- Sisley, S., Smith, K., Sandoval, D.A., and Seeley, R.J. (2014). Differences in acute anorectic effects of long-acting GLP-1 receptor agonists in rats. *Peptides* 58, 1-6.
- Smart, J.L., Tolle, V., Otero-Corchon, V., and Low, M.J. (2007). Central dysregulation of the hypothalamic-pituitary-adrenal axis in neuron-specific proopiomelanocortin-deficient mice. *Endocrinology* 148, 647-659.
- Snijder, M.B., Heine, R.J., Seidell, J.C., Bouter, L.M., Stehouwer, C.D., Nijpels, G., Funahashi, T., Matsuzawa, Y., Shimomura, I., and Dekker, J.M. (2006). Associations of adiponectin levels with incident impaired glucose metabolism and type 2 diabetes in older men and women: the hoorn study. *Diabetes Care* 29, 2498-2503.
- Sohn, J.W., Xu, Y., Jones, J.E., Wickman, K., Williams, K.W., and Elmquist, J.K. (2011). Serotonin 2C receptor activates a distinct population of arcuate pro-opiomelanocortin neurons via TRPC channels. *Neuron* 71, 488-497.
- Stanley, B.G., and Leibowitz, S.F. (1984). Neuropeptide Y: stimulation of feeding and drinking by injection into the paraventricular nucleus. *Life Sci* 35, 2635-2642.
- Steculorum, S.M., Ruud, J., Karakasilioti, I., Backes, H., Engstrom Ruud, L., Timper, K., Hess, M.E., Tsaousidou, E., Mauer, J., Vogt, M.C., *et al.* (2016). AgRP Neurons Control Systemic Insulin Sensitivity via Myostatin Expression in Brown Adipose Tissue. *Cell* 165, 125-138.
- Sternson, S.M., Atasoy, D., Betley, J.N., Henry, F.E., and Xu, S. (2016). An Emerging Technology Framework for the Neurobiology of Appetite. *Cell Metab* 23, 234-253.
- Stuber, G.D., and Wise, R.A. (2016). Lateral hypothalamic circuits for feeding and reward. *Nat Neurosci* 19, 198-205.
- Swanson, L.W., and Kuypers, H.G. (1980). The paraventricular nucleus of the hypothalamus: cytoarchitectonic subdivisions and organization of projections to the pituitary, dorsal vagal complex, and spinal cord as demonstrated by retrograde fluorescence double-labeling methods. *J Comp Neurol* 194, 555-570.
- Ten Kulve, J.S., van Bloemendaal, L., Balesar, R., RG, I.J., Swaab, D.F., Diamant, M., la Fleur, S.E., and Alkemade, A. (2016). Decreased Hypothalamic Glucagon-Like Peptide-1 Receptor Expression in Type 2 Diabetes Patients. *J Clin Endocrinol Metab* 101, 2122-2129.
- Thompson, R.H., and Swanson, L.W. (1998). Organization of inputs to the dorsomedial nucleus of the hypothalamus: a reexamination with Fluorogold and PHAL in the rat. *Brain Res Brain Res Rev* 27, 89-118.
- Timper, K., and Bruning, J.C. (2017). Hypothalamic circuits regulating appetite and energy homeostasis: pathways to obesity. *Dis Model Mech* 10, 679-689.
- Toda, C., Santoro, A., Kim, J.D., and Diano, S. (2017). POMC Neurons: From Birth to Death. *Annu Rev Physiol* 79, 209-236.
- Urban, D.J., and Roth, B.L. (2015). DREADDs (designer receptors exclusively activated by designer drugs): chemogenetic tools with therapeutic utility. *Annu Rev Pharmacol Toxicol* 55, 399-417.
- Vahl, T.P., Tauchi, M., Durler, T.S., Elfers, E.E., Fernandes, T.M., Bitner, R.D., Ellis, K.S., Woods, S.C., Seeley, R.J., Herman, J.P., *et al.* (2007). Glucagon-like peptide-1 (GLP-1) receptors expressed on nerve terminals in the portal vein mediate the effects of endogenous GLP-1 on glucose tolerance in rats. *Endocrinology* 148, 4965-4973.
- Van der Ploeg, L.H., Martin, W.J., Howard, A.D., Nargund, R.P., Austin, C.P., Guan, X., Drisko, J., Cashen, D., Sebbat, I., Patchett, A.A., *et al.* (2002). A role for the melanocortin 4 receptor in sexual function. *Proc Natl Acad Sci U S A* 99, 11381-11386.

- Vasudevan, A.R., Burns, A., and Fonseca, V.A. (2006). The effectiveness of intensive glycemic control for the prevention of vascular complications in diabetes mellitus. *Treat Endocrinol* 5, 273-286.
- Wang, C., He, Y., Xu, P., Yang, Y., Saito, K., Xia, Y., Yan, X., Hinton, A., Jr., Yan, C., Ding, H., *et al.* (2018). TAp63 contributes to sexual dimorphism in POMC neuron functions and energy homeostasis. *Nat Commun* 9, 1544.
- Wang, D., He, X., Zhao, Z., Feng, Q., Lin, R., Sun, Y., Ding, T., Xu, F., Luo, M., and Zhan, C. (2015). Whole-brain mapping of the direct inputs and axonal projections of POMC and AgRP neurons. *Front Neuroanat* 9, 40.
- Wang, Z., do Carmo, J.M., da Silva, A.A., Bailey, K.C., Aberdein, N., Moak, S.P., and Hall, J.E. (2019). Role of SOCS3 in POMC neurons in metabolic and cardiovascular regulation. *Am J Physiol Regul Integr Comp Physiol* 316, R338-R351.
- Wardlaw, S.L., McCarthy, K.C., and Conwell, I.M. (1998). Glucocorticoid regulation of hypothalamic proopiomelanocortin. *Neuroendocrinology* 67, 51-57.
- Waterson, M.J., and Horvath, T.L. (2015). Neuronal Regulation of Energy Homeostasis: Beyond the Hypothalamus and Feeding. *Cell Metab* 22, 962-970.
- Wikberg, J.E., Muceniece, R., Mandrika, I., Prusis, P., Lindblom, J., Post, C., and Skottner, A. (2000). New aspects on the melanocortins and their receptors. *Pharmacol Res* 42, 393-420.
- Williams, K.W., Margatho, L.O., Lee, C.E., Choi, M., Lee, S., Scott, M.M., Elias, C.F., and Elmquist, J.K. (2010). Segregation of acute leptin and insulin effects in distinct populations of arcuate proopiomelanocortin neurons. *J Neurosci* 30, 2472-2479.
- Xia, Y., Wikberg, J.E., and Chhajlani, V. (1995). Expression of melanocortin 1 receptor in periaqueductal gray matter. *Neuroreport* 6, 2193-2196.
- Xu, J., Bartolome, C.L., Low, C.S., Yi, X., Chien, C.H., Wang, P., and Kong, D. (2018). Genetic identification of leptin neural circuits in energy and glucose homeostases. *Nature* 556, 505-509.
- Yang, Y., Atasoy, D., Su, H.H., and Sternson, S.M. (2011). Hunger states switch a flip-flop memory circuit via a synaptic AMPK-dependent positive feedback loop. *Cell* 146, 992-1003.
- Yang, Y., Moghadam, A.A., Corder, Z.A., Liang, N.C., and Moran, T.H. (2014). Long term exendin-4 treatment reduces food intake and body weight and alters expression of brain homeostatic and reward markers. *Endocrinology* 155, 3473-3483.
- Yaswen, L., Diehl, N., Brennan, M.B., and Hochgeschwender, U. (1999). Obesity in the mouse model of pro-opiomelanocortin deficiency responds to peripheral melanocortin. *Nat Med* 5, 1066-1070.
- Yates, A., Beal, K., Keenan, S., McLaren, W., Pignatelli, M., Ritchie, G.R., Ruffier, M., Taylor, K., Vullo, A., and Flicek, P. (2015). The Ensembl REST API: Ensembl Data for Any Language. *Bioinformatics* 31, 143-145.
- Ye, J.H., Zhang, J., Xiao, C., and Kong, J.Q. (2006). Patch-clamp studies in the CNS illustrate a simple new method for obtaining viable neurons in rat brain slices: glycerol replacement of NaCl protects CNS neurons. *J Neurosci Methods* 158, 251-259.
- Yu, G., Wang, L.G., Han, Y., and He, Q.Y. (2012). clusterProfiler: an R package for comparing biological themes among gene clusters. *OMICS* 16, 284-287.
- Zambrowicz, B.P., Imamoto, A., Fiering, S., Herzenberg, L.A., Kerr, W.G., and Soriano, P. (1997). Disruption of overlapping transcripts in the ROSA beta geo 26 gene trap strain leads to widespread expression of beta-galactosidase in mouse embryos and hematopoietic cells. *Proc Natl Acad Sci U S A* 94, 3789-3794.

- Zhan, C., Zhou, J., Feng, Q., Zhang, J.E., Lin, S., Bao, J., Wu, P., and Luo, M. (2013). Acute and long-term suppression of feeding behavior by POMC neurons in the brainstem and hypothalamus, respectively. *J Neurosci* 33, 3624-3632.
- Zheng, H., Patterson, L.M., Phifer, C.B., and Berthoud, H.R. (2005). Brain stem melanocortinerigic modulation of meal size and identification of hypothalamic POMC projections. *Am J Physiol Regul Integr Comp Physiol* 289, R247-258.
- Zhu, X., Zhou, A., Dey, A., Norrbom, C., Carroll, R., Zhang, C., Laurent, V., Lindberg, I., Ugleholdt, R., Holst, J.J., *et al.* (2002). Disruption of PC1/3 expression in mice causes dwarfism and multiple neuroendocrine peptide processing defects. *Proc Natl Acad Sci U S A* 99, 10293-10298.

6 Summary

The anorexigenic pro-opiomelanocortin (*Pomc*)-expressing neurons of the arcuate nucleus of the hypothalamus (ARC) are constituents of the melanocortin system, and their function is pivotal in control of systemic energy homeostasis. Adjacency to the median eminence and a fenestrated blood-brain barrier exposes the neurons of the melanocortin system to hormones and stimuli from the periphery. These signals are integrated and serve as a basis for the exertion of optimal responses in the regulation of homeostatic processes.

Defined by the expression of POMC, it has been assumed that these neurons are a uniform group; however, cumulative electrophysiological and single-cell sequencing evidence hint at both functional and molecular heterogeneity of POMC neurons. Deciphering this heterogeneity is crucial in understanding how a wide range of stimuli are integrated and unraveling the intricacies in metabolic control mediated by different POMC subpopulations.

In the present study, we utilize intersectional Cre/Dre-dependent transgenic mouse models to successfully target distinct leptin receptor (*Lepr*) and glucagon-like peptide receptor (*Glp1r*) expressing POMC neurons. This system enabled a detailed description of anatomical distribution, translational profiling, and functional characterization of these two POMC subpopulations. Our experiments reveal that $POMC^{Lepr+}$ and $POMC^{Glp1r+}$ neurons exhibit distinct anatomical distribution patterns within the ARC by using tissue clearing and three-dimensional image assessment. In addition, electrophysiological recordings from these neurons illustrated variations in their key intrinsic properties. Molecular profiling revealed a differential expression in receptors for energy state communicating hormones and neurotransmitters. Finally, employing the Cre/Dre-dependent activatory chemogenetic system for both neuronal groups demonstrated differential regulation of the two subpopulations with regards to food intake. Collectively, this work reveals heterogeneity of critical metabolism-regulatory POMC neurons.

7 Zusammenfassung

Die anorexigenen pro-opiomelanocortin (POMC)-exprimierenden Neuronen des *Nucleus arcuatus* (ARC) des Hypothalamus sind wesentliche Bestandteile des Melanocortin-Systems und ihre Funktion ist entscheidend für die Kontrolle der systemischen Energiehomöostase. Durch die unmittelbare Nähe zur *Eminentia mediana* und einer fenestrierten Blut-Hirn-Schranke sind die Neurone des Melanocortin-Systems Hormonen und Stimuli aus der Peripherie ausgesetzt. Diese Signale werden integriert und dienen als Grundlage zur Ausübung optimaler Reaktionen in der Regulation homöostatischer Prozesse.

Definiert durch die Expression von POMC, wurde davon ausgegangen, dass diese Neuronen eine einheitliche Gruppe bilden, allerdings deutet eine zunehmende Anzahl an Befunden aus elektrophysiologischen Untersuchungen und Einzelzell-Sequenzierungen auf eine funktionelle und molekulare Heterogenität der POMC-Neuronen hin. Die Entschlüsselung dieser Diversifikation ist entscheidend um zu verstehen, wie verschiedene Stimuli aus der Peripherie integriert werden und inwiefern verschiedene POMC-Subpopulationen an der Feinjustierung der metabolischen Homöostase beteiligt sind.

In der vorliegenden Studie verwenden wir intersektionale Cre/Dre-abhängige transgene Mausmodelle zur gezielten Manipulation von POMC Neuronen, die entweder den Leptin-Rezeptor (*Lepr*) oder den *Glucagon-like peptide 1* (*Glp1*)-Rezeptor ausprägen. Dieses System ermöglicht eine detaillierte Beschreibung der anatomischen Lokalisierung, translatorisches Profiling und eine funktionelle Charakterisierung dieser beiden POMC-Subpopulationen. Mittels Gewebe-Clearing und dreidimensionaler Bildgebung zeigte sich, dass POMC^{Lepr+} und POMC^{Glp1r+} Neuronen deutlich voneinander zu unterscheidende anatomische Verteilungsmuster innerhalb des ARC aufweisen. Darüber hinaus zeigte die elektrophysiologische Charakterisierung dieser Neuronensubpopulationen Unterschiede in ihren wichtigsten intrinsischen Eigenschaften. Molekulares Profiling ergab zudem eine unterschiedliche Expression von Neurotransmittern und Rezeptoren Energiehaushalts-regulierender Hormone. Schließlich zeigte der Einsatz des Cre/Dre-abhängigen aktivierenden chemogenetischen Systems in den beiden Neuronengruppen eine unterschiedliche Regulation hinsichtlich der Nahrungsaufnahme. Zusammenfassend identifiziert diese Arbeit die Heterogenität kritischer stoffwechselregulierender POMC-Neuronen.

8 Erklärung

Hiermit versichere ich an Eides statt, dass ich die vorliegende Dissertation selbstständig und ohne die Benutzung anderer als der angegebenen Hilfsmittel und Literatur angefertigt habe. Alle Stellen, die wörtlich oder sinngemäß aus veröffentlichten und nicht veröffentlichten Werken dem Wortlaut oder dem Sinn nach entnommen wurden, sind als solche kenntlich gemacht. Ich versichere an Eides statt, dass diese Dissertation noch keiner anderen Fakultät oder Universität zur Prüfung vorgelegen hat; dass sie - abgesehen von unten angegebenen Teilpublikationen und eingebundenen Artikeln und Manuskripten - noch nicht veröffentlicht worden ist sowie, dass ich eine Veröffentlichung der Dissertation vor Abschluss der Promotion nicht ohne Genehmigung des Promotionsausschusses vornehmen werde. Die Bestimmungen dieser Ordnung sind mir bekannt. Darüber hinaus erkläre ich hiermit, dass ich die Ordnung zur Sicherung guter wissenschaftlicher Praxis und zum Umgang mit wissenschaftlichem Fehlverhalten der Universität zu Köln gelesen und sie bei der Durchführung der Dissertation zugrundeliegenden Arbeiten und der schriftlich verfassten Dissertation beachtet habe und verpflichte mich hiermit, die dort genannten Vorgaben bei allen wissenschaftlichen Tätigkeiten zu beachten und umzusetzen. Ich versichere, dass die eingereichte elektronische Fassung der eingereichten Druckfassung vollständig entspricht.

Teilpublikationen:

Biglari, N., Gaziano, I., Schumacher, J. *et al.* Functionally distinct POMC-expressing neuron subpopulations in hypothalamus revealed by intersectional targeting. *Nat Neurosci* 24, 913–929 (2021). <https://doi.org/10.1038/s41593-021-00854-0>

Nasim Biglari

July 2021

9 Acknowledgements

Thank you to all past and present members of AG Brüning and AG Wunderlich for creating an unbelievably wonderful working atmosphere that has been both mentally stimulating and fun. I would like to give particular thanks to

Prof. Dr. Jens Brüning: Thank you for giving me the opportunity to join the group and work on this great project. I thank you even more for your amazing support, your inquisitive approach to science and optimism throughout the challenging periods.

Prof. Dr. Peter Kloppenburg: Thank you for the amazing collaboration on this project. I truly enjoyed all the discussions in endeavoring to understand the complexity of POMC neurons!

Prof. Dr. Matthias Hammerschmidt: Thank you for being a part of my thesis committee and for the stimulating discussions over the years. It's been an honor.

Dr. Ursula Lichtenberg: Thank you for organizing everything all these years! Without you the lab wouldn't survive.

Cornelius Iovan: Thank you for all many many PCRs and the incredibly organized system you created. Also, for the fun conversations!

Lars Paeger, Jan Radermacher and Svenja Corneliussen from the Kloppenburg group: I cannot thank you enough for all work you have done during our collaboration over the years. It would not have been possible without you.

Weiye, Paul, Corinna, Maggie, Elisa, Anna, Pia and Daria thank you for creating a fun atmosphere.

Dr. Stefan Vollmar, Michael Sue, Ingo Alt, David Hitze and Jürgen Schneppe: Thank you for your patience and your help with all our incessant requests.

Dank an alle Tierpfleger, vor allem Michael Keltz and Johannes van der Burgwal.
And a big thanks to Hella and Karina!

Jonas: thanks for sharing this project with me. Thinking back to the time you were in the lab always puts a smile on my face.

Maggie and Philipp: Thank you both for taking the time to read my thesis.

Philipp: I truly appreciated having you there in the lab on a daily basis, discussing science and talking about everything else. It was great having you as a companion in all these years, throughout the highs and lows.

Sinika: Thank you for sharing an office with me. Even more so, for your wonderfully generous and kind nature.

Isabella (and baby): It was such a joy working with you. I thank you for your amazingly upbeat nature and for all your help on this project.

To my wonderful parents and my brother: I couldn't have asked for a more supportive and loving family. I thank you for your patience in all these years and I love you all, more than I can express in words.